



UNIVERSIDAD DE CHILE
FACULTAD DE CIENCIAS FÍSICAS Y MATEMÁTICAS
DEPARTAMENTO DE ASTRONOMÍA

**UNBIASED CHARACTERIZATION OF EXOATMOSPHERES USING
TRANSMISSION SPECTROSCOPY**

TESIS PARA OPTAR AL GRADO DE MAGÍSTER EN CIENCIAS, MENCIÓN
ASTRONOMÍA

ARTURO ALBERTO LIRA BARRIA

PROFESOR GUÍA:

PATRICIO MICHEL ROJO RUBKE

PROFESOR CO-GUÍA

RENÉ ALEJANDRO MÉNDEZ BUSSARD

MIEMBROS DE LA COMISIÓN:

GUILLERMO ALBERTO NEVILLE BLANC MENDIBERRI

NICOLA ASTUDILLO DEFRO

SANTIAGO DE CHILE

2020

RESUMEN DE LA MEMORIA PARA OPTAR
AL TÍTULO DE: Magíster en Ciencias
Mención Astronomía
POR: **Arturo Alberto Lira Barria**
FECHA: 13/11/2020
PROF. GUÍA: Patricio Michel Rojo Rubke

UNBIASED CHARACTERIZATION OF EXOATMOSPHERES USING TRANSMISSION SPECTROSCOPY

Hasta el momento, la técnica más exitosa para caracterizar atmósferas de planetas ha sido la espectroscopía de tránsito, tanto en variedad de sustancias químicas detectadas como en el número de exoatmósferas encontradas. Este método aprovecha el hecho de que las sustancias químicas que están presentes en la atmósfera de un exoplaneta absorben luz de manera diferenciada como función de la longitud de onda. Este trabajo se basa en los métodos de Astudillo-Defru y Rojo [2013] para desarrollar un algoritmo de búsqueda ciega que explora cada transición atómica en espectros de tránsitos, para encontrar absorción relativa. El algoritmo fue aplicado para analizar datos de archivo de HDS en Subaru, HiRes en Keck, UVES en VLT y HARPS en La Silla, en cuatro objetos, cubriendo un rango de longitud de onda que va desde los ~ 5000 a los $\sim 7000\text{\AA}$. Reportamos una detección tentativa de Mn I en HD 209458b, con algunos candidatos prometedores de detección que destacamos para la futura búsqueda de especies químicas.

RESUMEN DE LA MEMORIA PARA OPTAR
AL TÍTULO DE: Magíster en Ciencias
Mención Astronomía
POR: **Arturo Alberto Lira Barria**
FECHA: 13/11/2020
PROF. GUÍA: Patricio Michel Rojo Rubke

UNBIASED CHARACTERIZATION OF EXOATMOSPHERES USING TRANSMISSION SPECTROSCOPY

So far, the most successful technique to characterize atmospheres of exoplanets has been transit spectroscopy, both in terms of the variety of species detected and the number of exoatmospheres proved. This method uses the fact that the chemical species that are present in an exoplanet atmosphere absorb light differently as a function of wavelength. We build on the Astudillo-Defru and Rojo [2013] method to perform a blind-search algorithm that looks for relative absorption at every qualified atomic transition in spectral transit data. We applied this algorithm to analyze archival data of HDS@Subaru, HiRes@Keck, UVES@VLT and HARPS@LaSilla on four targets covering the wavelength range from ~ 5000 to $\sim 7000\text{\AA}$. We report a tentative detection of Mn I in HD 209458b, with some promising candidates of detection that we highlight for future searches for species.

Para Víctor y Fresia,

*cuyo recuerdo y apoyo ha sido un
aliciente para seguir en esta carrera.*

Agradecimientos

En primer lugar, agradezco a mis padres por haberme encauzado hacia las ciencias, respondiendo mis preguntas complicadas, pero sobre todo enseñándome a responderlas por mí mismo. A mi padre por su odisea para comprar mi telescopio, a mi madre por siempre estar pendiente, y a mi hermana por los vídeos chistosos. Con mucho cariño menciono a mi tía abuela Fresia y mi abuelo Víctor, por su constante interés en mi carrera, y a que los tres nos pasamos la vida leyendo.

La importancia del trabajo, el pensamiento crítico, y la seguridad que viene del estudio se las agradezco todas a la institución que alimentó tanto mi curiosidad como mi ambición, el Instituto Nacional. En particular, agradezco a la Academia de Astronomía y por supuesto a la profesora a cargo, María Angélica López, cuya motivación por la física ha contagiado al menos a una decena de sus alumnos a seguir carreras de ciencia.

Menciono también a mi profesor guía, Patricio Rojo, quien desde el principio se mostró muy paciente y amable, reconociendo siempre cuando había avances. También quiero agradecer al profesor René Méndez por toda su ayuda, tanto en la edición de esta tesis, como monetaria. Ésta última pagó varias comidas humanas y gatunas.

A riesgo de parecer Mario Hugo en mi enumeración, usaré un poco de tinta para nombrar a mis gatos, que siempre endulzan la vida. Pienso en el Félix, el Maquiavelo y el Copérnico. También mi Vitali, el Pericles, el César, Cesarito, Zorbas y Tiberio. Galileo, José María, la Flor y la Burbuja. Sir Lancelot, Blanca, Camilito, Ámbar, Ágatha y la Lucy. La Shakira con el Elvis, que empezaron una generación. El Rechoncito, el Santino y el Cósmico. Más recientemente, la Ginger con el Archie, que trajeron la camada de Valterio, Paquita, Arlito y la Nieves. El Tony con la Mashiro, que llegaron chiquitos y asustados. La María Antonieta trajo a Sombras, al Chiqui, a Richi, Teodoro y Lunita. El Carlos, la Dulcinea y mi Stefanina que hoy (4 de Noviembre) tuvo 4 gatitos más. Mención especial a los perros, el Tito, la Josefina, Wolfie, Lucas y Snoopy.

Contents

1. Introduction	1
1.1. Exoplanetary Atmospheres: The way forward	3
2. The algorithm	6
2.1. Data preparation and corrections	8
2.2. Analysis	9
3. Observations	11
4. Results	15
4.1. HDS@Subaru (HD 209458b)	17
4.2. HD 189733b	23
4.3. TRES-2b	23
5. Conclusions	24
Appendix A. Algorithm steps	26
A.1. Normalization process	27
A.2. Summary plots	31
Appendix B. HD 209458b extensive analysis	33
B.1. Global element analysis	33
B.2. Algorithm parameters:	35
B.2.1. Object information:	35
B.3. Elements with detections	36
B.3.1. 0.75 angstrom band	36
B.3.2. 1.0 angstrom band	40

B.4. Detected elements transitions	44
B.4.1. 0.75 angstrom band	44
B.4.2. 1.0 angstrom band	49
Appendix C. HD 189733b extensive analysis (UVES dataset)	54
C.1. Global element analysis	54
C.2. Algorithm parameters:	56
C.2.1. Object information:	56
C.3. Elements with detections	58
C.3.1. 0.75 angstrom band	58
C.3.2. 1.0 angstrom band	62
C.4. Detected elements transitions	66
C.4.1. 0.75 angstrom band	66
C.4.2. 1.0 angstrom band	70
Appendix D. HD 189733b extensive analysis (HARPS dataset)	74
D.1. Global element analysis	74
D.2. Algorithm parameters:	76
D.2.1. Object information:	76
D.3. Elements with detections	78
D.3.1. 0.75 angstrom band	78
D.3.2. 1.0 angstrom band	80
D.4. Detected elements transitions	82
D.4.1. 0.75 angstrom band	82
D.4.2. 1.0 angstrom band	85
Appendix E. TrES-2b extensive analysis	88
E.1. Global element analysis	88
E.2. Algorithm parameters:	90
E.2.1. Object information:	91
E.3. Elements with detections	92
E.3.1. 0.75 angstrom band	92
E.3.2. 1.0 angstrom band	96

E.4. Detected elements transitions	100
E.4.1. 0.75 angstrom band	100
E.4.2. 1.0 angstrom band	105
Bibliography	110

List of Tables

3.1. Archival spectral data analyzed in this paper. S/N was calculated empirically from the qualified transitions. For each planet, we used this value to calculate the continuum residuals boundary used in the QT. Below the bold line we see datasets whose transitions had approved the QT but were discarded by insufficient transit coverage or expected number of photons in the exo-atmosphere. In the binning column, 2s means that we binned two pixels in wavelength, and 4t that we binned 4 frames in time. TrES-2b was a special binning case, as we did a non-uniform time binning. 14

4.1. Summary of highlighted elements in all objects analyzed. 16

4.2. Sigmas of detection for elements in HD 209458b. The σ_{In-Out} column shows the distance from the In-Out center to zero, divided by the with of the In-Out histogram. In contrast, σ_{rel} shows the distance between the in-out center to the center of the noise histogram with the maximum with, and we took the with of the latter to normalize. To match with plots like figure 4.3, the values of absorption are shown as positive. 20

List of Figures

- 1.1. Signal-to-noise ratio computed from the equilibrium temperature, flux of the star, and diameter of the telescope, for all analyzed objects in this work (HAT p 2b and WASP 74b were discarded, as we explain in Chapter 3). 5
- 2.1. Flowchart of our search and detection method. 7
- 2.2. Graphical representation of the bootstrap scenarios described in the text, namely, *In-Out scenario*: To avoid the situation where a few frames might be dominating the absorption, we remove increasingly and randomly some in-transit epochs to calculate the relative absorption (starting with 2 and ending at half of the sample). *Noise scenarios*: For the Out-Out scenario, we ignore all the in-transit epochs and label some of the remaining epochs as in-transit to calculate the absorption. The In-In scenario is the same as Out-Out, but ignoring the out-transit epochs. The distribution of the In-Out scenario is expected to be centered at the actual relative absorption, while noise scenarios should be centered at zero. We use 1σ of the In-Out histogram as our uncertainty. Additionally, 3000 iterations of these scenarios are made for each transition, or the maximum allowed by the combinatorics when the frames were few. 10
- 3.1. Transit coverage of all planets analyzed. Each line represents an epoch, and the length of the line is calculated using the exposure time of that epoch. Note the dispersion of exposure times. 13
- 4.1. Periodic table of this spectral survey. In cyan we indicate elements whose transitions were accepted by QT, and in green elements detected by this work. Previously detected elements, by literature, are in bold. 15

4.2.	<p>Examples of global analysis of two of the four datasets with detections. We show different rates with which we were able to analyze for each element. When two or more lines from the database are closer than 1 FWHM to an observed transition, we ranked the lines using oscillator strength. ST group are considered within the strong detections/total strong lines rate (d_s/T_s, s for strong). We also calculated the total detections/total transitions ($(d_s+d_w)/(T_s+T_w)$, w for weak) rate, and the total strong transitions/total transitions ($T_s/(T_s+T_w)$).</p>	17
4.3.	<p>Element absorption in the 0.75 Å band of all the transitions approved by QT, for interesting elements in HD 209458b. (<i>Up left:</i> Ca I, <i>Up right:</i> Mn I, <i>Low left:</i> Sc II, <i>Low right:</i> Co I). The ordinate shows $(C_{noise} - C_{IO})/\sigma_{noise}$ where $\sigma_{noise} = \max(\sigma_{II}, \sigma_{OO})$. The color shows sigmas of detection ($-C_{IO}/\sigma_{IO}$), where green is $\geq 3\sigma$ and red is $\leq 1\sigma$. Additionally, to deal with contamination from transitions of other species closer than 1 FWHM, we show the ones without contamination as circles (○), with the strongest oscillator strength at that element as triangles pointing up (△). Otherwise, we show them with triangles pointing down (▽).</p>	19
4.4.	<p>Summary plots for previously detected Calcium I (6493.8, 6162.3Å) and Scandium II (5526.8 Å), and revalidated in this work. For every single plot, we have at: <i>Left:</i> From top to bottom, we see the telluric spectra, the normalized flux of the line and the transit seen along wavelength, since we integrated the flux in time. <i>Center:</i> Snellen et al. [2008] transmission light curve. <i>Right, bottom:</i> MCMC distribution, where we can see the distribution of the scenarios explained in Fig. 2.2. Green corresponds to In-Out scenario, blue to Out-Out scenario and red to In-In scenario. We can also see the widths of the histograms at right. <i>Right, top:</i> Boxes with the center of the line found in data (different from database due to Doppler effect), the In-Out histogram center and its distance from zero in terms of In-Out histogram width.</p>	21
4.5.	<p>Summary plots for the tentative detection of Mn I (from top to bottom, 6021.8, 5718.2 6016.7Å). Note that despite 5573.7 transition is the strongest for this element, its σ_c is also very high (see Table 4.2).</p>	22

A.1.	Transition approved by the QT. <i>Top, left:</i> The selected pixels for the fitting of the continuum (CP) are shown inside the light orange band. <i>Top, right:</i> CP are shown in violet, while the window for selecting the minimum flux of the transition (to calculate the observed wavelength) is shown as a violet band. <i>Down, left:</i> After the normalization of the flux, the gaussian profile fitting is shown in dark red. <i>Down, right:</i> The light orange band shows the region that will be used for the analysis (the center band, explained at chapter 2). The residuals of the gaussian profile are shown as a dotted line, while the violet star shows the center of the line, for visual inspection.	27
A.2.	Example of transition discarded by center. Note that in panel <i>top, right</i> we could see two violet bands. The window for selecting the minimum flux of the transition (to calculate the observed wavelength) is shown as a violet band. The light violet band shows the window before the radial velocity correction. . . .	28
A.3.	Example of transition discarded by center and amplitude.	29
A.4.	Example of transition discarded by center and error percent of the CP.	30
A.5.	Example of a summary plot of a transition analysed in HD 209458b (HDS) data. Graphics like this are explained in the caption of Fig. 4.4	31
A.6.	Example of a summary plot of a transition analysed in HD 189733b (UVES) data. Graphics like this are explained in the caption of Fig. 4.4	31
A.7.	Example of a summary plot of a transition analysed in HD 189733b (HARPS) data. Graphics like this are explained in the caption of Fig. 4.4	32
B.1.	Summary for elements on band 0.75	33
B.2.	Summary for elements on band 1.0	34
C.1.	Summary for elements on band 0.75	54
C.2.	Summary for elements on band 1.0	55
D.1.	Summary for elements on band 0.75	74
D.2.	Summary for elements on band 1.0	75
E.1.	Summary for elements on band 0.75	88
E.2.	Summary for elements on band 1.0	89

Chapter 1

Introduction

Old as humanity itself, the question about our place in the universe remains unanswered. For the first time in history, scientists could be near to the answer. This complex question requires the collaboration of several fields, but astronomy and particularly, exoplanetary science, have a leading role in the matter. In the near future, these sciences will be able to place the Solar System, and the Earth, in a cosmic context.

Since the first discovery of an exoplanet orbiting a Sun-like star [Mayor and Queloz, 1995], thousands of new planets have been found. As it was suspected centuries ago, they are abundant. At least in our solar neighbourhood, the fraction of stars with detectable planets is near 75% [Mayor et al., 2011]. Although this may make us think that there are many systems like ours, current statistics suggest that our Solar System is not a representative sample of the planetary systems discovered. Mordasini [2018] mentions several facts that support this statement:

- The frequency of close-in planets (< 100 d) is very high (50 – 60%),
- Planets with a mass lower than $1M_{\oplus}$ and radius lower than $4R_{\oplus}$ have a very high frequency (20 – 50%). They are often found in multiple and tight planetary systems, very different from ours,
- Jupiter may be an outlier, as giant planets ($> 300M_{\oplus}$) within 5-10 AU have a frequency of 10 – 20%. This value gets even lower at distances of tens to hundreds of AU ($\sim 1\%$), and,
- Although eccentricities are restricted to lower values in planets with a mass lower than

$30M_{\oplus}$, they are found in a very broad distribution for all planets, reaching values sometimes bigger than 0.9.

This panorama was impossible to visualize even two decades ago, and it is impressive how much we have learnt from bulk parameters. Indeed, planet formation theory succeeded in explaining a break in the mass distribution at masses near $30M_{\oplus}$ (Howard et al. [2010], Mordasini [2018]). Additionally, a lack of planets known as the Fulton Gap, was found at radii near to $\sim 1.7R_{\oplus}$ [Fulton et al., 2017]. Although simulations seem to be struggling to explain this particular feature of the radii distribution [Venturini et al., 2020], it may suggest a transition between super-Earths and sub-Neptunes. On the other hand, there have been several attempts to classify exoplanets using the estimated density (e.g. Otegi et al. [2020], Odrzywolek and Rafelski [2018]). A standard classification comprehends the *rocky/icy planets* ($< 5M_{\oplus}$), the *transitional planets* ($5 - 15M_{\oplus}$), and the *volatile* or *gas-rich planets* ($> 15M_{\oplus}$), depending on what we expect about their composition [Tinetti et al., 2018]. It should be noted that in our system, there is no planet belonging to that *transitional* class, in which we expect to have either massive super-Earths or sub-Neptunian gaseous planets. In fact, regarding the radii distribution, we note that the majority of planets occupy the size ranging from super-Earth and mini-Neptune [Fulton and Petigura, 2018].

Although this is obviously a first distinction, we can not forget that there are large degeneracies when trying to derive properties using mass and radius alone, because very little empirical correlation exists in the mass-radius space. To name a few examples, Kepler-10c has only $\sim 2R_{\oplus}$, while its mass is $\sim 17M_{\oplus}$ [Dumusque et al., 2014]. On the other hand, the packed planets orbiting Kepler-11, show masses ranging from $\sim 2M_{\oplus}$ to $\sim 13M_{\oplus}$, and densities that differ by a factor of six [Lissauer et al., 2011]. Moreover, when trying to classify with bulk parameters, we should remember a crucial fact: Earth and Venus are very near to each other in a mass-radius space, and yet they have tremendously different atmospheric conditions. That is why exoplanetary scientists have developed ingenious techniques to characterize not only bulk parameters, but also the atmospheres of exoplanets.

1.1. Exoplanetary Atmospheres: The way forward

The field is putting efforts and focusing on obtaining a large set of atmosphere's examples. This is motivated by the lack of a unifying theory, that could link the overall chemistry of an exoplanet to its formation environment, evolution, or host star characteristics. Another reason is that exoplanetary characterization seems to be the only way to find bio-signatures. In the following years, the dream to detect O_2 in an Earth-like exoplanet will be very challenging, but possible. Upcoming facilities like the E-ELT could be able to achieve this, although it would require several years of observation and data of the same planet [Fressin et al., 2013].

Since the first detection of an exoplanet atmosphere [Charbonneau et al., 2002], nearly one hundred more have been probed, 79 exoplanets have at least one chemical species detected, and nearly 50 different species have been found ¹. Detections of species are clearly biased towards warm planets, particularly hot Jupiters. Their study represents an unprecedented opportunity to measure directly the composition of planets. Unlike our solar system, condensation is less likely to trap molecules and elements in lower layers of their atmospheres. This also help us to comprehend different evolution, formation and migration scenarios, since these processes contribute to the overall exoplanet composition. On the other hand, advancements have been made on detecting clouds and hazes, measuring temperature profiles and atmospheric dynamics, and even measuring winds [Madhusudhan, 2019].

All these advancements were achieved thanks to three observational methods: high-resolution spectroscopy (HRS), direct imaging (DI), and transit spectroscopy. HRS uses the fact that planetary spectra is shifted due to radial velocity, and it has provided detections of species in nearly ten hot Jupiters, although its capacity of constraining abundances is marginal. On the other hand, DI has provided high S/N emission spectra directly for about ten exoplanets, located relatively far from their host stars. In the future, combining high-contrast imaging with HRS could provide the first detection of species in super-Earths and Earth-like planets [Snellen et al., 2015]. However, the most successful technique of characterization so far is transit spectroscopy (TS), by the number and variety of species detected as well as the number of exoplanets probed.

TS uses the fact that the chemical species that are present in an exoplanet atmosphere

¹ <http://exoplanet.eu>. July 2020

absorb differently as a function of wavelength, causing a wavelength-dependent effective planetary radius. This technique can be used during a primary eclipse to obtain an absorption spectrum of the planet, or during a secondary eclipse to obtain an emission spectrum. The first has provided more quantity detections of species on more planets, but the second has provided detections of more molecules. Hereafter, we will focus on primary eclipse TS, which has provided several molecules detections, including H_2O , TiO , AlO (Sánchez-López et al. [2019], Sedaghati et al. [2017], von Essen et al. [2019]). Even sub-Neptunes have already been characterized with this technique [Benneke et al., 2019]. When TS is used in high resolution spectrographs, individual atomic species are resolved. Some detections include Na , K , Mg . (Welbanks and Madhusudhan [2019b], Wyttenbach et al. [2017], Gebek and Oza [2020], Hoeijmakers et al. [2020]). Recently, the sample has been extended to include He I (Nortmann et al. [2018]; Allart et al. [2019]; Welbanks and Madhusudhan [2019a]; Welbanks and Madhusudhan [2019a]), and Fe I (Hoeijmakers et al. [2018], Cubillos et al. [2020], Stangret et al. [2020]). A complete summary of all atoms detected can be found in Fig. 4.1.

At temperatures above ~ 2000 K, the emergence of the new category of Ultra-hot Jupiters foresees an increase in the sample of atoms detected. In fact, it has already been able to not just add another discovery of sodium [Chen et al., 2020], but also add Cr I and V I to the chemical species probed [Ben-Yami et al., 2020]. Just in one planet, Cr I, Co I, Sr II and Fe II were all detected for the first time in a cross-correlation survey performed by Hoeijmakers et al. [2019]. In this context, it is likely that the field would benefit from broad spectral surveys for species. The field has already taught us, repeatedly, that we should expect surprises.

An early case of a survey was presented in Astudillo-Defru and Rojo [2013], who pioneered an unbiased blind-search algorithm. It analyzes any atomic spectral line, not only in those positions where models predict absorption. In this work, we improve that algorithm to uniformly analyze archival spectra from several telescopes, including HDS@Subaru, HiRes@Keck, UVES@VLT and HARPS@LaSilla. The objective was to expand the sample of species detected, using data of transits mostly taken to perform Rossiter-McLaughlin methods, as they need conditions similar than ours. We believe that an algorithm like ours could benefit the field to make transit spectroscopy surveys easier, since it will be available freely to be used by anyone. We already have some tentative detections, and thanks to the versatility

of the code, many other planets can be analyzed with it.

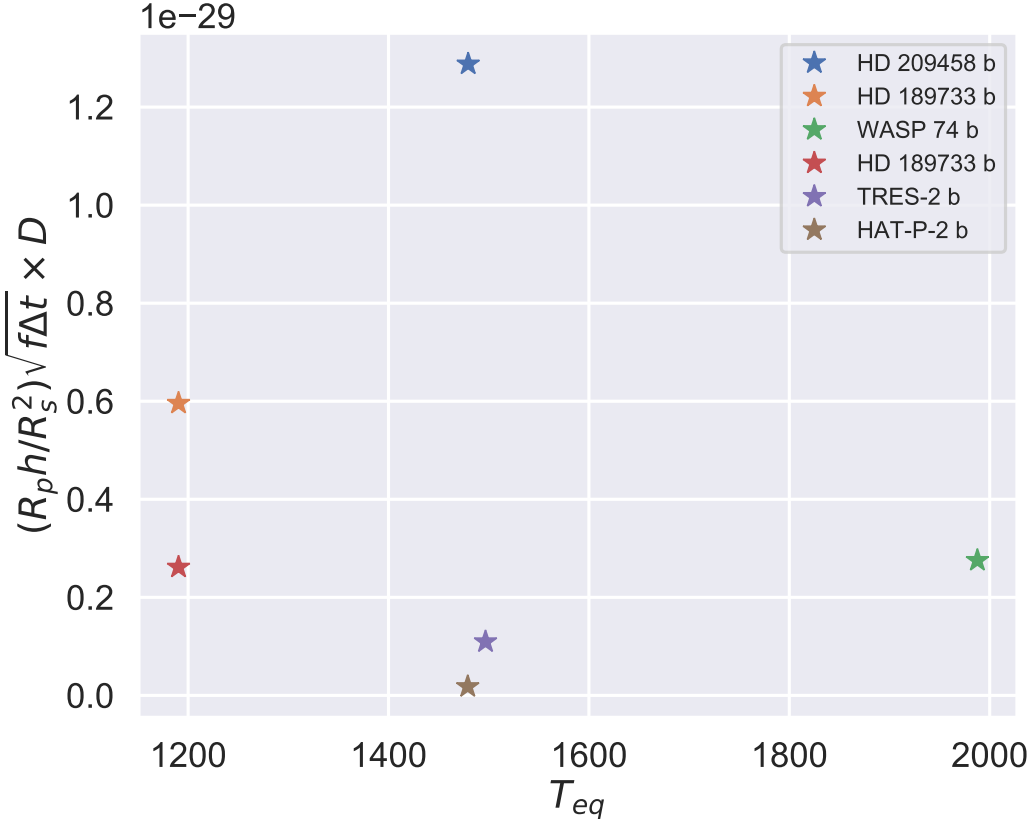


Figure 1.1: Signal-to-noise ratio computed from the equilibrium temperature, flux of the star, and diameter of the telescope, for all analyzed objects in this work (HAT p 2b and WASP 74b were discarded, as we explain in Chapter 3).

Chapter 2

The algorithm

Our code is written in Python 3.7, and will be available on GitHub ¹. It has multiprocessing implemented, and most of the numerical parameters mentioned below can be customized. Our algorithm can be used to blindly search for absorption features over the entire wavelength range of transit spectral time series, but also to perform a directed search for one particular species. A typical transit observed with an optical echelle spectrograph can be analyzed in a few days using 20 cores.

Our approach is based on the methods described by Astudillo-Defru and Rojo [2013] (ADR2013 from now on). The algorithm is designed to analyze every transition approved by our Qualifying Tests (see 2.1.5) to search for relative absorption. This is achieved by comparing zones where the flux should remain constant with those where a relative decrease is expected, both along time and wavelength. The latter is studied with a band centered at the transition, which is compared with the continuum. Along time, the algorithm compares in and out-transit data. Finally, to calculate the confidence of any possible absorption, the code takes several random samples (bootstrap) of the time series. It compares cases when only a few in-transit data are ignored (to avoid possible outliers), with cases without the relative absorption. The latter is achieved by only taking out(in) transit data, to calculate the relative decrease of flux. For details, see Fig. 2.2.

If a particular species is present in the exo-atmosphere, a consistent detection should exhibit absorption in several of its qualified transitions. That is why the code groups them to be reviewed by the scientist, on an automated document congregating graphics like figure 4.3.

¹ <https://github.com/alirabarria/TotalBlindSearch>

We now list the steps of the algorithm in detail (noting explicitly the modifications from ADR2013):

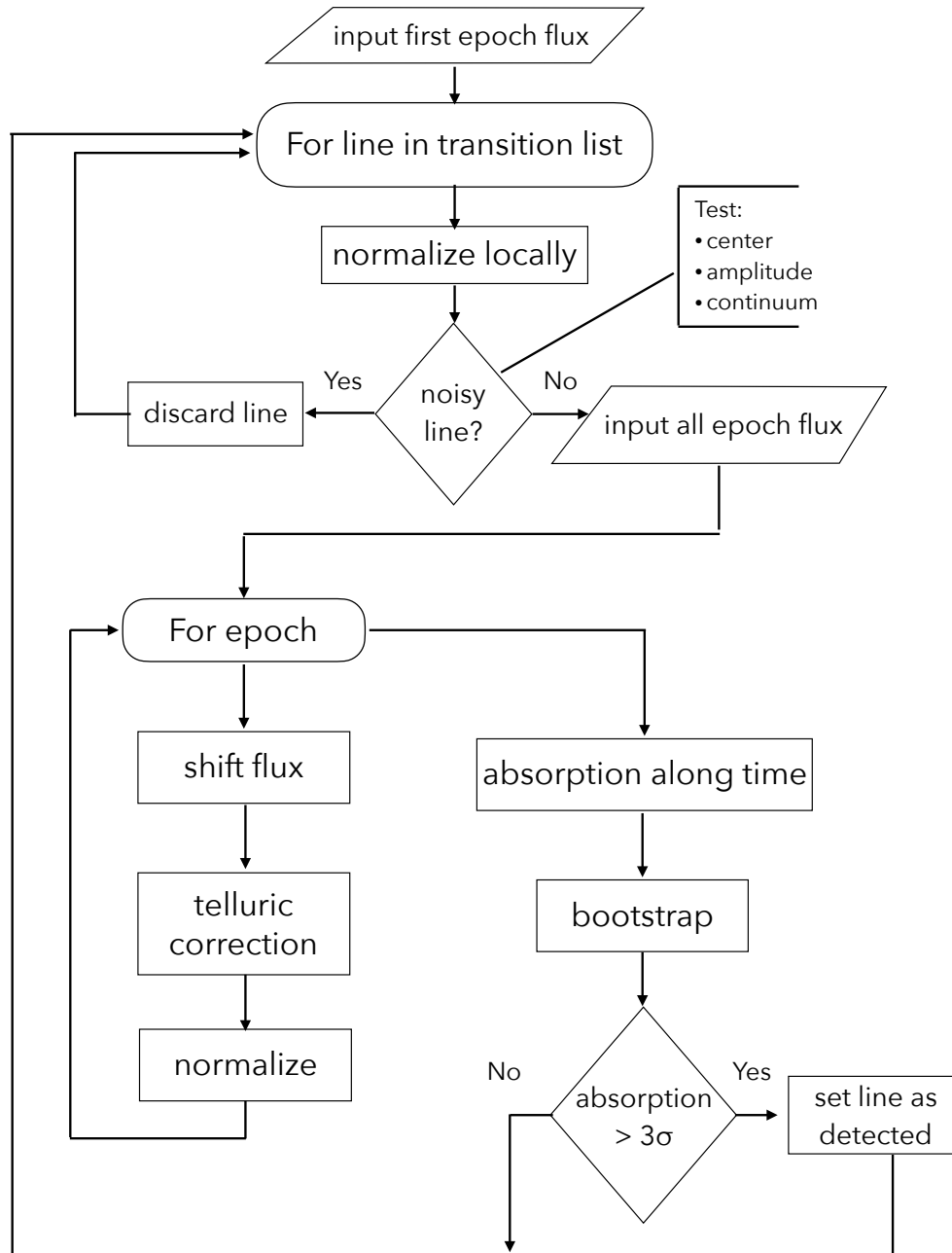


Figure 2.1: Flowchart of our search and detection method.

2.1. Data preparation and corrections

1. To localize the known transitions, we used the entire solar Spectroweb transition list [Lobel, 2008]. We skipped all molecular transitions, and differently from ADR2013, no line depth filter was applied. We also added the Helium transitions from VALD [Kupka et al., 1999].
2. We made a first spectral shift correction by considering Doppler shift. We iteratively refined the radial velocity obtained from the catalogue by considering a selection of strong features ($\log gf > -1$, solar line depth $> 20\%$) discarding outliers, until the scatter on the residuals was $\leq 0.2\text{\AA}$.
3. For all the following steps, we used a reduced local range of $30 \times FWHM$ centered at each transition provided by the database.
4. To normalize the spectra, continuum pixels (CP) are selected within 3.5 Poisson-statistic sigmas from a median filter. The latter was applied using a kernel of $5 \times$ the FWHM. Then, we fit a third order polynomial to the CP, and divide it from the spectra. At this step, Poisson statistics were calculated using the telescope gain and the counts; only UVES' pipeline provided a more precise noise that included the sky subtraction.
5. To discard noisy or blended lines, we tested the transitions by fitting a Gaussian profile to the first epoch of each observed transition. Accepted lines had to pass the Qualifying Tests (QT), described in the following:
 - *Amplitude*: The amplitude of the fit must be closer than 0.06 to the normalized minimum flux.
 - *Center*: The wavelength at the minimum flux must be closer than 0.06\AA from the center of the fit.
 - *Residuals*: the 70 % of CP must be closer than $2 \times$ the expected sigma noise ² to the median of the CP.

The following 4 steps are modifications from ADR2013:

² Calculated from the empirical S/N.

6. To avoid misalignment between the same transition at different epochs, we used cross-correlation. For each transition on each frame, the algorithm tests 2500 intervals in a range of $\pm 1\text{\AA}$, and always compares to the interpolated flux of the first epoch.
7. To increase S/N, the pipeline can average data along wavelength or time. The binning along wavelength is made before normalization, while time binning is made after performing the misalignment correction. For this work, we did not use this feature for all planets (see Chapter 3).
8. To calculate a telluric spectrum, we fitted the intensity to the airmass $I = I_0 \exp\{(Nk_\lambda s)\}$. We used an exponential model, in order to maintain error consistency.³
9. After performing the misalignment and telluric correction we renormalize each line, at each epoch. Then, following Hoeijmakers et al. [2015], we divided each pixel by its median in time. Since the planet signal shifts due to the movement of the planet in front of the star, we are keeping the planet signal but reducing the star contribution. This addition to the previous method help us to improve the detection significance of the previous Calcium detection (see Fig. 4.4).

2.2. Analysis

The algorithm’s main objective is to search for relative absorption in flux on different axes. A robust detection will show a match on the following:

Along wavelength: The transmission spectrum is obtained by averaging the in- and out-transit epochs and then calculating $(F_{In} - F_{Out})/F_{Out}$ at each pixel. If the transition shows absorption, we should see a Voigt profile.

Along time: Following Snellen et al. [2008] we created a pass-band centered at the transition and two control pass-bands at the sides (we tried lengths of 0.75 and 1 \AA for every object analyzed). We averaged the bands and compared the flux at the feature’s center with the control pass-bands to calculate the relative absorption at each transition. If absorption is present, we should see a transit-shape curve.

Absorption corroboration: Following Redfield et al. [2008], and using the same bands from the previous analysis, we bootstrap three types of scenarios to estimate uncertainties. For

³ ADR2013 used a linear model to the logarithm of the flux, which was not statistically correct.

each scenario, the relative absorption is calculated by sub-sampling data to search for false positives and to test the robustness of a detection. The In-Out scenario tests whether the result is robust against a few frames biasing the absorption, while the Out-Out and In-In scenarios test against the possibility of random noise generating the signal. (Fig. 2.2 details the bootstrap algorithm).

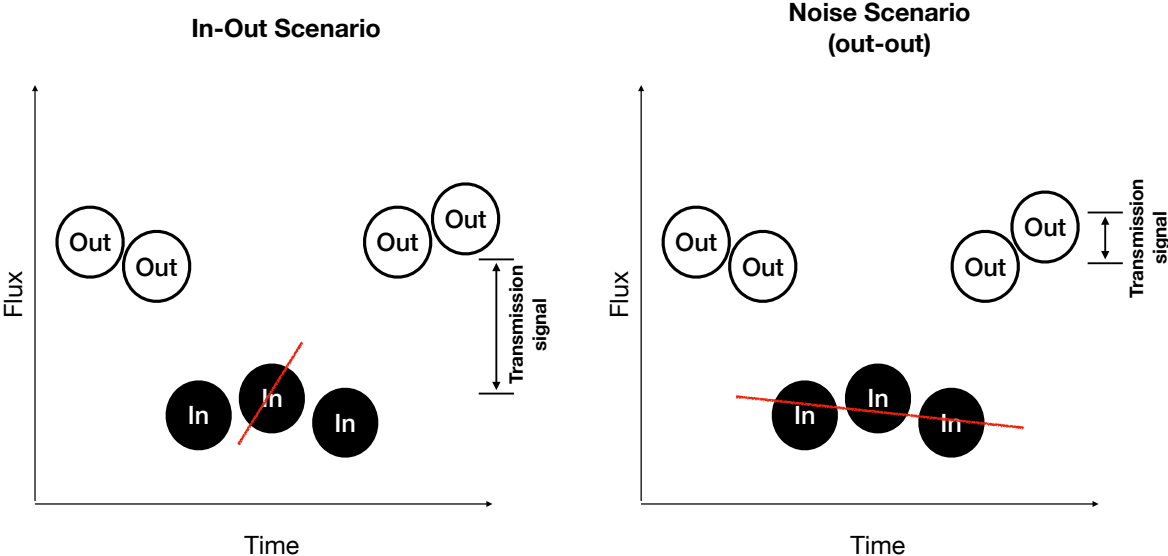


Figure 2.2: Graphical representation of the bootstrap scenarios described in the text, namely, *In-Out scenario*: To avoid the situation where a few frames might be dominating the absorption, we remove increasingly and randomly some in-transit epochs to calculate the relative absorption (starting with 2 and ending at half of the sample). *Noise scenarios*: For the Out-Out scenario, we ignore all the in-transit epochs and label some of the remaining epochs as in-transit to calculate the absorption. The In-In scenario is the same as Out-Out, but ignoring the out-transit epochs. The distribution of the In-Out scenario is expected to be centered at the actual relative absorption, while noise scenarios should be centered at zero. We use 1σ of the In-Out histogram as our uncertainty. Additionally, 3000 iterations of these scenarios are made for each transition, or the maximum allowed by the combinatorics when the frames were few.

Chapter 3

Observations

We considered all planets with Rossiter-McLaughlin measurements and archival data available. Additionally, we included a few other planets with archival data. We used some prominent transits to test every object, and we discarded the data if none of these transits would pass the QT (see 2.1.5). The objects whose transits passed the QT are listed in Table 3.1, with the ID's we use here. We discarded data with insufficient transit baseline coverage since our telluric corrections methods need pre- and post-transit frames. In addition, we focus only on the system with the highest expected signal-to-noise ratio computed from the equilibrium temperature, flux of the star, and diameter of the telescope (see Fig. 1.1).

Our datasets were observed mostly by telescopes with diameters greater than 8m, being LaSilla the only exception (3.6m). We only selected data from high-resolution spectrographs, in order to resolve atomic transitions. They all lie in the 50000-70000 range, being HARPS the only with a resolving power of 110000.

For HARPS, after testing a few objects (WASP-167b, GJ 436 b) we realized that, for objects fainter than ~ 10.5 mag, the signal was too low to be analyzed by our method, as no transit was passed the QT. However, for HiRes, we could analyze until magnitude 11.41, corresponding to target TrES 2b.

HiRes data was reduced with the automated pipeline called MAKEE [Tran et al., 2016]. HARPS and UVES science data was obtained from the ESO archive, and the HDS data (1) was already reduced by Astudillo-Defru and Rojo [2013]. This previous work applied the non-linearity correction that Snellen et al. [2008] suggested for HDS. We used the data already corrected by them, and we did not analyze other objects observed by this spectrograph due

to the lack of this correction. Albrecht et al. [2009] suggested a non-linearity correction for an effect ~ 3 times smaller in UVES data than in HDS. Khalafinejad et al. [2017] did not apply this correction, and neither do we. Additionally, we discarded the UVES data set taken by Albrecht et al. [2009], because they lacked observations of pre-transit time.

Based in our transition lists, we concentrated on the bands that fit in the wavelength range from ~ 5000 to $\sim 7000\text{\AA}$. This corresponded to the red CCD on dataset (1), the red band on the UVES dataset (2),¹ and the green CCD on the HiRes dataset (4). In the latter, we also noted that its noise level was low compared to the blue CCD of the same spectrograph. On the other hand, HARPS dataset (3) was analyzed entirely.

From Table 3.1 we see that (1) has a S/N considerably bigger than every other dataset. In order to increase S/N of the other analyzed objects, we binned in wavelength and/or time if possible. Wavelength binning was only performed if the number of pixels per \AA was bigger than HDS', while time binning was only applied if we could maintain the number of in-transit epochs similar in all analyzed objects, as we need a similar number of combinations to perform the bootstrap analysis. The latter binning was always uniform, discarding frames right before or after the transit when necessary. TrES-2b (4) was a special case because we corrected the dispersion in exposure time, resulting in a non-uniform binning of frames.

¹ Despite it covers until 9400\AA , the analysis covered only until $\sim 7000\text{\AA}$.

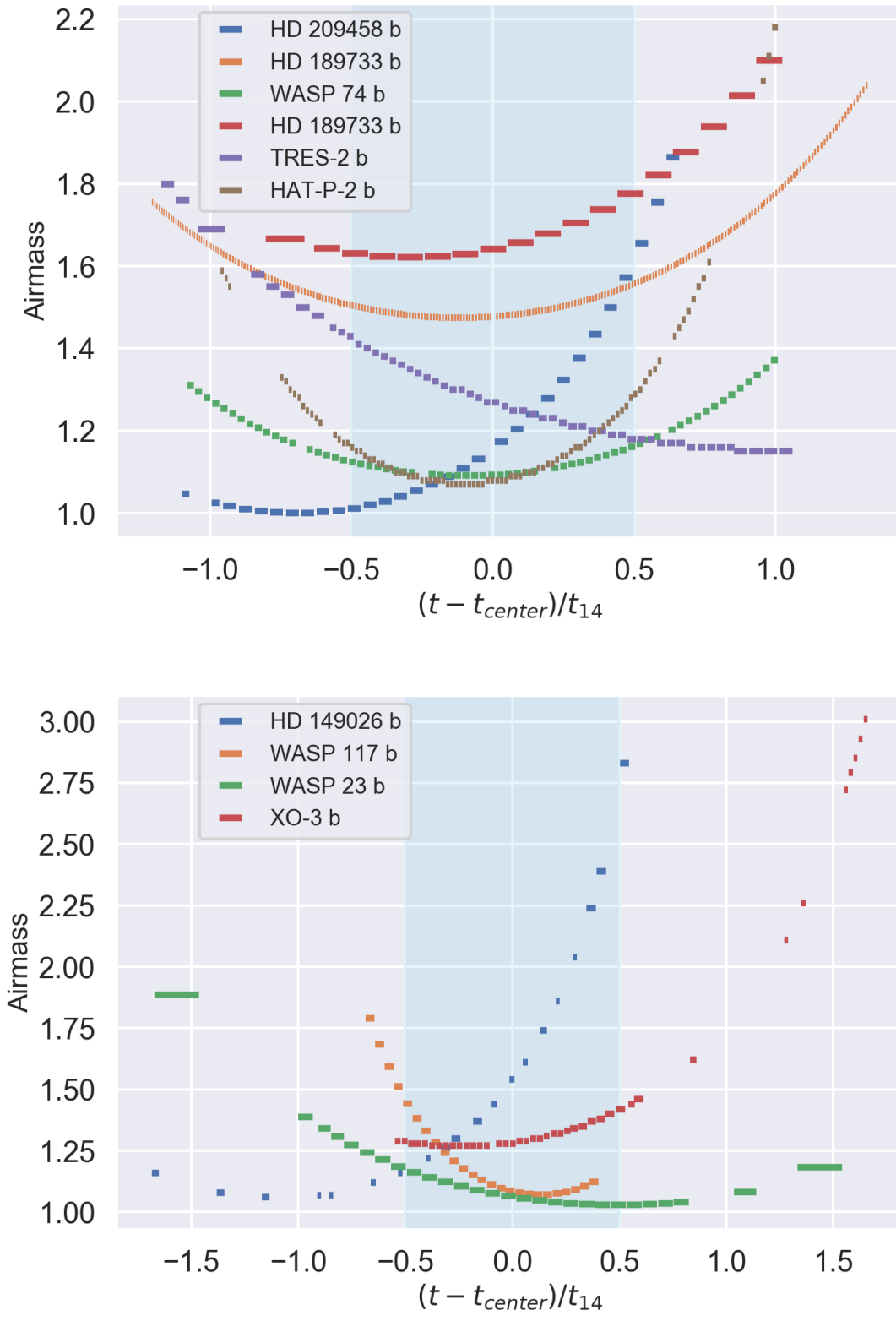


Figure 3.1: Transit coverage of all planets analyzed. Each line represents an epoch, and the length of the line is calculated using the exposure time of that epoch. Note the dispersion of exposure times.

Table 3.1: Archival spectral data analyzed in this paper. S/N was calculated empirically from the qualified transitions. For each planet, we used this value to calculate the continuum residuals boundary used in the QT. Below the bold line we see datasets whose transitions had approved the QT but were discarded by insufficient transit coverage or expected number of photons in the exo-atmosphere. In the binning column, 2s means that we binned two pixels in wavelength, and 4t that we binned 4 frames in time. TrES-2b was a special binning case, as we did a non-uniform time binning.

ID	Object	Date	Ref	Tele- scope	S/N (frame)	S/N (transit)	λ range (nm)	#In	Binned
1	HD 209458b	10-24-2002	2013	HDS @Subaru	24	4613	550 - 680	17	No
2	HD 189733 b	07-01-2012	2017	UVES @VLT	13	3620	560 - 940	92	2s, 4t
3	HD 189733b	09-07-06	072.C- 0488(E)	HARPS @LaSilla	15	1680	380 - 690	19	2s
4	TrES 2b	04-26-2007	2008	HiRes @Keck	6	1397	490 - 640	30	\sim 4t
5	WASP 74b	07-28-17	099.C- 0618	UVES @VLT	9	2660	560 - 940	14	2s
6	HD 149026 b	06-25-2006	2007	HiRes @Keck	-	-	-	-	-
7	HAT P 2b	06-06-2007	2007	HiRes @Keck	-	-	-	-	-
8	XO 3b	02-02-2009	2009	HiRes @Keck	-	-	-	-	-
9	WASP 117b	08-29-2013	2014	HARPS @LaSilla	-	-	-	-	-
10	WASP 23b	12-18-2009	2011	HARPS @LaSilla	-	-	-	-	-
11	HD 209458b	13-08-2006	2009	UVES @VLT	-	-	-	-	-

Chapter 4

Results

H																	He	
Li	Be											B	C	N	O	F	Ne	
Na	Mg											Al	Si	P	S	Cl	Ar	
K	Ca	Sc	Ti	V	Cr	<i>Mn</i>	Fe	Co	Ni	Cu	Zn	Ga	Ge	As	Se	Br	Kr	
	Ca II	Sc II	Ti II	V II	Cr II		Fe II											
Rb	Sr	Y	Zr	Nb	Mo	Tc	Ru	Rh	Pd	Ag	Cd	In	Sn	Sb	Te	I	Xe	
	Sr II	Y II	Zr II															
Cs	Ba	La	Hf	Ta	W	Re	Os	Ir	Pt	Au	Hg	Tl	Pb	Bi	Po	At	Rn	
	Ba II	La II																
Fr	Ra	Ac	Rf	Db	Sg	Bh	Hs	Mt	Ds	Rg	Cn	Nh	Fl	Mc	Lv	Ts	Og	
			Ce	Pr	Nd	Pm	Sm	Eu	Gd	Tb	Dy	Ho	Er	Tm	Yb	Lu		
			Ce II	Pr II	Nd II		Sm II											
			Th	Pa	U	Np	Pu	Am	Cm	Bk	Cf	Es	Fm	Md	No	Lr		

Figure 4.1: Periodic table of this spectral survey. In cyan we indicate elements whose transitions were accepted by QT, and in green elements detected by QT, and in bold previously detected elements, by literature, are in bold.

For each planet, we used Fig. 4.2 to guide our criteria. From left to right, it sorts our analyzed atomic species from roughly the most likely to be present to the least likely. Then, we examine the overall behavior of all the transitions in an atom (e.g. Fig. 4.3), and finally we look in detail at individual transitions (e.g. Fig. 4.4). The latter contains all the information of the relative absorption, depicted along wavelength, time, and the bootstrap distributions.

To decide if an atomic species ¹ was detected, we summarized every analyzed transition of each atom. From the histograms obtained for the distributions In-Out, In-In, Out-Out (see Fig. 2.2) we define C_{IO} , C_{II} , C_{OO} , as its respective medians, and σ_{IO} , σ_{II} , σ_{OO} as its

¹ We use element, atom or species interchangeably.

Table 4.1: Summary of highlighted elements in all objects analyzed.

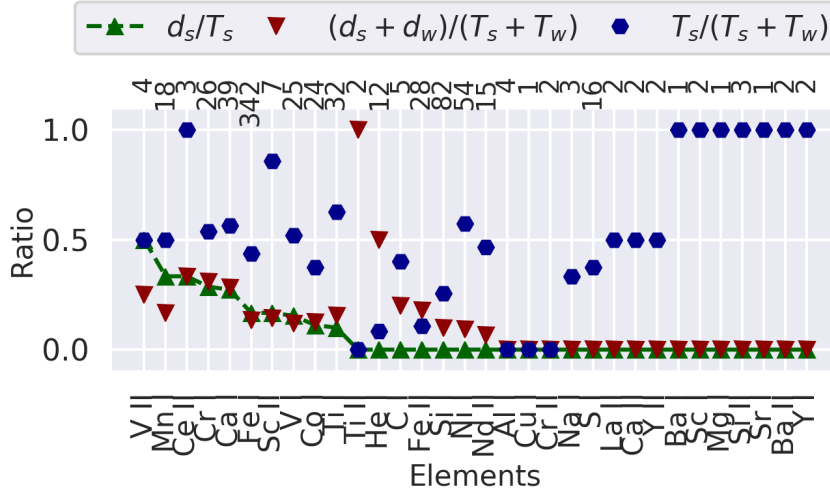
Object	Candidates	Promising	Rejected	Literature
HD 209458b	Mn I	Ca I, Sc II, V I, Co I	Ni I, Nd II, S I	C I, Fe I, H I, He I, K I, Mg I, Na I, O I
HD 189733b (UVES)	-	Ti I	Mn I	C I, H I, He I, K I, Na I, O I
Tres 2b	-	Cr I, La II, Si II	-	No previous de- tections

respective Gaussian widths. A transition is defined as detected when the distance between C_{IO} and zero is greater than $3\sigma_{IO}$. Moreover, we reduced the possibility of detecting species by chance asking that C_{IO} did not remain inside a noise distribution. To do this, we defined the histogram with the largest width as noise ($\sigma_{noise} = \max(\sigma_{II}, \sigma_{OO})$) and we required that:

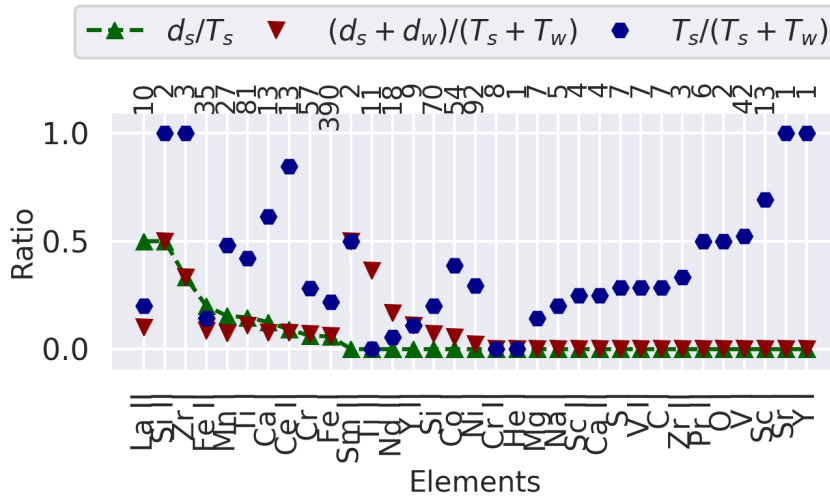
$$\sigma_{rel} = (C_{noise} - C_{IO})/\sigma_{noise} > 1$$

We used oscillator strength as a proxy of how strong is each spectral line. Besides, we searched for contamination from other transitions closer than 1 FWHM. If no other spectral line is found in the range, or it is the strongest, we consider it a Strong Transition (ST). Additionally, in our analysis we considered the noise of the continuum used to normalize the transition, defining σ_c as the standard deviation of the CP (see 2.1.4) at each spectral line.

Table 4.1 summarizes our findings for all species in all our planets analyzed, including a literature comparison. Note that we decided to omit WASP-74b from this section, because no atom showed a consistent detection across multiple transitions. In the following sections, we highlight the interesting species found in each planet analyzed. We listed the relevant parameters of the first ten ST of selected atoms of HD 209458b in Table 4.2. Equivalent tables are available for all other planets at appendices B to E. They include all elements with at least one qualified transition showing detection.



(a) HD 209458b



(b) TrES 2b

Figure 4.2: Examples of global analysis of two of the four datasets with detections. We show different rates with which we were able to analyze for each element. When two or more lines from the database are closer than 1 FWHM to an observed transition, we ranked the lines using oscillator strength. ST group are considered within the strong detections/total strong lines rate (d_s/T_s , s for strong). We also calculated the total detections/total transitions ($(d_s + d_w)/(T_s + T_w)$, w for weak) rate, and the total strong transitions/total transitions ($T_s/(T_s + T_w)$).

4.1. HDS@Subaru (HD 209458b)

Mn I is a promising detection for this planet since the transitions that show detection have also a smaller σ_c .² From Fig. 4.3 and Table 4.2, at 0.75Å band we see three spectral lines (6021.8, 5718.3 and 6016.7 Å) showing a robust absorption. Despite 5573.7 being the

² The three transitions referenced in text show a $\sigma_c \leq 0.006$, the median for this planet.

strongest transition at this element and showing no detection, its continuum residuals are more than two times bigger than those belonging to 6016.7.

Co I shows four ST with $> 3\sigma_{IO}$ of absorption, however, only one of these is outside the noise histograms. Thus, despite not qualifying as a detection, we think that the low σ_c of this group hints at a possible indicator of a tentative detection.

Regarding the previous detection that ADR2013 found, we find evidence of Ca I and possibly Sc II in the same data. We recovered all the transitions showing absorption for both (see Fig. 4.4). However, for Ca I we also found several non-detection in spectral lines with an oscillator strength of the same order. Additionally, despite the fact that the first line of Sc II shows absorption, it is one of the noisiest of every element. Therefore, we find that the previous detections are inconclusive. This does not mean that we are rejecting them, but that they should be revisited with better data. Notice that we did not analyze H I, because the transition of this element would need a special tuning of parameters (the prominence of it makes the algorithm to discard it).

Other works found detections of C I, Mg I, H I, O I [Rimmer and Helling, 2016]; Fe I [Cubillos et al., 2020]; He I [Welbanks and Madhusudhan, 2019a]; Na I, K I [Welbanks and Madhusudhan, 2019b]. However, we did not find detection of these species. In the case of C I, the only transition with detection is shared with Mn I (6016.7). The others lines of C I were non-detections (three with a bigger oscillator strength), and 6016.7 has a $\log(gf)$ of -1.83 at C I (vs -0.22 at Mn I), therefore we think that the absorption found in our data belongs to Mn I. Mg I did not show detection, but we only have one qualified transition at this spectral range. The only ST of He I did not show absorption. K I and O I have no qualified transitions. Fe I shows 46 detections from a total of 342 analyzed. The detections do not show a correlation with oscillator strength or continuum noise. We classified this element as inconclusive, as we could not explain the non-detections.

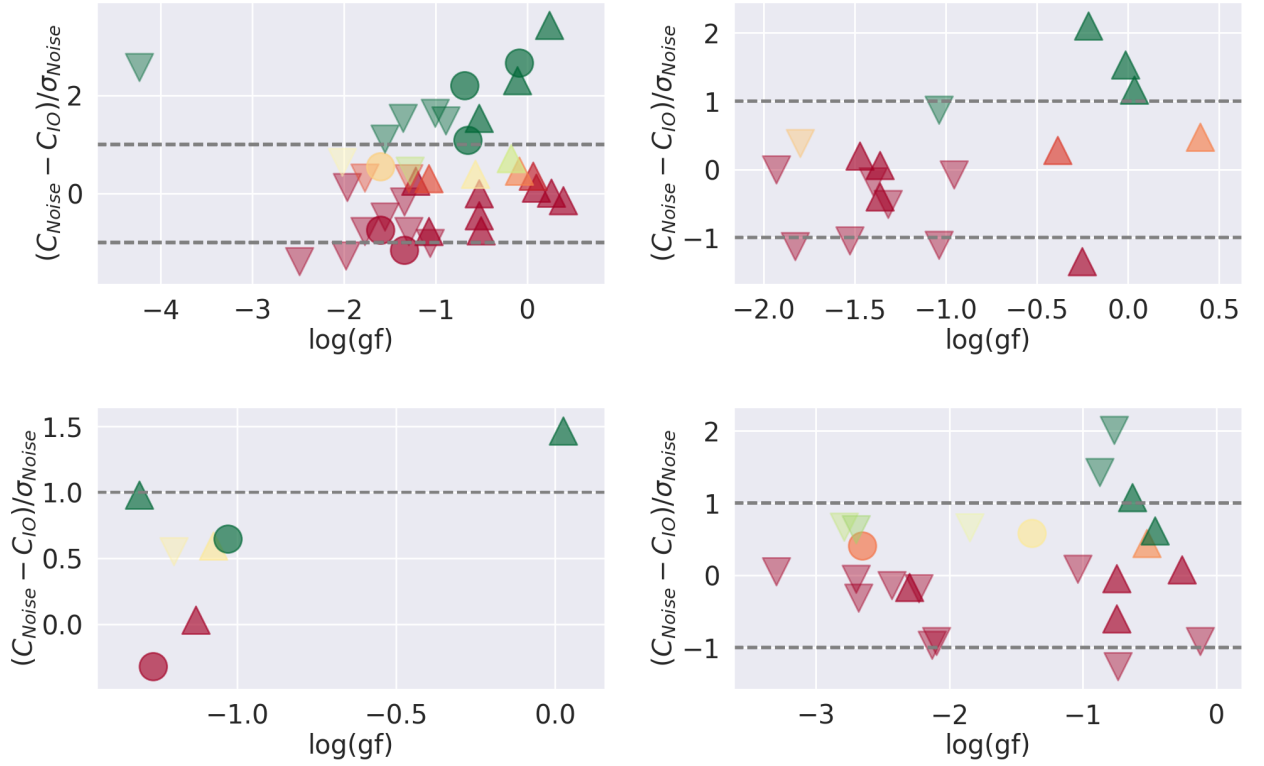


Figure 4.3: Element absorption in the 0.75 Å band of all the transitions approved by QT, for interesting elements in HD 209458b. (*Up left*: Ca I, *Up right*: Mn I, *Low left*: Sc II, *Low right*: Co I). The ordinate shows $(C_{noise} - C_{IO}) / \sigma_{noise}$ where $\sigma_{noise} = \max(\sigma_{II}, \sigma_{OO})$. The color shows sigmas of detection ($-C_{IO} / \sigma_{IO}$), where green is $\geq 3\sigma$ and red is $\leq 1\sigma$. Additionally, to deal with contamination from transitions of other species closer than 1 FWHM, we show the ones without contamination as circles (○), with the strongest oscillator strength at that element as triangles pointing up (△). Otherwise, we show them with triangles pointing down (▽).

Atom	$\lambda_{lab}(\lambda_{obs})$	log(gf)	normed			
			depth	σ_{In-Out}	σ_{rel}	σ_c
Ca I	△ 6439.075(.235)	0.39	0.58	-0.42	-0.14	0.005
	△ 6462.567(.734)	0.26	0.59	0.07	0.01	0.005
	△ 5857.451(.599)	0.24	0.52	10.63	3.43	0.007
	△ 5594.462(.607)	0.1	0.57	0.67	0.12	0.011
	△ 6318.109(.174)	0.06	0.41	1.12	0.36	0.007
	△ 5598.48(.605)	-0.09	0.55	1.47	0.46	0.008
	○ 6162.173(.331)	-0.09	0.63	10.9	2.67	0.008
	△ 6493.781(.945)	-0.11	0.49	6.99	2.31	0.006

	△	5991.798(.513)	-0.18	0.18	2.23	0.71	0.006
	△	6449.808(.968)	-0.5	0.42	-2.41	-0.76	0.005
	△	5601.277(.404)	-0.52	0.46	-2.34	-0.46	0.008
	△	5573.682(.014)	0.4	0.55	1.47	0.47	0.009
	△	6021.803(.937)	0.03	0.35	3.48	1.16	0.004
	△	5718.233(7.97)	-0.01	0.28	5.47	1.54	0.006
	△	6016.673(.776)	-0.22	0.34	6.4	2.11	0.004
Mn I	△	6013.513(.63)	-0.25	0.29	-6.42	-1.35	0.004
	△	5738.261(.357)	-0.39	0.05	1.24	0.28	0.005
	△	6586.304(.472)	-1.36	0.13	0.2	0.06	0.006
	△	6586.304(.469)	-1.36	0.14	-1.59	-0.4	0.005
	△	5557.684(8.086)	-1.48	0.24	0.59	0.2	0.006
	△	5526.79(.936)	0.02	0.42	4.48	1.47	0.01
	○	6245.637(.761)	-1.03	0.17	3.69	0.65	0.008
	△	5684.202(.614)	-1.07	0.27	1.85	0.59	0.009
Sc II	△	5641.001(.118)	-1.13	0.21	0.13	0.03	0.008
	○	6279.753(.907)	-1.26	0.25	-1.36	-0.32	0.007
	△	6604.601(.741)	-1.31	0.17	3.05	0.98	0.004

Table 4.2: Sigmas of detection for elements in HD 209458b. The σ_{In-Out} column shows the distance from the In-Out center to zero, divided by the with of the In-Out histogram. In contrast, σ_{rel} shows the distance between the in-out center to the center of the noise histogram with the maximum with, and we took the with of the latter to normalize. To match with plots like figure 4.3, the values of absorption are shown as positive.

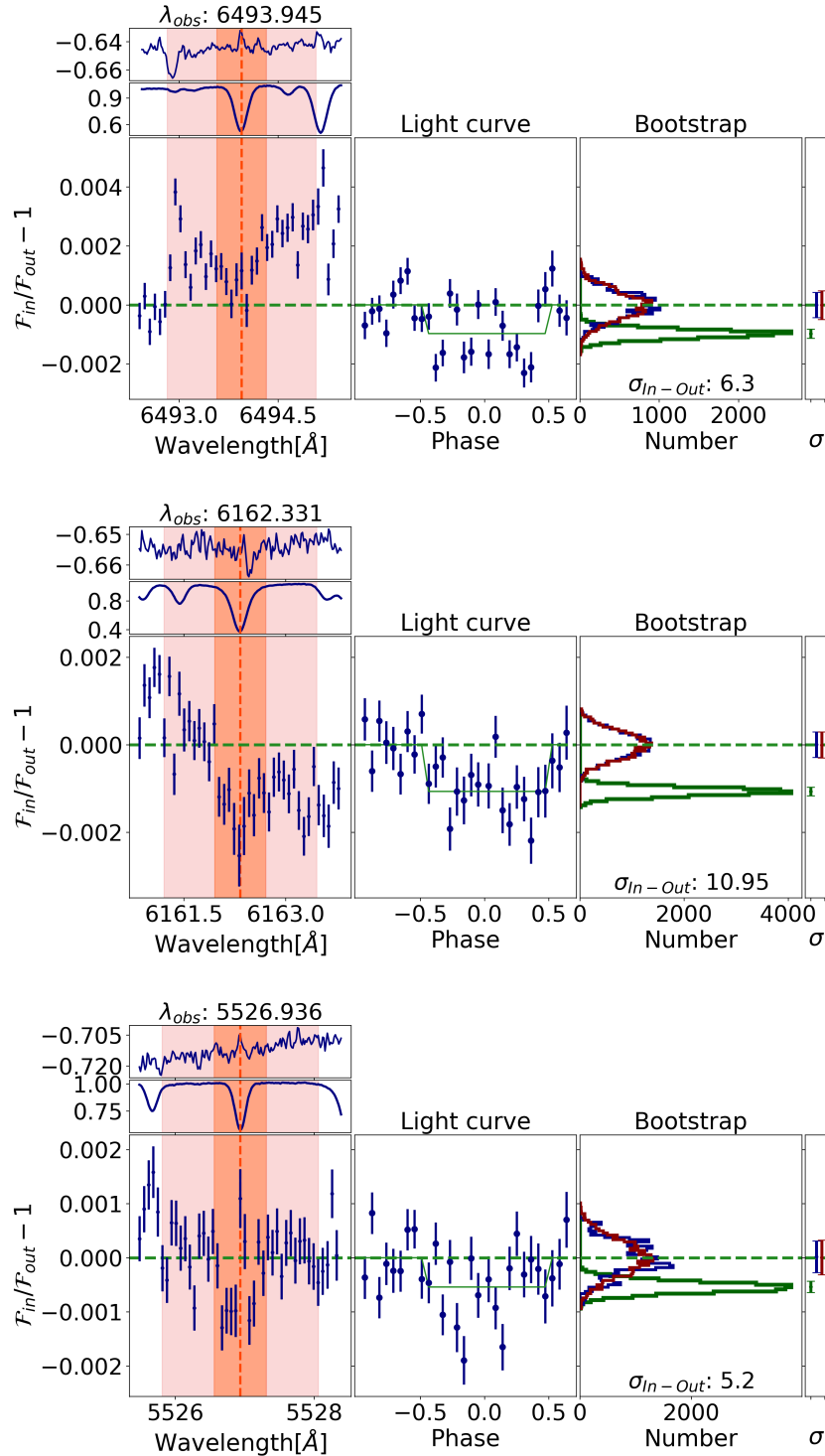


Figure 4.4: Summary plots for previously detected Calcium I (6493.8, 6162.3 Å) and Scandium II (5526.8 Å), and revalidated in this work. For every single plot, we have at:

Left: From top to bottom, we see the telluric spectra, the normalized flux of the line and the transit seen along wavelength, since we integrated the flux in time. *Center:* Snellen et al. [2008] transmission light curve. *Right, bottom:* MCMC distribution, where we can see the distribution of the scenarios explained in Fig. 2.2. Green corresponds to In-Out scenario, blue to Out-Out scenario and red to In-In scenario. We can also see the widths of the histograms at right. *Right, top:* Boxes with the center of the line found in data (different from database due to Doppler effect), the In-Out histogram center and its distance from zero in terms of In-Out histogram width.

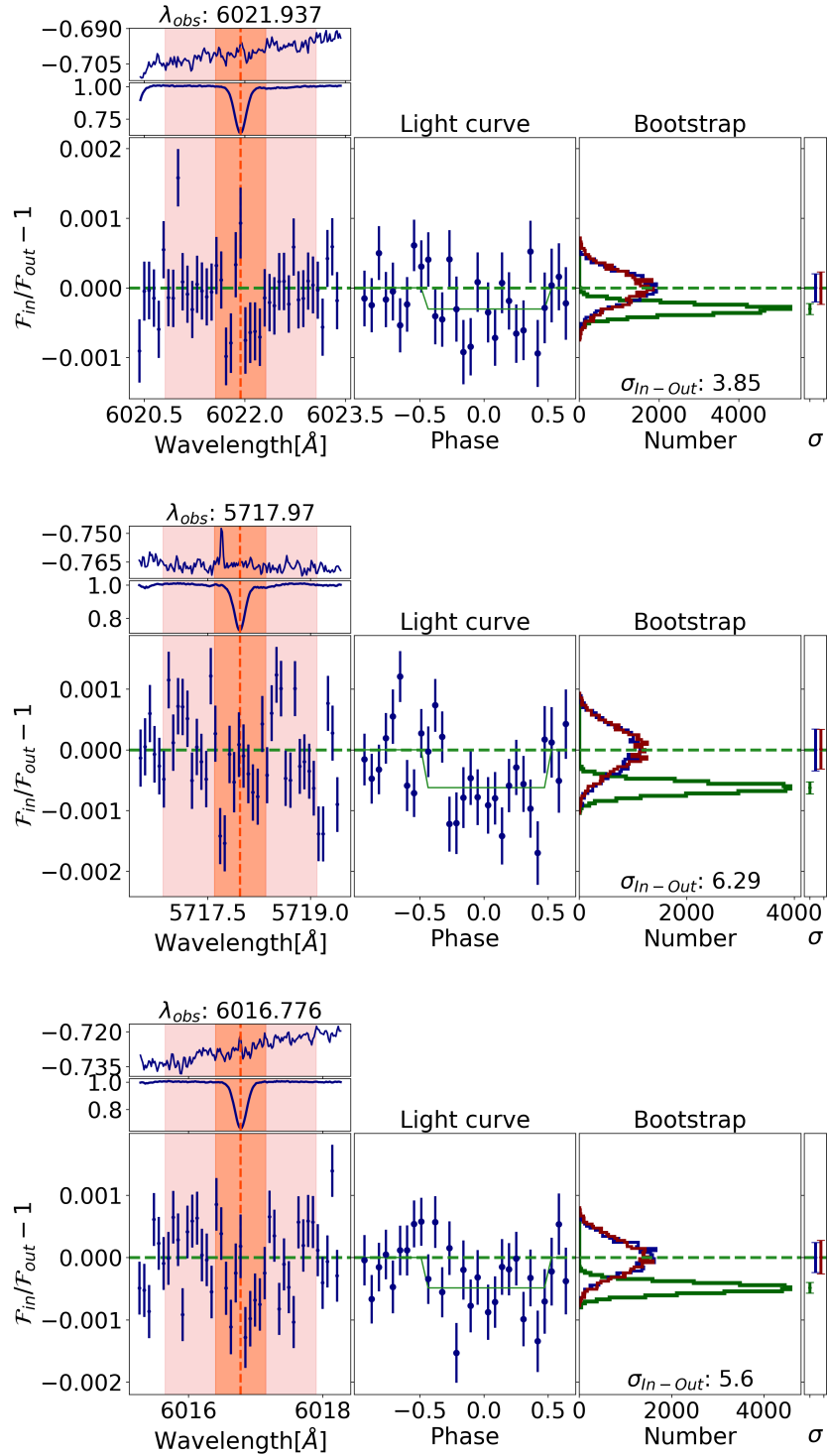


Figure 4.5: Summary plots for the tentative detection of Mn I (from top to bottom, 6021.8, 5718.2 6016.7 Å). Note that despite 5573.7 transition is the strongest for this element, its σ_c is also very high (see Table 4.2).

4.2. HD 189733b

In the HARPS dataset of this planet, we could see a very tentative detection of Si II. Only two lines were accepted by the tests on this element, but the stronger one shows relative absorption. This same transition was not qualified in UVES data, because of its width, and no other Si II transition showed absorption in this dataset. It should be noticed though that the transition showing absorption in HARPS is considerably stronger than the transitions accepted by the tests on UVES. However, we did not find any element showing absorption consistently on this planet. We noticed that several of the possible detections in the UVES data showed continuum contamination of close transitions, that reduced the stability of the control pass-bands.

We highlight Mn I at UVES, because it shows a consistent not detection among all transitions analyzed in this spectral range. Although several other elements show non-detections, this is the only one with several transitions approved by our QT.

This planet has some previous detections of C I [Benneke, 2015], H I [Bourrier et al., 2013], He I [Salz et al., 2018], Na I [Wytttenbach et al., 2015], K I [Gebek and Oza, 2020] and O I [Ben-Jaffel and Ballester, 2013]. No spectral lines of H I or O I were accepted by the QT. Na I and K I have only one transition qualified at each case, which was not sufficient to conclude that there is absorption, nor to deny it. C I and He I had a few more transitions accepted, but they do not show consistent absorption on the UVES data, and they did not present any detections on HARPS data. Therefore, we could not corroborate nor deny any of these previous detections.

4.3. TRES-2b

This planet has a S/N considerably lower than HD 209458b. Of the 19 elements in which at least one transition showed detection, we highlight two. La II has only two ST; they both show detection at band 1Å, but they are a little noisier than the median. Si II shows the less noisy transition with absorption, which is less noisy than the median of this object as well. Although these species seem to present a detection, they remain inconclusive at this level of sensitivity.

Chapter 5

Conclusions

We presented a blind-search algorithm designed to perform spectral surveys to search for atomic species in transiting exoplanets. In our work we revisited and expanded the dataset in which Astudillo-Defru and Rojo [2013] discovered Ca I and tentatively Sc II in HD 209458 b. We recovered their detections, but found several other transitions of the same element that did not show relative absorption. Therefore, we classify their species detections as inconclusive. On the other hand, we found a more robust detection of Mn I, which shows relative absorption consistently among the stronger transitions of that element.

Our search for species in other lower S/N datasets was not conclusive. Although we found a very tentative detection of Si II in the HARPS dataset of HD 189733b, we could not find evidence of that in the UVES dataset of the same planet. On the other hand, we highlight some possible detections of La II and Si II at Tres-2b, still not conclusive because of the low S/N.

Recently, Casasayas-Barris et al. [2020] has contested the sodium detection of Charbonneau et al. [2002], measuring the RM and CLV effects on HD 209458b transits. For a more definitive conclusion, it will be necessary to correct for these effects in our analysis. Those effects have not been precisely quantified for an algorithm like ours, as there are claims pointing for and against the importance of those corrections (Chen et al. [2020], Seidel et al. [2020]). Despite we could only find one atomic species with consistent absorption, forthcoming facilities like JWST and E-ELT will provide data with considerably higher S/N. For example, our Si II tentative absorption in the HARPS dataset of HD 189733b shows a $\sim 4\sigma$ relative absorption. If we observe the same transition with EELT-HIRES, the certainty would theoretically be ~ 10 times bigger, under similar conditions, providing a powerful tech-

nique to model-independently discover and constrain the overall composition of exoplanetary atmospheres.

Appendix A

Algorithm steps

This appendix contains figures of the main processes of the algorithm. At section A.1 we show examples of the normalization and Qualifying Tests. At section A.2 we show examples of the summary plots of the algorithm, which show the telluric spectra, the analysis along wavelength and time, and the bootstrap process. We choose to show the same transition qualified in three of the four planets analysed in this work.

A.1. Normalization process

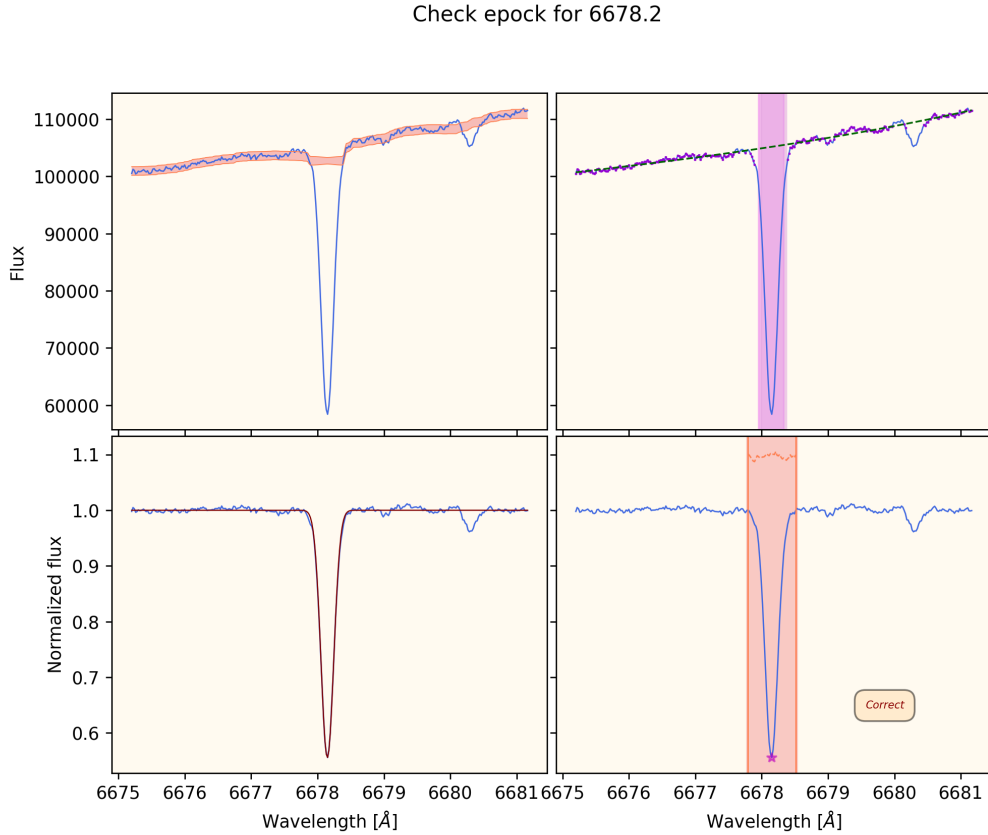


Figure A.1: Transition approved by the QT. *Top, left:* The selected pixels for the fitting of the continuum (CP) are shown inside the light orange band. *Top, right:* CP are shown in violet, while the window for selecting the minimum flux of the transition (to calculate the observed wavelength) is shown as a violet band. *Down, left:* After the normalization of the flux, the gaussian profile fitting is shown in dark red. *Down, right:* The light orange band shows the region that will be used for the analysis (the center band, explained at chapter 2). The residuals of the gaussian profile are shown as a dotted line, while the violet star shows the center of the line, for visual inspection.

Check epoch for 5804.259

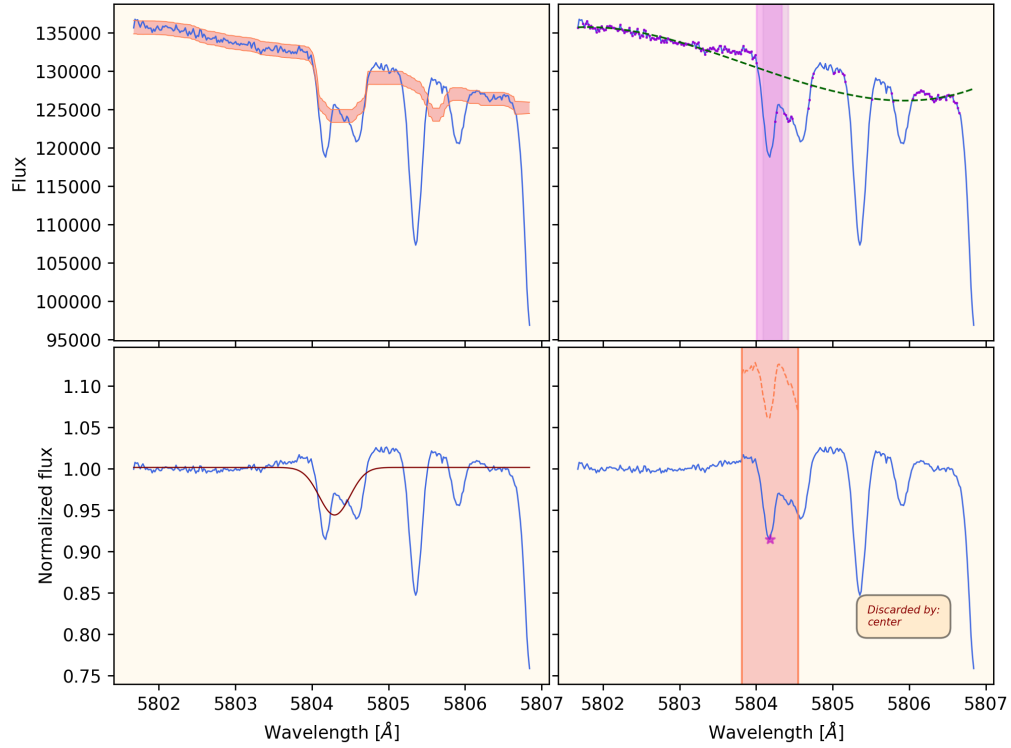


Figure A.2: Example of transition discarded by center. Note that in panel *top, right* we could see two violet bands. The window for selecting the minimum flux of the transition (to calculate the observed wavelength) is shown as a violet band. The light violet band shows the window before the radial velocity correction.

Check epoch for 5694.731

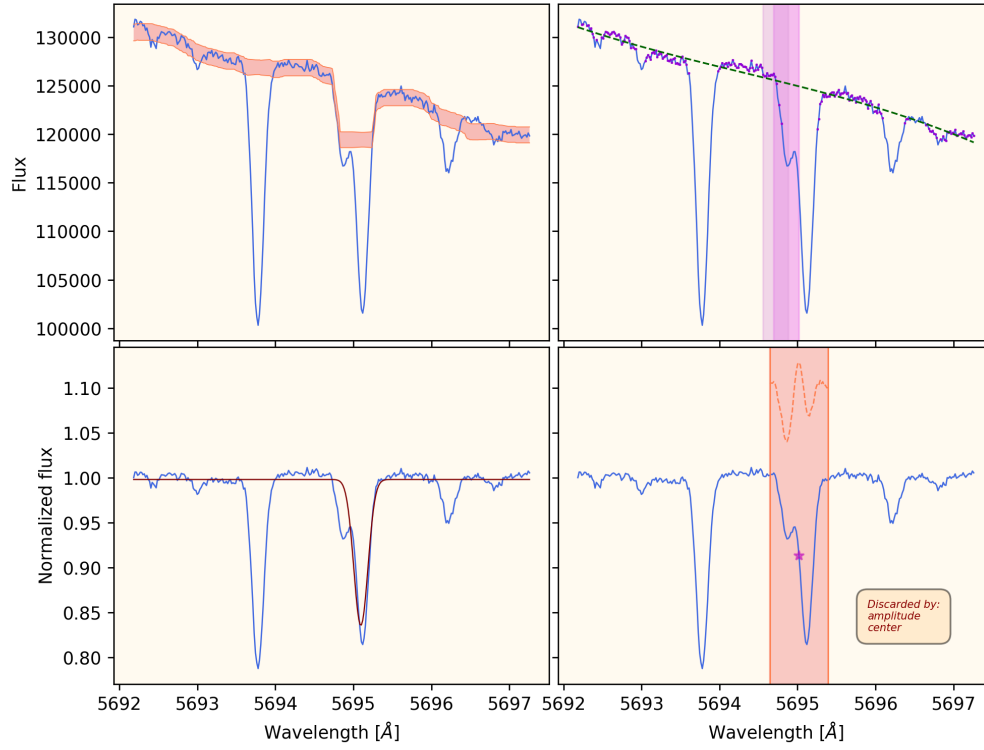


Figure A.3: Example of transition discarded by center and amplitude.

Check epoch for 5786.156

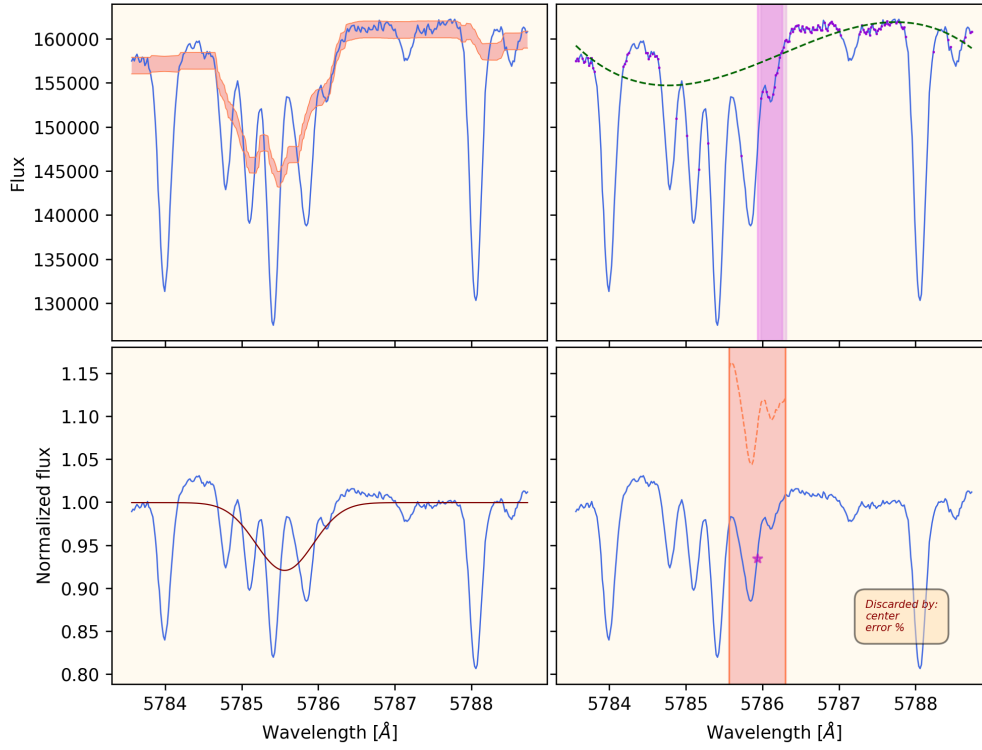


Figure A.4: Example of transition discarded by center and error percent of the CP.

A.2. Summary plots

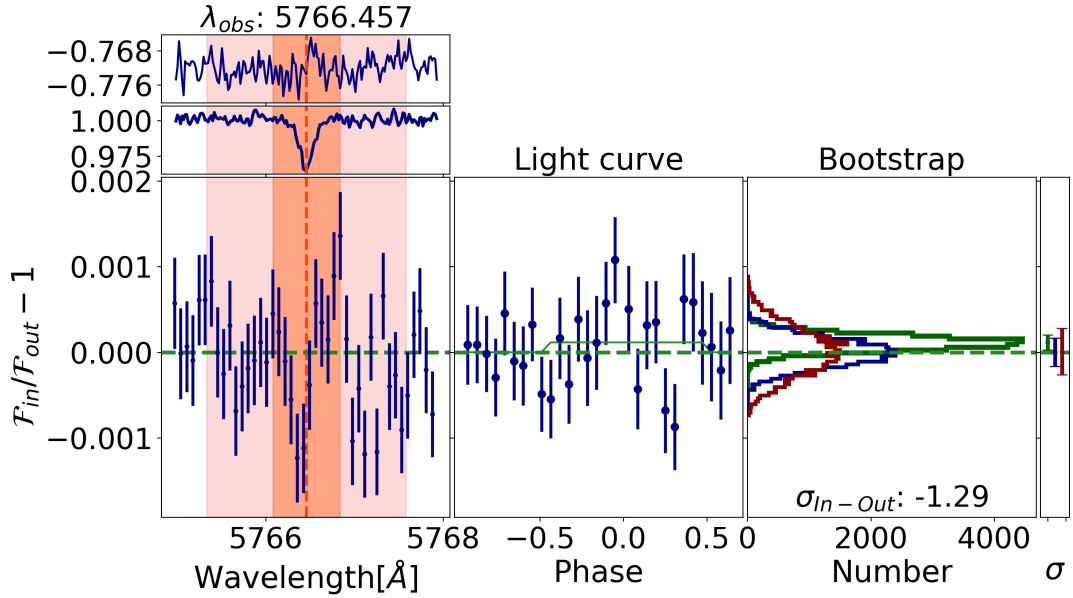


Figure A.5: Example of a summary plot of a transition analysed in HD 209458b (HDS) data. Graphics like this are explained in the caption of Fig. 4.4

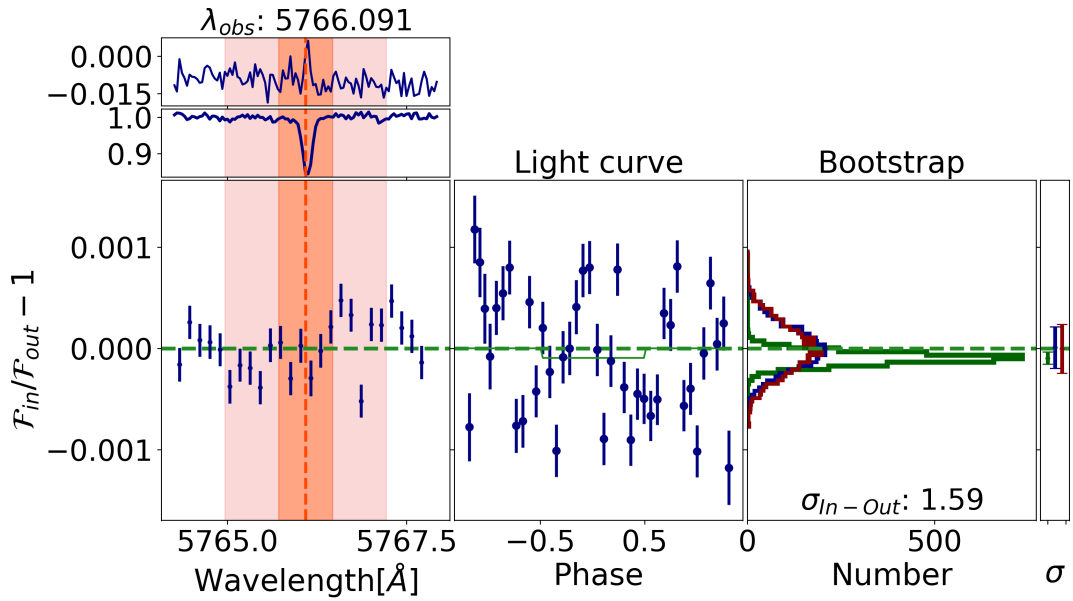


Figure A.6: Example of a summary plot of a transition analysed in HD 189733b (UVES) data. Graphics like this are explained in the caption of Fig. 4.4

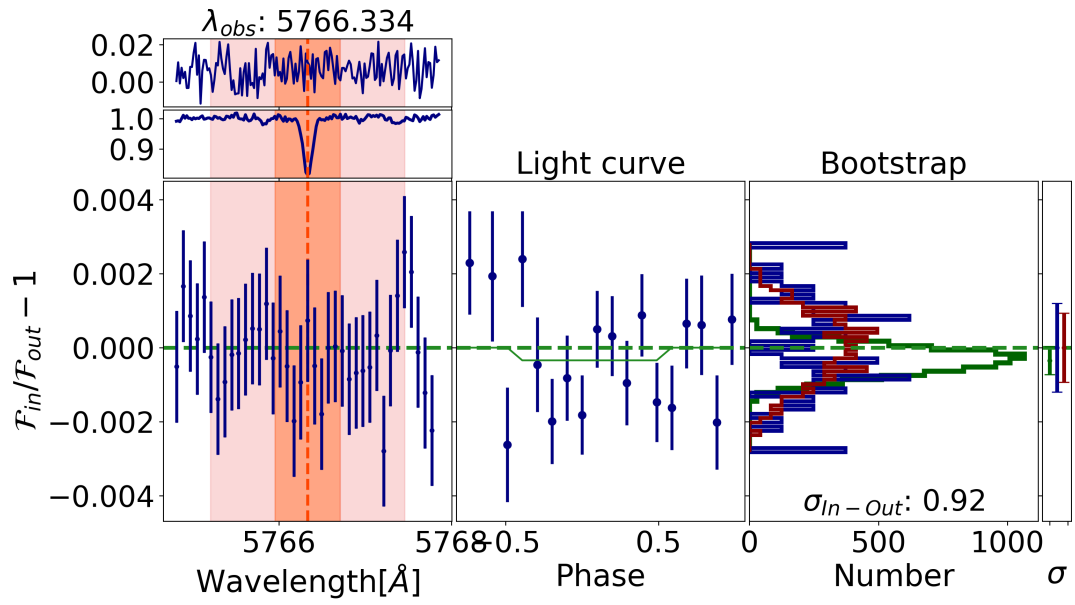


Figure A.7: Example of a summary plot of a transition analysed in HD 189733b (HARPS) data. Graphics like this are explained in the caption of Fig. 4.4

Appendix B

HD 209458b extensive analysis

B.1. Global element analysis

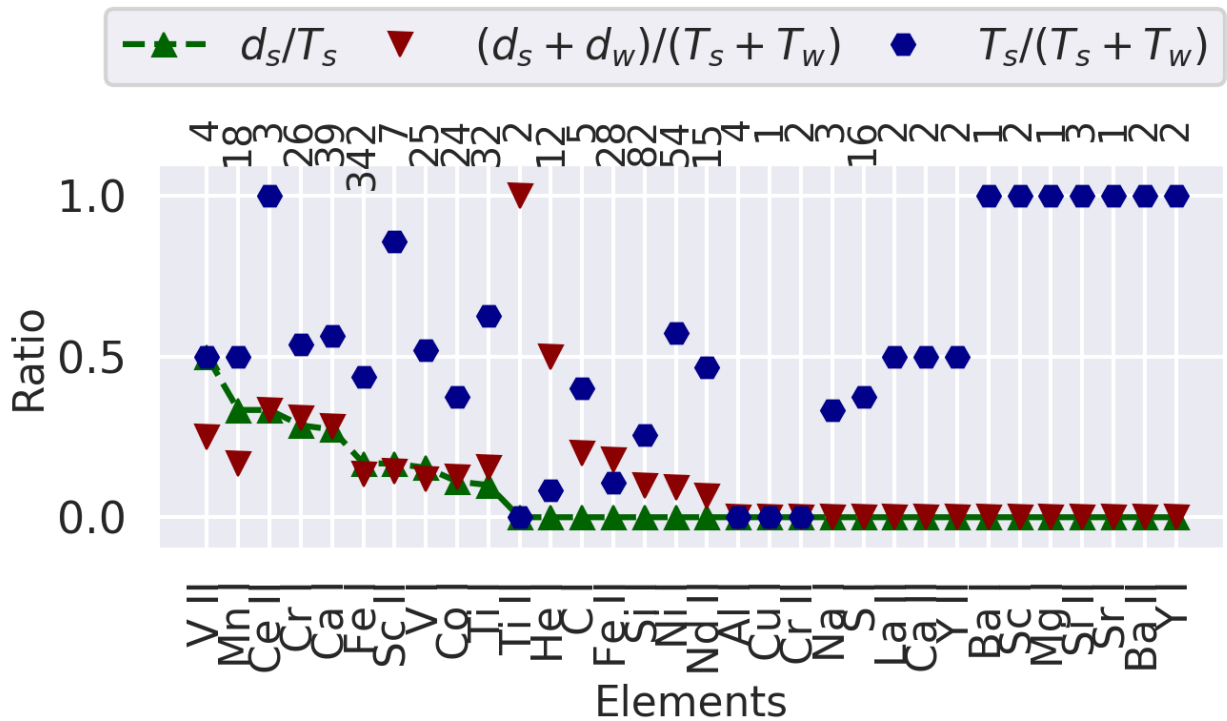


Figure B.1: Summary for elements on band 0.75

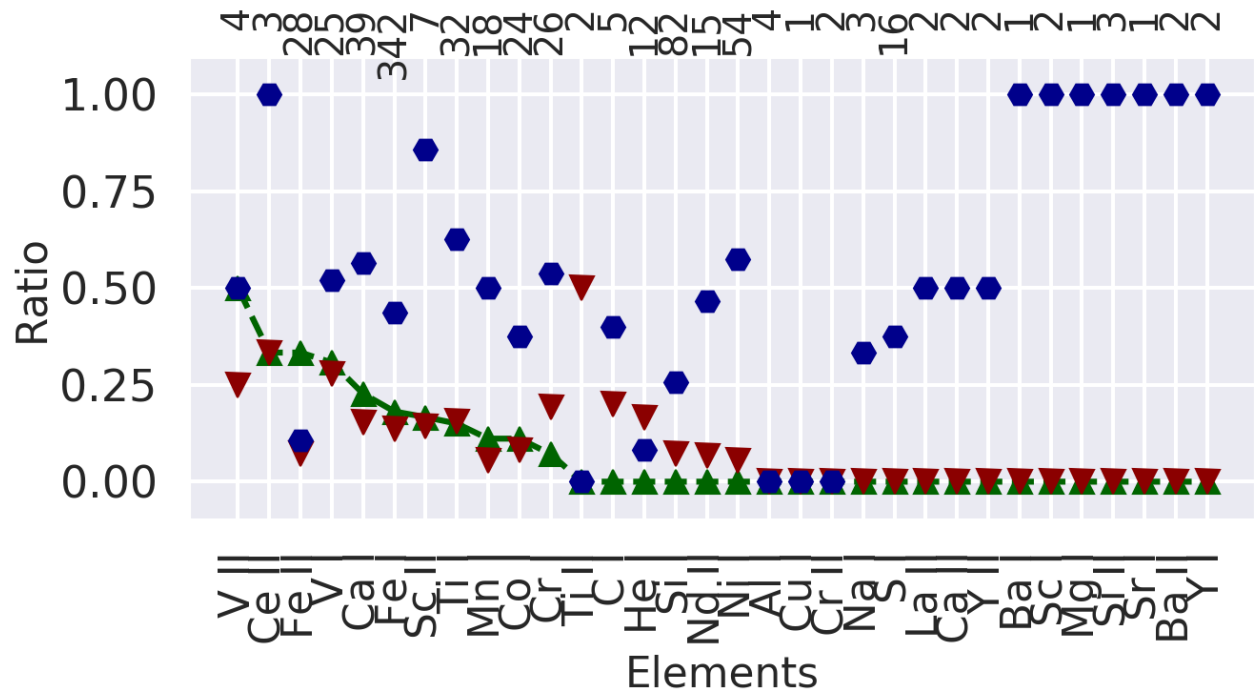


Figure B.2: Summary for elements on band 1.0

B.2. Algorithm parameters:

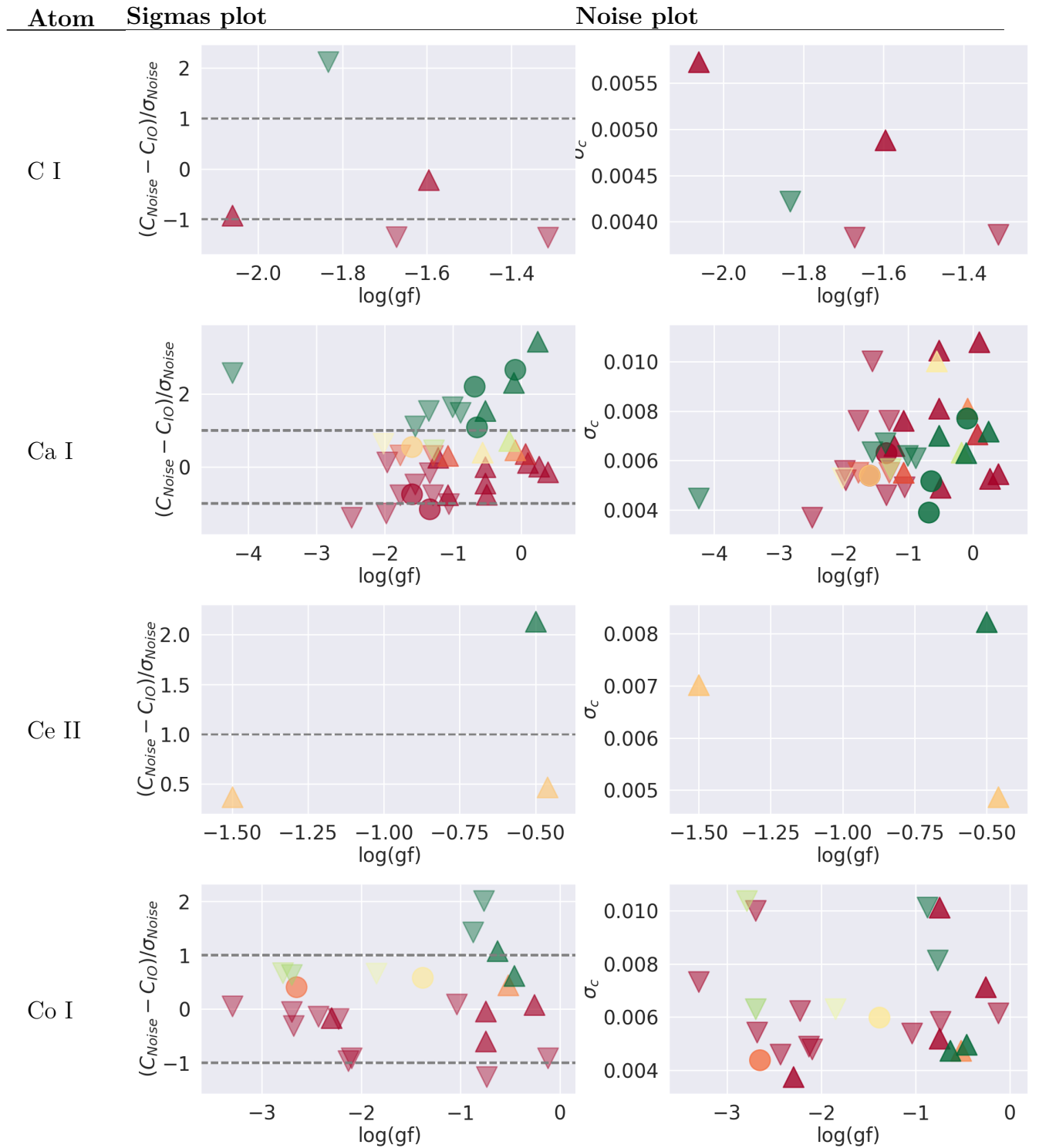
Parameter name	Value
N_pixs	700
N_shifts	2500
cut_order	100
delta_max_shift	1
dlt_epochs	0
do_1stdopp	False
doppler_pixs	500
dtransit	0.127951389
error_gain	1.6
general_warnings	nan
in_epochs	17
indexFWHM	10
interpolate_ref	True
merge_epoch_as	
n_binning	3
n_epoch_merge	0
n_epochs	29
near_indline	20
near_tolerance	0.001
norm_high	3
norm_min_pixs	1
norm_polyorder	3
norm_width	5
normalize_hists	False
orders	22
orders_length	0.01832280506588094
period	3.52474859
radial_velocity	0
redf_loops	3000
redfield_bins	50
renorm_scale	1
smart_merge	True
t_start	52572.282646825275
t_transit	2452826.628521
telescope	subaru
tell_only_out	True
test_boundary	0.011
test_percent	0.7
test_pixs_near	15
test_times_near	10
test_var_amplitude	0.06
test_var_mu	0.06
time_average_corr	True
times_indline	2
wave_binning	0

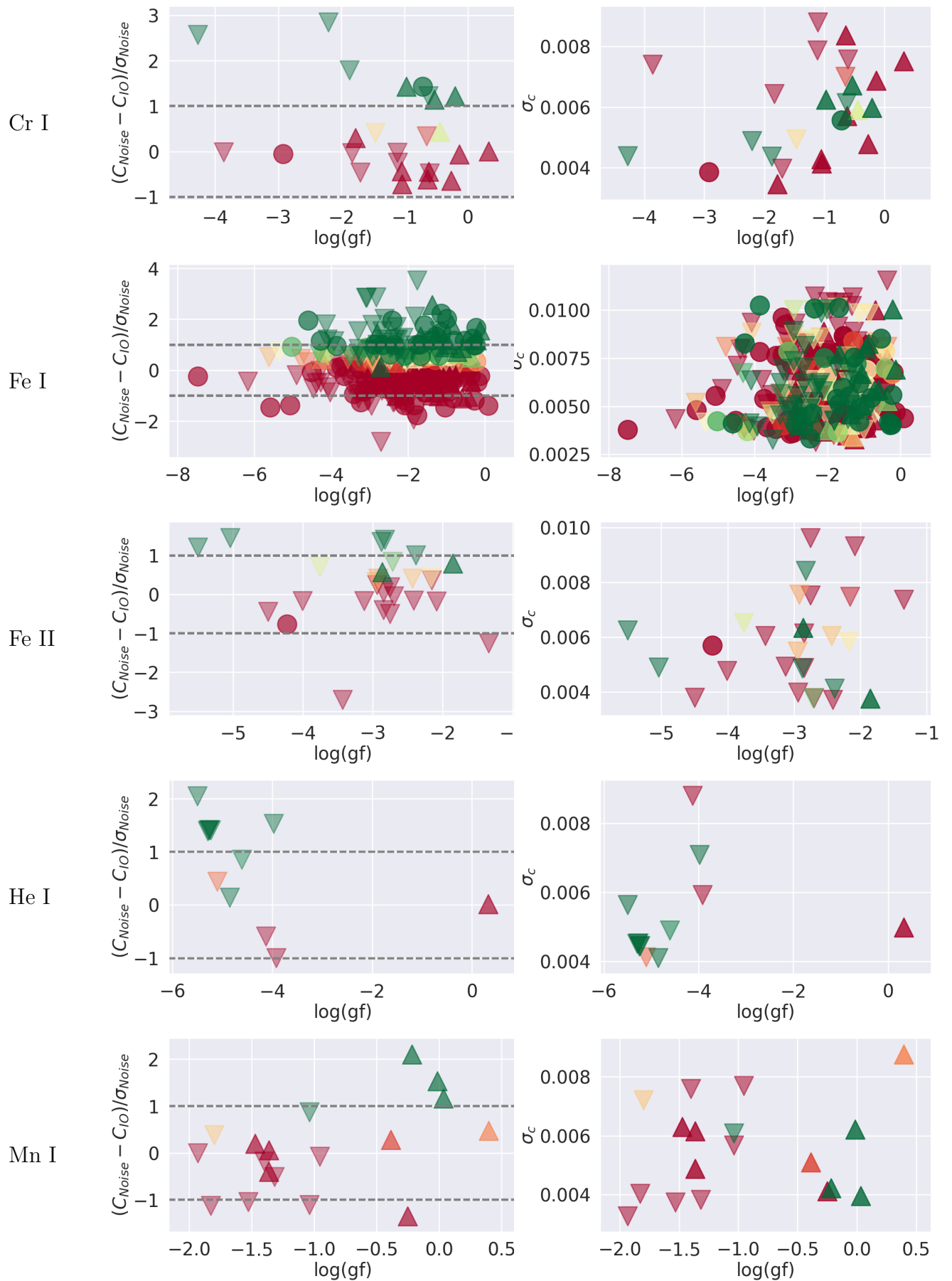
B.2.1. Object information:

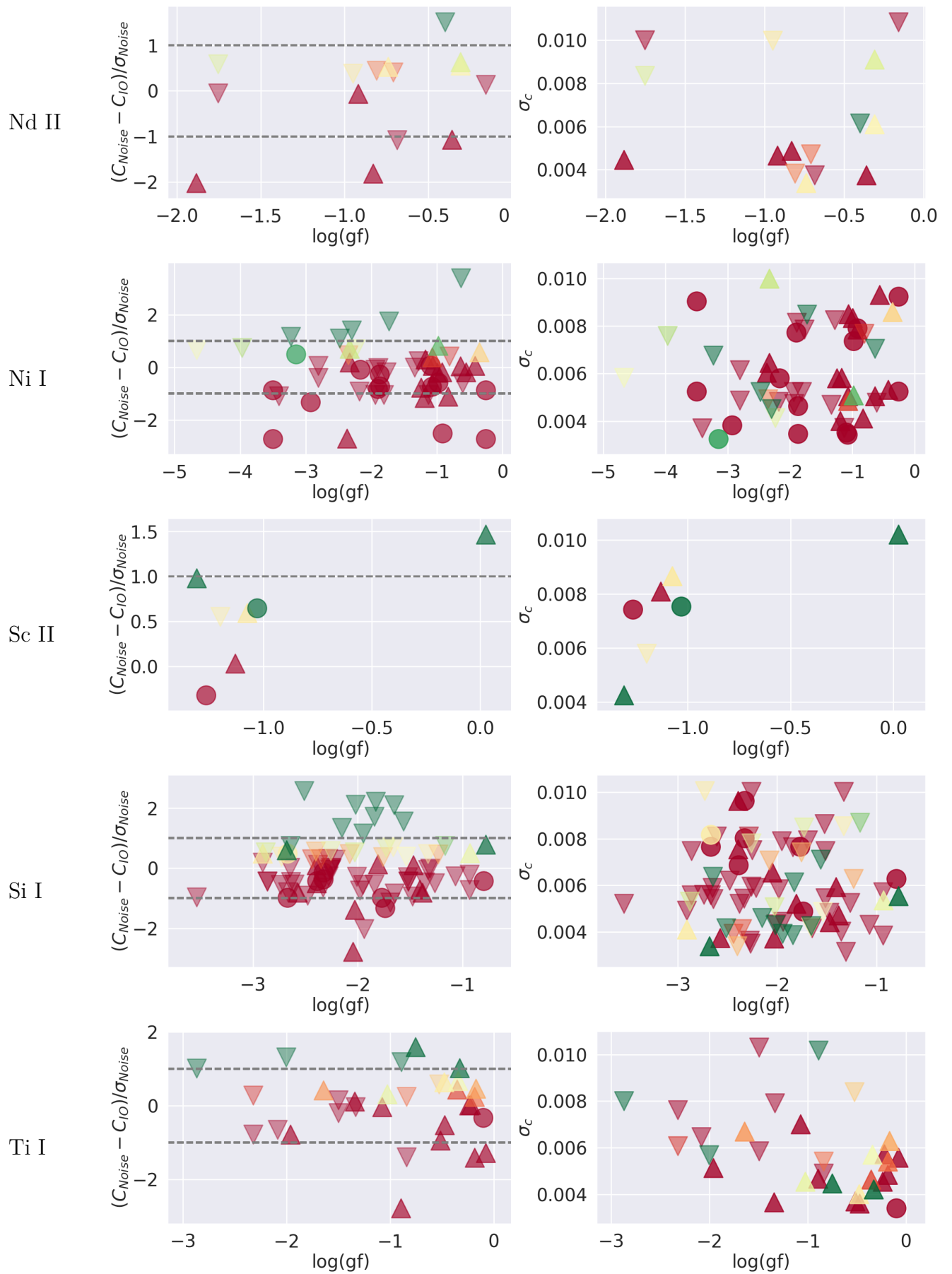
Parameter name	Value
TELESCOP	SUBARU
INSTRUME	HDS
OBJECT	HD209458
DATE	2011-11-09T00:48:21

B.3. Elements with detections

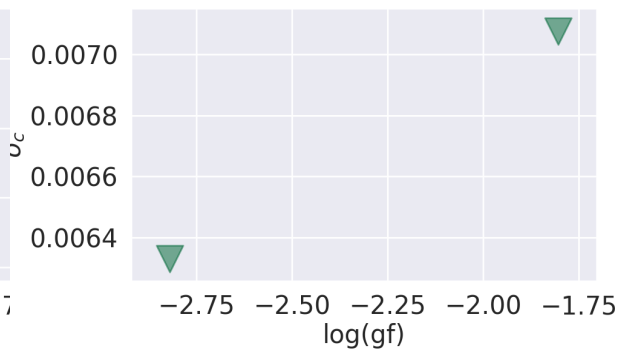
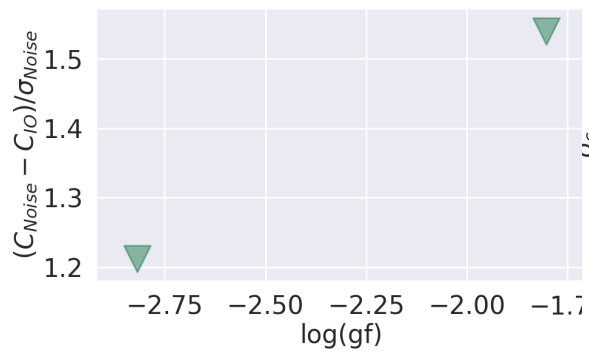
B.3.1. 0.75 angstrom band



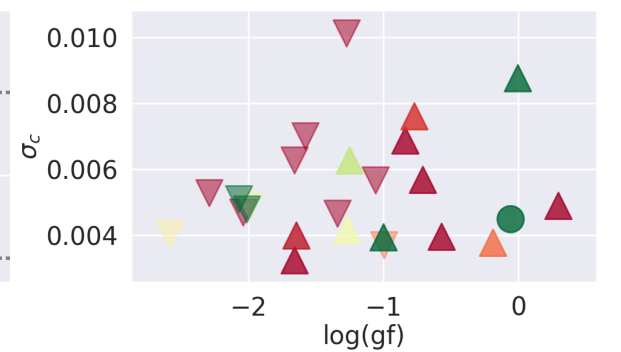
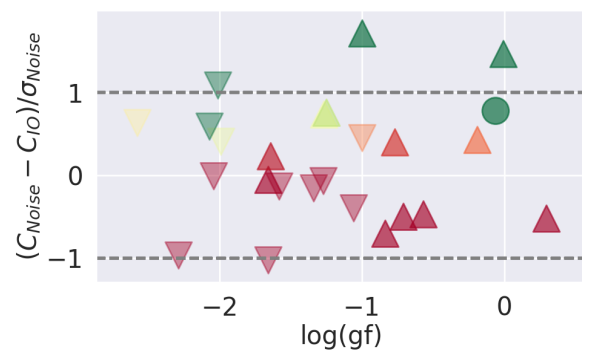




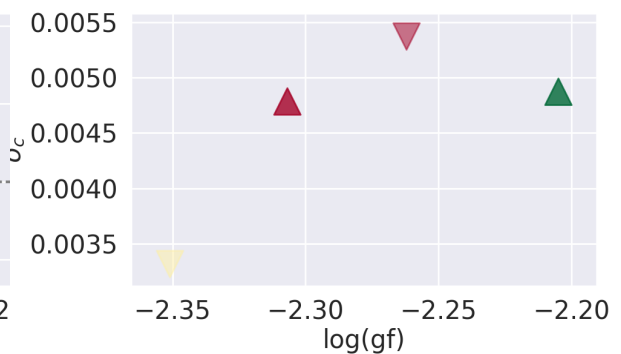
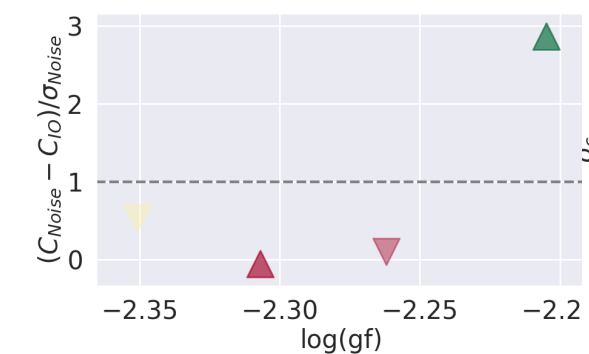
Ti II



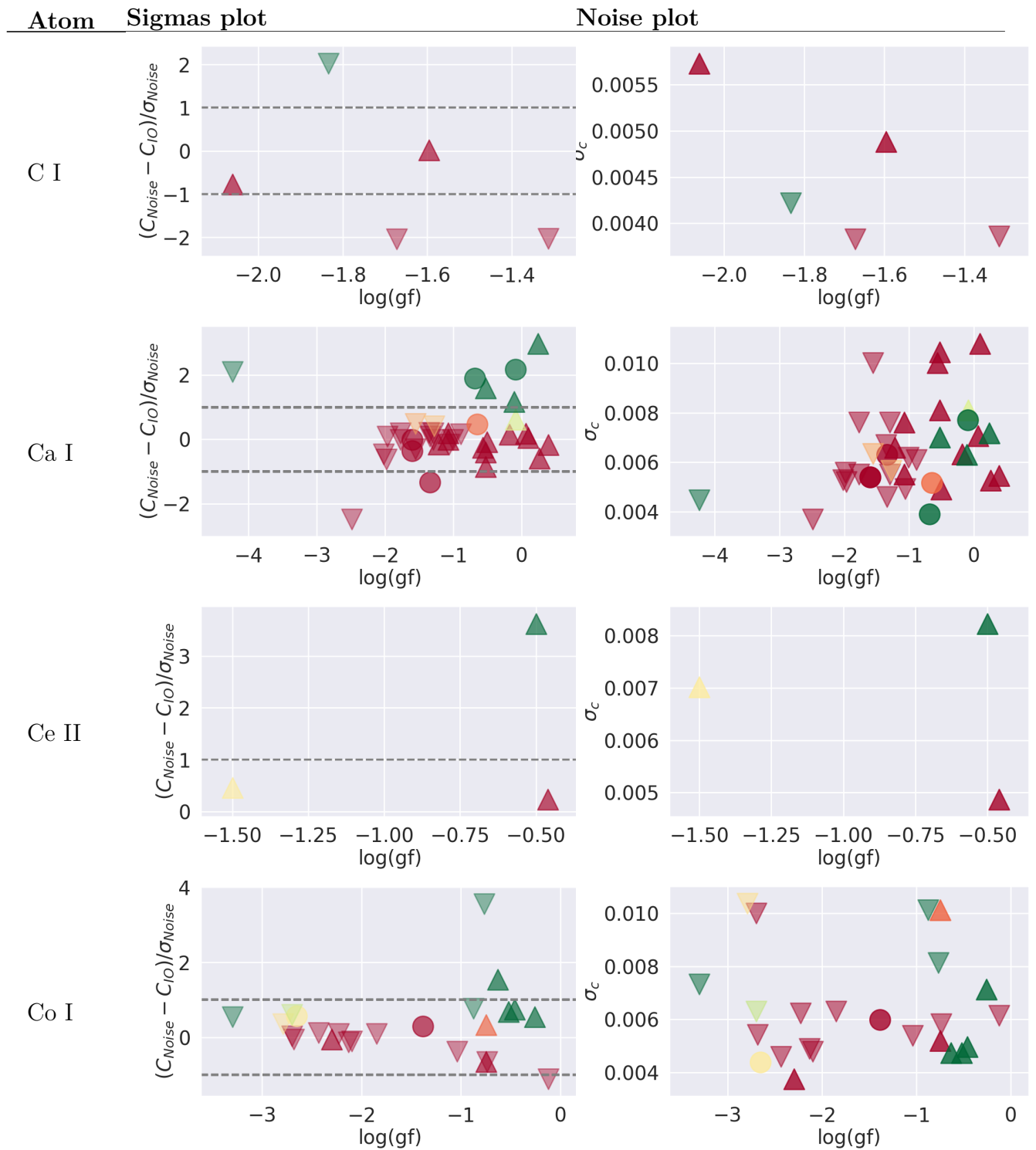
V I

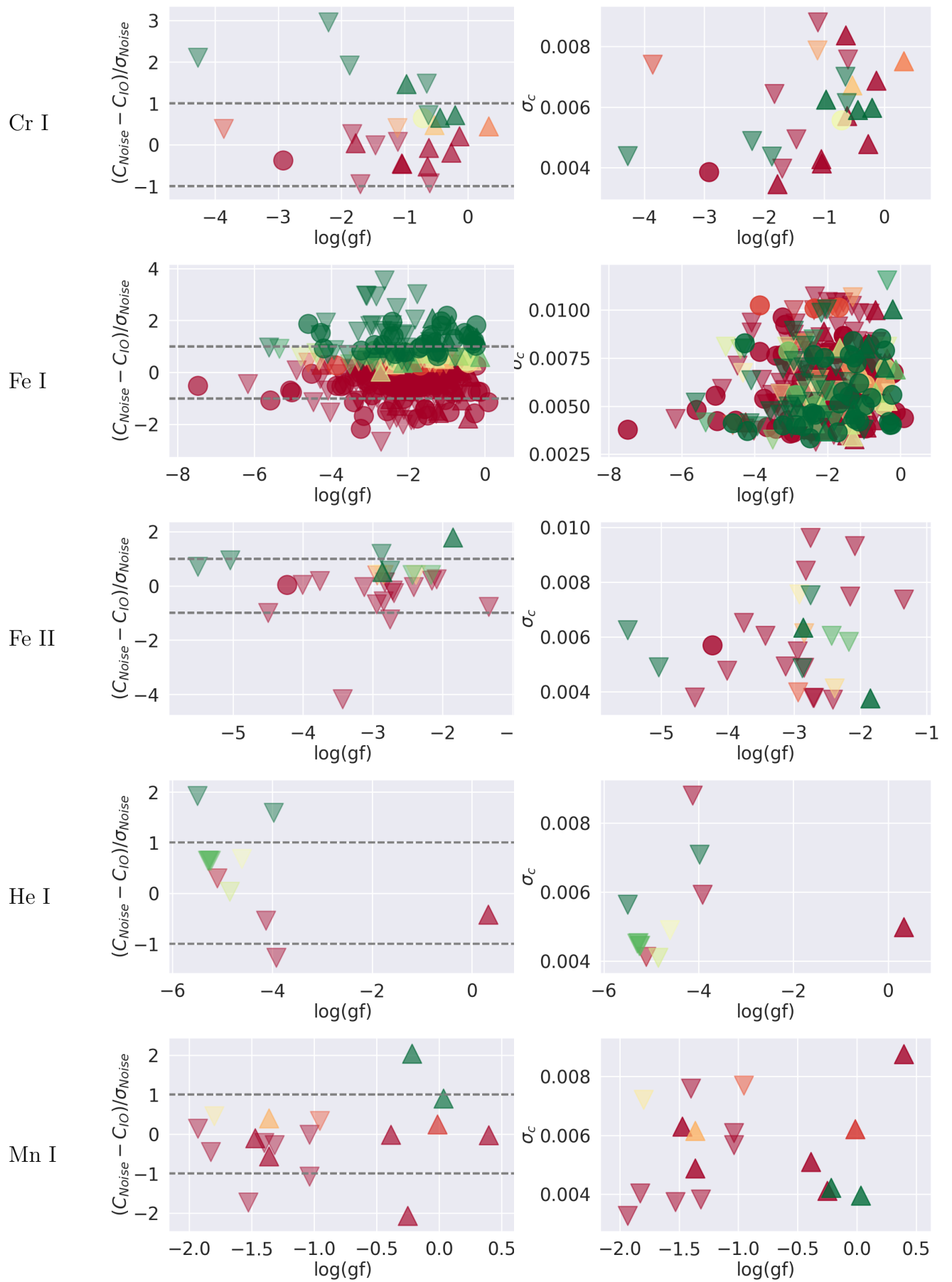


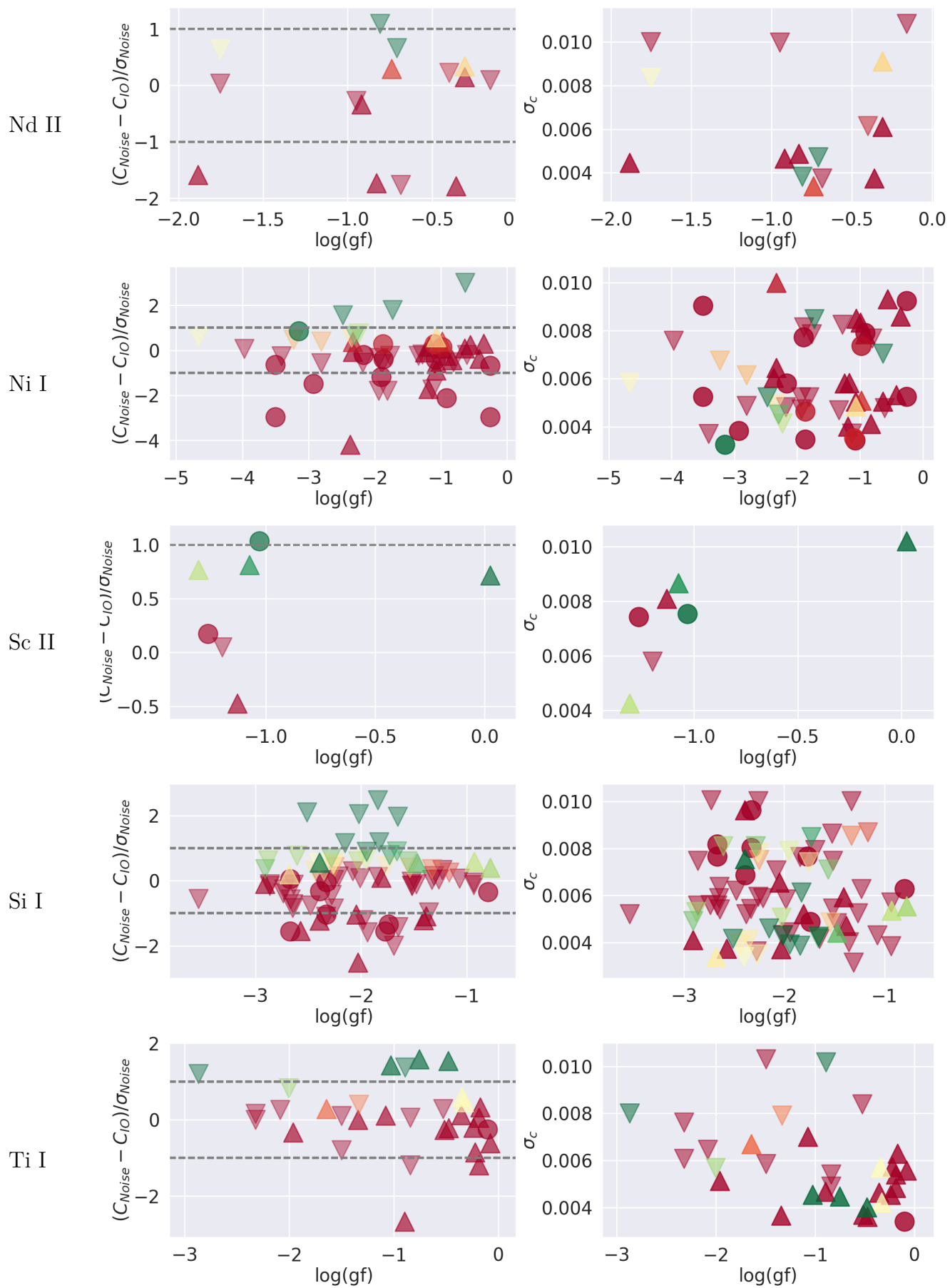
V II

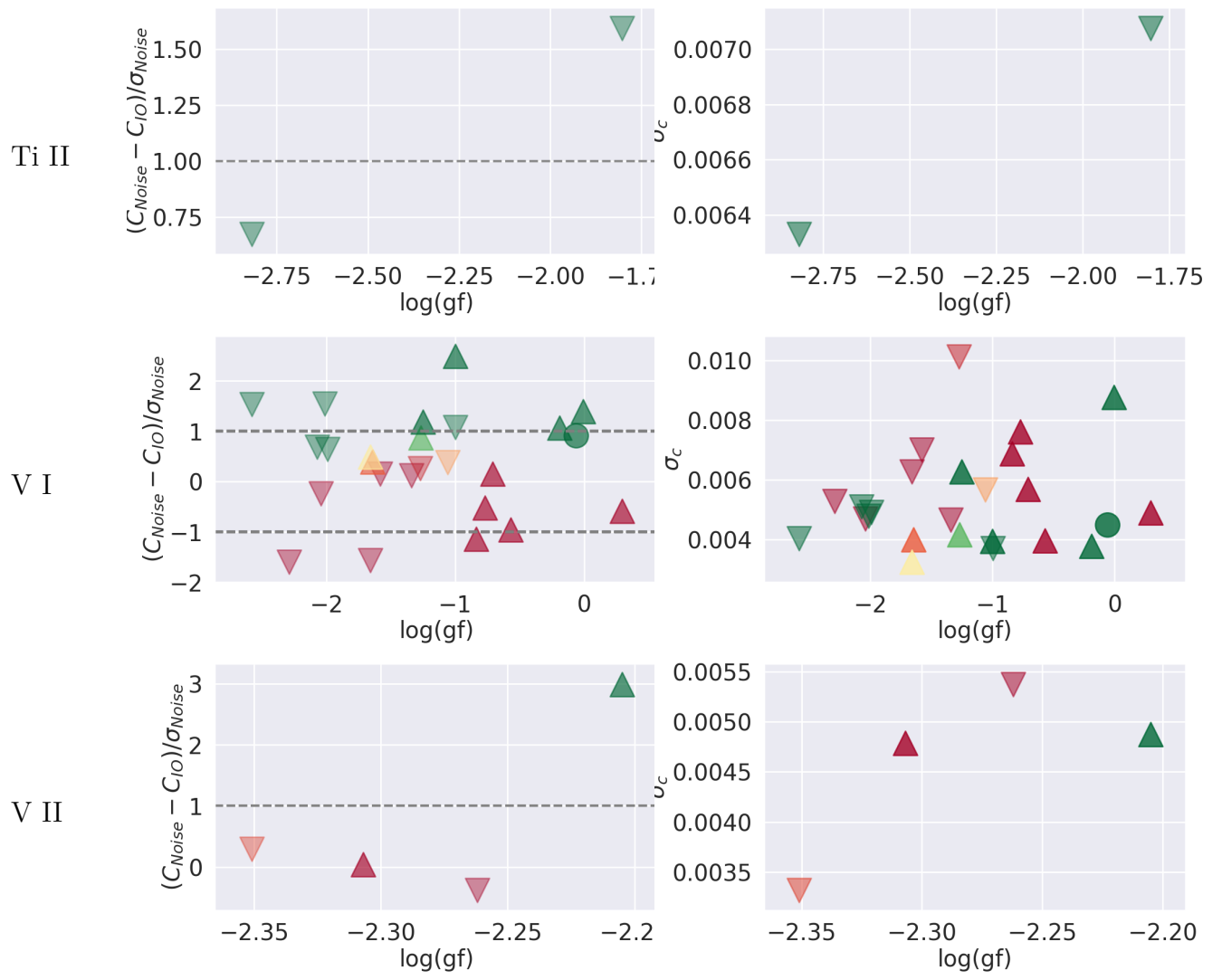


B.3.2. 1.0 angstrom band









B.4. Detected elements transitions

B.4.1. 0.75 angstrom band

Atom		$\lambda_{lab}(\lambda_{obs})$	log(gf)	normed depth	σ_{In-Out}	σ_{rel}	σ_c
C I	△	6587.61(.796)	-1.6	0.07	-0.58	-0.22	0.005
	△	5793.12(.214)	-2.06	0.2	-4.63	-0.92	0.006
Ca I	△	6439.075(.235)	0.39	0.58	-0.42	-0.14	0.005
	△	6462.567(.734)	0.26	0.59	0.07	0.01	0.005
	△	5857.451(.599)	0.24	0.52	10.63	3.43	0.007
	△	5594.462(.607)	0.1	0.57	0.67	0.12	0.011
	△	6318.109(.174)	0.06	0.41	1.12	0.36	0.007
	△	5598.48(.605)	-0.09	0.55	1.47	0.46	0.008
	○	6162.173(.331)	-0.09	0.63	10.9	2.67	0.008
	△	6493.781(.945)	-0.11	0.49	6.99	2.31	0.006
	△	5991.798(.513)	-0.18	0.18	2.23	0.71	0.006
	△	6449.808(.968)	-0.5	0.42	-2.41	-0.76	0.005
Ce II	△	5601.277(.404)	-0.52	0.46	-2.34	-0.46	0.008
	△	5975.818(.502)	-0.46	0.2	1.7	0.47	0.005
	△	5637.358(.536)	-0.5	0.2	8.63	2.13	0.008
Co I	△	6343.963(4.294)	-1.5	0.23	1.68	0.37	0.007
	△	5984.252(3.817)	-0.26	0.3	0.44	0.08	0.007
	△	6232.383(.781)	-0.46	0.33	3.66	0.62	0.005
	△	6082.422(.856)	-0.52	0.12	1.5	0.45	0.005
	△	6257.047(6.506)	-0.63	0.37	3.57	1.08	0.005
	△	5546.965(.64)	-0.75	0.24	-0.14	-0.04	0.01
	△	5546.965(.631)	-0.75	0.24	-3.76	-0.6	0.005
○	5558.818(.902)	-1.38	0.0	1.85	0.59	0.006	

	△	6384.245(3.848)	-2.3	0.05	-0.54	-0.16	0.004
	○	6623.763(4.037)	-2.65	0.02	1.42	0.42	0.004
	△	5790.957(1.121)	0.32	0.36	0.03	0.01	0.008
	△	5787.918(8.06)	-0.13	0.19	-0.22	-0.06	0.007
	△	6218.951(9.439)	-0.21	0.37	5.74	1.22	0.006
	△	5694.731(5.12)	-0.27	0.18	-3.44	-0.64	0.005
Cr I	△	6214.144(3.583)	-0.44	0.35	2.18	0.43	0.006
	△	5553.549(.721)	-0.53	0.21	3.77	1.15	0.007
	△	5935.017(4.8)	-0.62	0.32	-1.69	-0.44	0.006
	△	5781.826(2.248)	-0.64	0.2	-2.34	-0.61	0.008
	○	6729.734(.228)	-0.71	0.03	4.4	1.44	0.006
	△	6715.473(.526)	-0.97	0.08	5.48	1.43	0.006
	△	6597.55(.737)	-1.04	0.17	-5.74	-0.71	0.004
	○	6024.049(.203)	0.09	0.44	-4.43	-1.39	0.004
	△	5862.357(.489)	-0.13	0.37	7.12	1.56	0.007
	○	5914.201(.3)	-0.13	0.47	-1.06	-0.23	0.005
	○	5984.815(.956)	-0.2	0.34	-2.97	-0.46	0.007
Fe I	△	5565.704(.833)	-0.21	0.39	3.5	1.18	0.01
	○	5930.173(.328)	-0.23	0.38	5.43	1.68	0.006
	○	5930.173(.313)	-0.23	0.37	1.51	0.36	0.007
	○	6419.942(0.103)	-0.24	0.34	4.74	0.99	0.004
	○	5633.946(4.072)	-0.27	0.31	-6.11	-1.19	0.005
	○	6020.17(.301)	-0.28	0.4	3.45	0.98	0.004
	○	6078.491(.625)	-0.32	0.32	3.9	1.25	0.004
	△	6482.204(.009)	-1.85	0.24	3.01	0.79	0.004
Fe II	△	5534.847(.959)	-2.87	0.34	4.73	0.57	0.006
	○	6369.462(.621)	-4.23	0.11	-2.42	-0.77	0.006

He I	△	6678.154(.152)	0.33	0.45	0.11	0.02	0.005	
	△	5573.682(.014)	0.4	0.55	1.47	0.47	0.009	
Mn I	△	6021.803(.937)	0.03	0.35	3.48	1.16	0.004	
	△	5718.233(7.97)	-0.01	0.28	5.47	1.54	0.006	
	△	6016.673(.776)	-0.22	0.34	6.4	2.11	0.004	
	△	6013.513(.63)	-0.25	0.29	-6.42	-1.35	0.004	
	△	5738.261(.357)	-0.39	0.05	1.24	0.28	0.005	
	△	6586.304(.472)	-1.36	0.13	0.2	0.06	0.006	
	△	6586.304(.469)	-1.36	0.14	-1.59	-0.4	0.005	
	△	5557.684(8.086)	-1.48	0.24	0.59	0.2	0.006	
	Nd II	△	5668.857(9.17)	-0.31	0.19	1.94	0.56	0.006
		△	5688.518(.348)	-0.31	0.48	2.16	0.64	0.009
△		6385.19(4.822)	-0.36	0.08	-3.28	-1.07	0.004	
△		6031.27(.161)	-0.74	0.02	1.91	0.53	0.003	
△		5742.087(1.99)	-0.83	0.13	-	-1.81	0.005	
△		6183.897(.731)	-0.92	0.05	-0.19	-0.06	0.005	
△		6514.959(.766)	-1.88	0.05	-6.38	-2.02	0.004	
Ni I	○	6176.807(.968)	-0.26	0.26	-2.8	-0.87	0.009	
	○	6176.807(.969)	-0.26	0.25	-	-2.71	0.005	
	△	5715.066(.211)	-0.35	0.3	11.29	0.58	0.009	
	△	6086.276(.434)	-0.42	0.17	1.75	0.06	0.005	
	△	6175.36(.522)	-0.56	0.2	0.2	-0.18	0.005	
	△	5805.213(.356)	-0.64	0.16	-0.57	0.04	0.005	
	△	6378.247(.401)	-0.83	0.12	0.11	-1.11	0.004	
	○	6782.495(.348)	-0.92	0.04	-3.27	-2.51	0.008	
	△	6314.659(.807)	-0.92	0.28	-8.53	-0.19	0.008	
	○	6772.313(.469)	-0.98	0.17	-0.58	-0.57	0.007	

	△	6223.981(4.145)	-0.98	0.1	2.63	0.82	0.005
	△	5526.79(.936)	0.02	0.42	4.48	1.47	0.01
	○	6245.637(.761)	-1.03	0.17	3.69	0.65	0.008
Sc II	△	5684.202(.614)	-1.07	0.27	1.85	0.59	0.009
	△	5641.001(.118)	-1.13	0.21	0.13	0.03	0.008
	○	6279.753(.907)	-1.26	0.25	-1.36	-0.32	0.007
	△	6604.601(.741)	-1.31	0.17	3.05	0.98	0.004
	△	5948.541(.688)	-0.78	0.35	3.76	0.78	0.006
	○	6155.134(.287)	-0.8	0.32	-2.72	-0.43	0.006
	△	6254.188(.391)	-0.93	0.43	2.1	0.51	0.005
Si I	△	6152.292(1.765)	-1.38	0.19	-2.41	-0.81	0.005
	△	6518.129(.521)	-1.41	0.21	-2.13	-0.71	0.006
	△	6091.919(2.063)	-1.47	0.12	0.54	0.1	0.004
	○	6583.707(.873)	-1.74	0.05	-8.55	-1.32	0.005
	○	6243.815(.954)	-1.77	0.19	-3.66	-0.98	0.008
	△	6087.805(.959)	-1.81	0.07	0.62	0.14	0.005
	△	6509.068(.01)	-2.03	0.03	-5.61	-1.38	0.004
	△	5943.075(2.599)	-2.05	0.05	-	-2.77	0.007
	△	5877.657(.926)	-0.08	0.06	-3.98	-1.28	0.006
	○	6548.325(.66)	-0.1	0.04	-1.01	-0.33	0.003
	△	5675.41(.551)	-0.17	0.25	1.58	0.46	0.006
	△	5866.368(.592)	-0.19	0.17	-4.69	-1.41	0.005
Ti I	△	5866.368(.606)	-0.19	0.16	1.4	0.24	0.005
	△	6215.233(.288)	-0.22	0.25	0.08	0.02	0.006
	△	6258.706(.846)	-0.24	0.22	0.13	0.0	0.005
	△	5953.16(2.854)	-0.33	0.25	3.78	1.02	0.004
	△	6180.303(.359)	-0.34	0.21	2.05	0.67	0.006

	△	6258.102(.266)	-0.35	0.18	1.27	0.44	0.005
	△	5965.828(.976)	-0.47	0.09	-2.36	-0.52	0.004
	△	5807.085(6.861)	0.29	0.23	-1.69	-0.52	0.005
	△	5784.365(3.995)	-0.01	0.15	4.63	1.47	0.009
	○	6090.214(.375)	-0.06	0.09	3.91	0.78	0.004
	△	5727.048(.187)	-0.19	0.11	1.39	0.43	0.004
V I	△	5772.411(.286)	-0.57	0.23	-2.07	-0.47	0.004
	△	5624.596(.673)	-0.71	0.5	-2.1	-0.5	0.006
	△	6339.084(.017)	-0.77	0.17	1.19	0.4	0.008
	△	6358.817(.821)	-0.84	0.29	-2.19	-0.71	0.007
	△	6430.472(.997)	-1.0	0.43	6.04	1.72	0.004
	△	6216.354(.511)	-1.25	0.11	2.28	0.76	0.006
	△	6624.839(5.181)	-1.27	0.03	2.06	0.73	0.004
V II	△	5916.354(.399)	-2.21	0.22	8.97	2.87	0.005
	△	6083.81(4.236)	-2.31	0.12	-0.13	-0.05	0.005

B.4.2. 1.0 angstrom band

Atom		$\lambda_{lab}(\lambda_{obs})$	$\log(gf)$	normed depth	σ_{In-Out}	σ_{rel}	σ_c
C I	Δ	6587.61(.796)	-1.6	0.07	0.05	0.01	0.005
	Δ	5793.12(.214)	-2.06	0.2	-2.3	-0.77	0.006
Ca I	Δ	6439.075(.235)	0.39	0.58	-0.62	-0.17	0.005
	Δ	6462.567(.734)	0.26	0.59	-2.16	-0.58	0.005
	Δ	5857.451(.599)	0.24	0.52	10.72	2.98	0.007
	Δ	5594.462(.607)	0.1	0.57	0.47	0.05	0.011
	Δ	6318.109(.174)	0.06	0.41	0.54	0.18	0.007
	Δ	5598.48(.605)	-0.09	0.55	2.17	0.62	0.008
	\circ	6162.173(.331)	-0.09	0.63	10.93	2.17	0.008
	Δ	6493.781(.945)	-0.11	0.49	5.2	1.17	0.006
	Δ	5991.798(.513)	-0.18	0.18	0.45	0.15	0.006
	Δ	6449.808(.968)	-0.5	0.42	-0.17	-0.08	0.005
Ce II	Δ	5601.277(.404)	-0.52	0.46	-1.95	-0.41	0.008
	Δ	5975.818(.502)	-0.46	0.2	0.73	0.24	0.005
	Δ	5637.358(.536)	-0.5	0.2	11.33	3.63	0.008
Co I	Δ	6343.963(4.294)	-1.5	0.23	1.88	0.45	0.007
	Δ	5984.252(3.817)	-0.26	0.3	4.59	0.55	0.007
	Δ	6232.383(.781)	-0.46	0.33	3.66	0.74	0.005
	Δ	6082.422(.856)	-0.52	0.12	3.11	0.68	0.005
	Δ	6257.047(6.506)	-0.63	0.37	5.26	1.54	0.005
	Δ	5546.965(.64)	-0.75	0.24	1.37	0.33	0.01
	Δ	5546.965(.631)	-0.75	0.24	-3.85	-0.65	0.005
	\circ	5558.818(.902)	-1.38	0.0	0.93	0.3	0.006
	Δ	6384.245(3.848)	-2.3	0.05	-0.19	-0.06	0.004

	○	6623.763(4.037)	-2.65	0.02	1.87	0.57	0.004
	△	5790.957(1.121)	0.32	0.36	1.45	0.44	0.008
	△	5787.918(8.06)	-0.13	0.19	0.73	0.21	0.007
	△	6218.951(9.439)	-0.21	0.37	4.31	0.72	0.006
	△	5694.731(5.12)	-0.27	0.18	-0.99	-0.19	0.005
Cr I	△	6214.144(3.583)	-0.44	0.35	5.52	0.65	0.006
	△	5553.549(.721)	-0.53	0.21	1.69	0.48	0.007
	△	5935.017(4.8)	-0.62	0.32	-0.26	-0.07	0.006
	△	5781.826(2.248)	-0.64	0.2	-1.6	-0.52	0.008
	○	6729.734(.228)	-0.71	0.03	2.07	0.65	0.006
	△	6715.473(.526)	-0.97	0.08	6.92	1.47	0.006
	△	6597.55(.737)	-1.04	0.17	-2.74	-0.46	0.004
	○	6024.049(.203)	0.09	0.44	-3.51	-1.14	0.004
	△	5862.357(.489)	-0.13	0.37	2.63	0.61	0.007
	○	5914.201(.3)	-0.13	0.47	-2.66	-0.74	0.005
	○	5984.815(.956)	-0.2	0.34	-3.79	-0.72	0.007
Fe I	△	5565.704(.833)	-0.21	0.39	4.18	1.35	0.01
	○	5930.173(.328)	-0.23	0.38	7.45	1.82	0.006
	○	5930.173(.313)	-0.23	0.37	0.82	0.27	0.007
	○	6419.942(0.103)	-0.24	0.34	8.04	1.03	0.004
	○	5633.946(4.072)	-0.27	0.31	13.52	-1.58	0.005
	○	6020.17(.301)	-0.28	0.4	3.69	1.22	0.004
	○	6078.491(.625)	-0.32	0.32	3.65	1.11	0.004
	△	6482.204(.009)	-1.85	0.24	5.33	1.78	0.004
Fe II	△	5534.847(.959)	-2.87	0.34	4.1	0.51	0.006
	○	6369.462(.621)	-4.23	0.11	0.16	0.04	0.006
He I	△	6678.154(.152)	0.33	0.45	-2.55	-0.42	0.005

	△	5573.682(.014)	0.4	0.55	-0.09	-0.02	0.009
	△	6021.803(.937)	0.03	0.35	2.98	0.9	0.004
	△	5718.233(7.97)	-0.01	0.28	1.19	0.24	0.006
	△	6016.673(.776)	-0.22	0.34	7.68	2.03	0.004
Mn I	△	6013.513(.63)	-0.25	0.29	-9.28	-2.06	0.004
	△	5738.261(.357)	-0.39	0.05	-0.09	-0.01	0.005
	△	6586.304(.472)	-1.36	0.13	1.62	0.4	0.006
	△	6586.304(.469)	-1.36	0.14	-2.16	-0.56	0.005
	△	5557.684(8.086)	-1.48	0.24	-0.23	-0.1	0.006
	△	5688.518(.348)	-0.31	0.48	1.76	0.34	0.009
	△	5668.857(9.17)	-0.31	0.19	0.81	0.15	0.006
	△	6385.19(4.822)	-0.36	0.08	-5.83	-1.78	0.004
Nd II	△	6031.27(.161)	-0.74	0.02	1.23	0.29	0.003
	△	5742.087(1.99)	-0.83	0.13	-	-1.73	0.005
	△	6183.897(.731)	-0.92	0.05	-0.89	-0.34	0.005
	△	6514.959(.766)	-1.88	0.05	-4.82	-1.59	0.004
	○	6176.807(.968)	-0.26	0.26	-2.98	-0.68	0.009
	○	6176.807(.969)	-0.26	0.25	-	-2.96	0.005
	△	5715.066(.211)	-0.35	0.3	13.57	0.29	0.009
	△	6086.276(.434)	-0.42	0.17	0.87	-0.38	0.005
Ni I	△	6175.36(.522)	-0.56	0.2	-1.77	0.25	0.009
	△	5805.213(.356)	-0.64	0.16	0.66	0.08	0.005
	△	6378.247(.401)	-0.83	0.12	0.29	-0.44	0.004
	○	6782.495(.348)	-0.92	0.04	-1.85	-2.11	0.008
	△	6314.659(.807)	-0.92	0.28	-7.79	-0.24	0.008
	△	6223.981(4.145)	-0.98	0.1	-0.77	0.39	0.005
	○	6772.313(.469)	-0.98	0.17	1.18	0.14	0.007

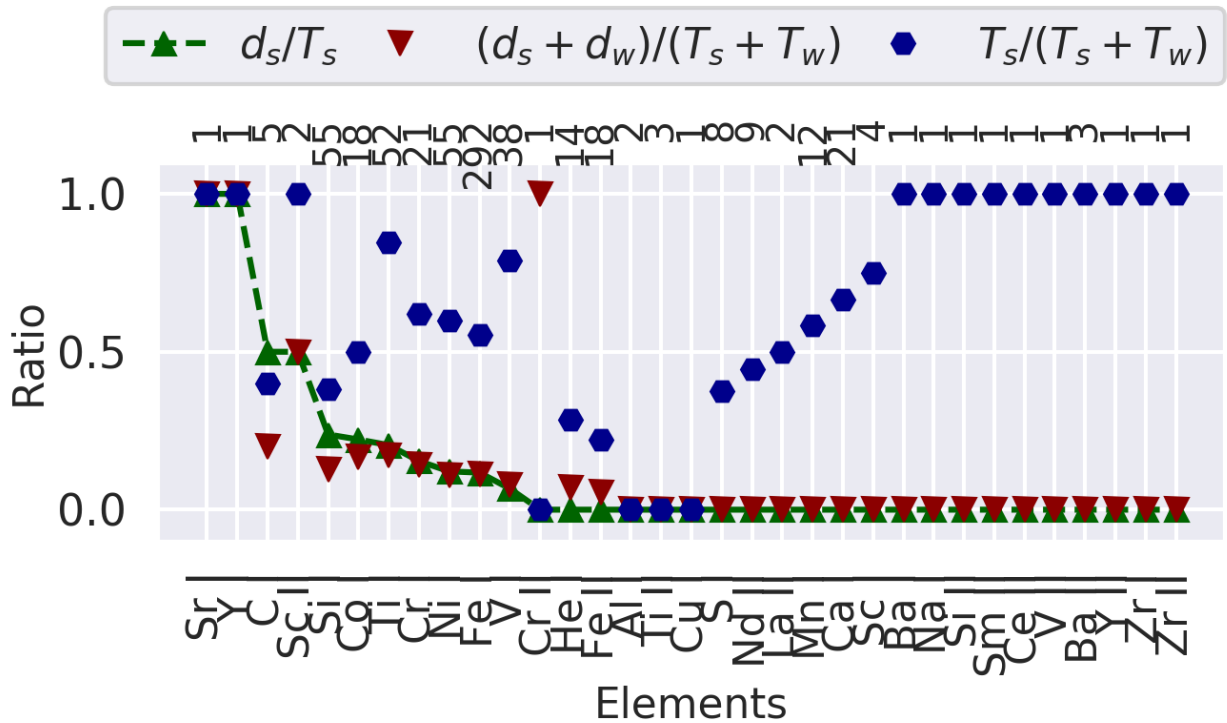
Sc II	△	5526.79(.936)	0.02	0.42	3.09	0.72	0.01
	○	6245.637(.761)	-1.03	0.17	8.32	1.04	0.008
	△	5684.202(.614)	-1.07	0.27	2.83	0.81	0.009
	△	5641.001(.118)	-1.13	0.21	-2.41	-0.47	0.008
	○	6279.753(.907)	-1.26	0.25	0.86	0.17	0.007
	△	6604.601(.741)	-1.31	0.17	2.31	0.77	0.004
Si I	△	5948.541(.688)	-0.78	0.35	2.39	0.4	0.006
	○	6155.134(.287)	-0.8	0.32	-3.85	-0.35	0.006
	△	6254.188(.391)	-0.93	0.43	2.29	0.58	0.005
	△	6152.292(1.765)	-1.38	0.19	-4.02	-1.09	0.005
	△	6518.129(.521)	-1.41	0.21	-3.75	-1.2	0.006
	△	6091.919(2.063)	-1.47	0.12	2.62	0.55	0.004
	○	6583.707(.873)	-1.74	0.05	-	-1.34	0.005
	○	6243.815(.954)	-1.77	0.19	-4.95	-1.56	0.008
	△	6087.805(.959)	-1.81	0.07	0.45	0.09	0.005
	△	6509.068(.01)	-2.03	0.03	-9.74	-2.5	0.004
△	5943.075(2.599)	-2.05	0.05	-3.25	-1.04	0.007	
Ti I	△	5877.657(.926)	-0.08	0.06	-2.72	-0.61	0.006
	○	6548.325(.66)	-0.1	0.04	-0.66	-0.26	0.003
	△	5675.41(.551)	-0.17	0.25	0.93	0.33	0.006
	△	5866.368(.606)	-0.19	0.16	0.29	0.05	0.005
	△	5866.368(.592)	-0.19	0.17	-3.97	-1.19	0.005
	△	6215.233(.288)	-0.22	0.25	-4.09	-0.85	0.006
	△	6258.706(.846)	-0.24	0.22	-0.54	-0.21	0.005
	△	5953.16(2.854)	-0.33	0.25	1.97	0.46	0.004
	△	6180.303(.359)	-0.34	0.21	1.98	0.6	0.006
△	6258.102(.266)	-0.35	0.18	0.36	0.12	0.005	

	△	5965.828(.976)	-0.47	0.09	-1.37	-0.22	0.004
	△	5807.085(6.861)	0.29	0.23	-1.79	-0.58	0.005
	△	5784.365(3.995)	-0.01	0.15	5.52	1.39	0.009
	○	6090.214(.375)	-0.06	0.09	3.96	0.92	0.004
	△	5727.048(.187)	-0.19	0.11	3.29	1.07	0.004
V I	△	5772.411(.286)	-0.57	0.23	-3.85	-0.96	0.004
	△	5624.596(.673)	-0.71	0.5	0.71	0.15	0.006
	△	6339.084(.017)	-0.77	0.17	-1.82	-0.52	0.008
	△	6358.817(.821)	-0.84	0.29	-3.92	-1.13	0.007
	△	6430.472(.997)	-1.0	0.43	8.1	2.49	0.004
	△	6216.354(.511)	-1.25	0.11	4.54	1.18	0.006
	△	6624.839(5.181)	-1.27	0.03	2.63	0.87	0.004
V II	△	5916.354(.399)	-2.21	0.22	12.48	2.99	0.005
	△	6083.81(4.236)	-2.31	0.12	0.29	0.04	0.005

Appendix C

HD 189733b extensive analysis (UVES dataset)

C.1. Global element analysis



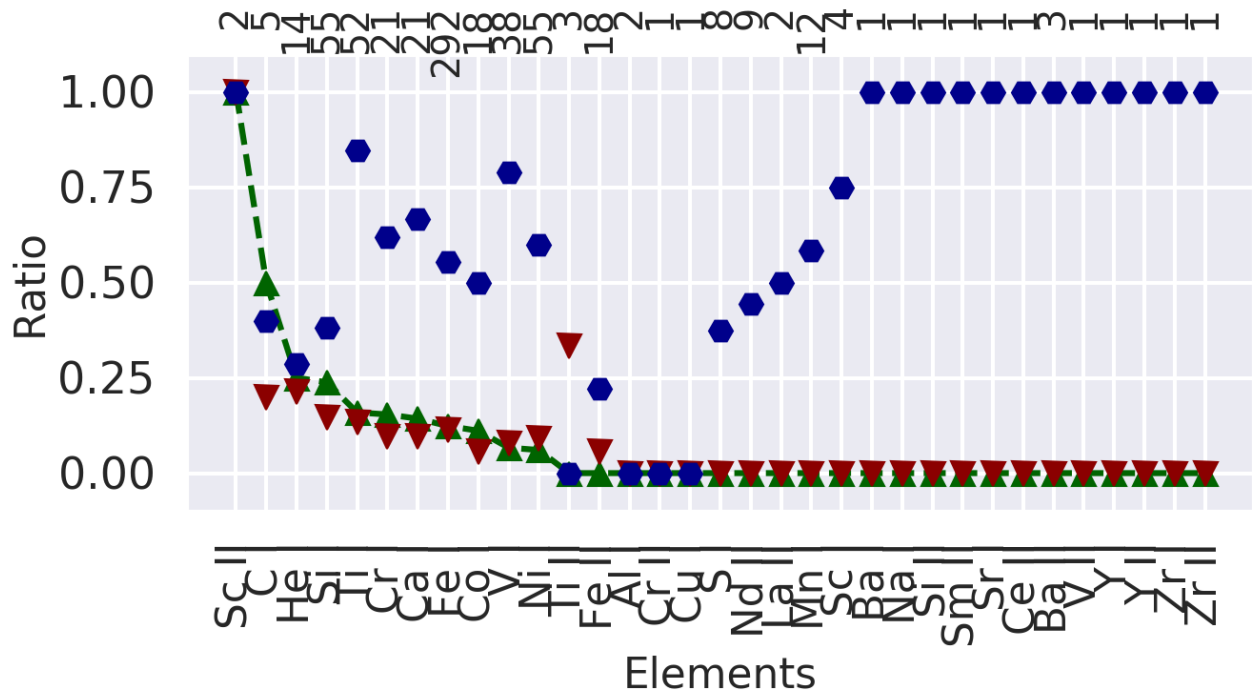


Figure C.2: Summary for elements on band 1.0

C.2. Algorithm parameters:

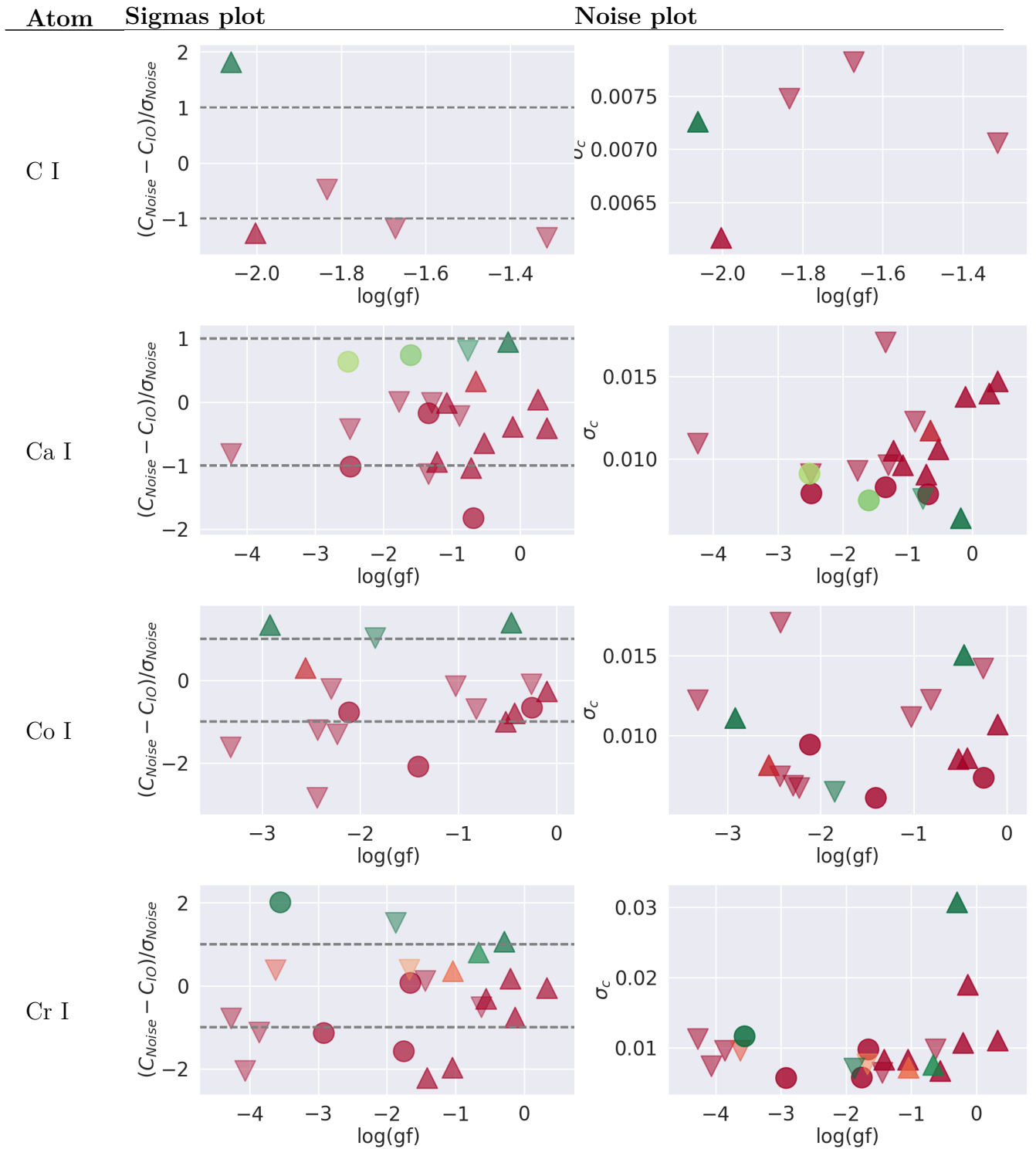
Parameter name	Value
N_FWHM	30
N_pixs	180
N_shifts	2500
cut_order	100
delta_max_shift	1
dlt_epochs	0
do_1stdopp	True
doppler_pixs	500
dtransit	0.07527
error_gain	1.36
general_warnings	indexFWHM and N_pixs changed due to wavelength binning
in_epochs	92
indexFWHM	6
interpolate_ref	True
merge_epoch_as	
n_binning	3
n_epoch_merge	4
n_epochs	244
near_incline	6
near_tolerance	0.001
norm_high	3
norm_min_pixs	1
norm_polyorder	3
norm_width	5
normalize_hists	False
orders	0
orders_length	0.020100829453440383
period	2.21857567
plot_time_binning	0
radial_velocity	-2.55
redf_loops	3000
redfield_bins	50
renorm_scale	1
smart_merge	True
t_start	56109.22400674862
t_transit	2454279.436714
telescope	uves
tell_only_out	True
test_boundary	0.021
test_percent	0.7
test_pixs_near	15
test_times_near	10
test_var_amplitude	0.06
test_var_mu	0.06
time_average_corr	True
times_incline	1
wave_binning	2

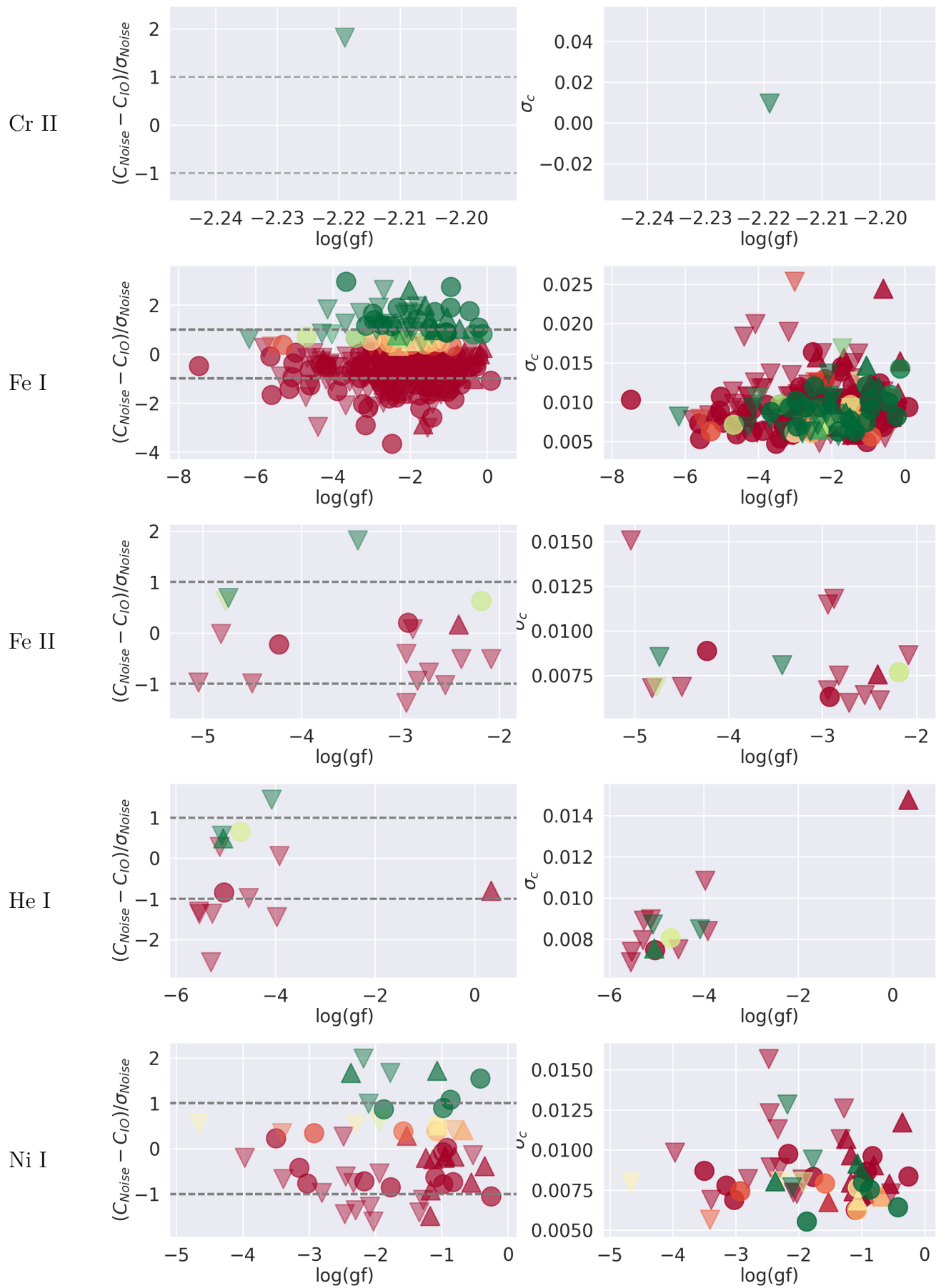
C.2.1. Object information:

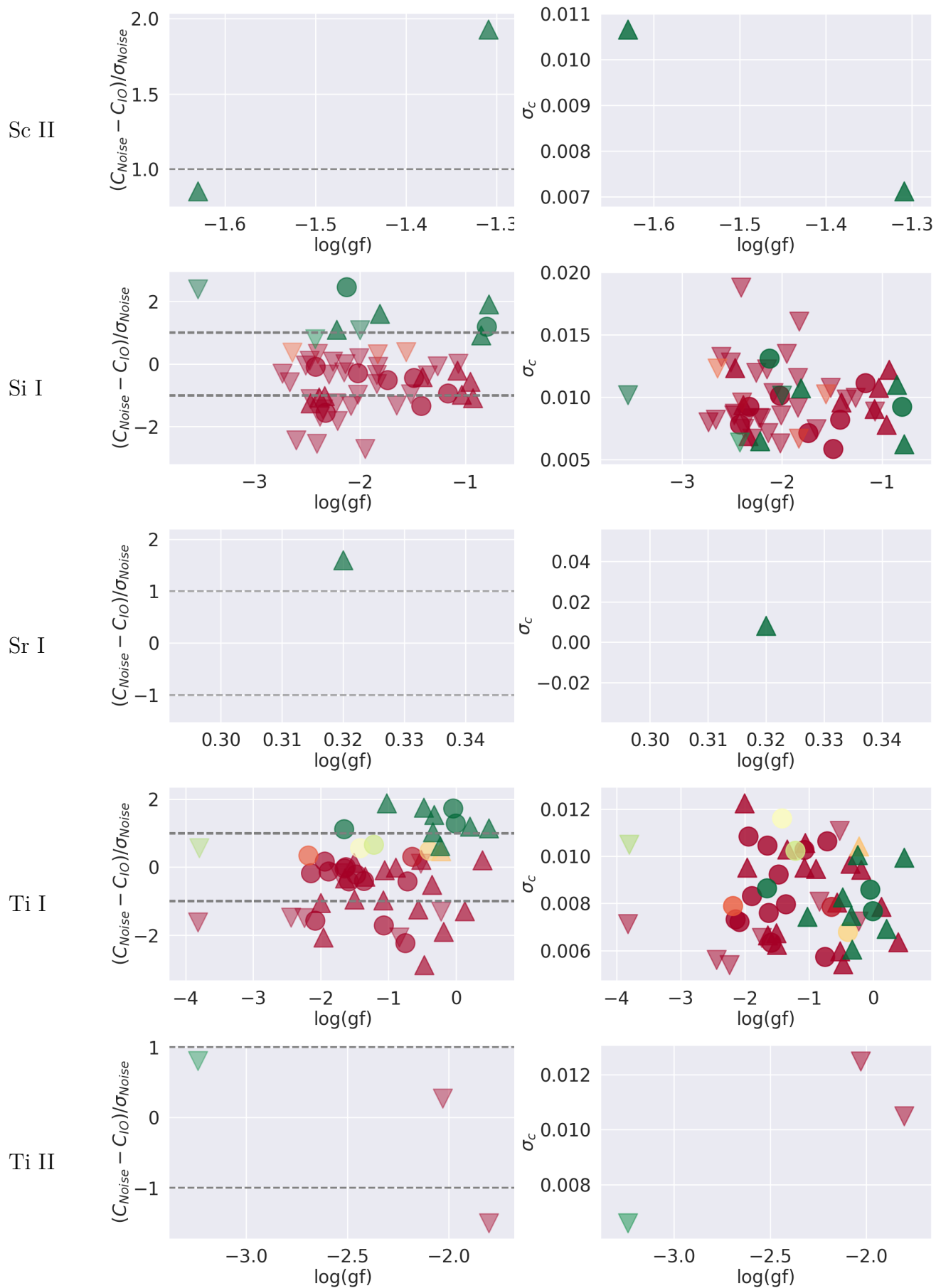
Parameter name	Value
TELESCOP	ESO-VLT-U2
INSTRUME	UVES
OBJECT	HD 189733
DATE	2013-05-23T09:55:11

C.3. Elements with detections

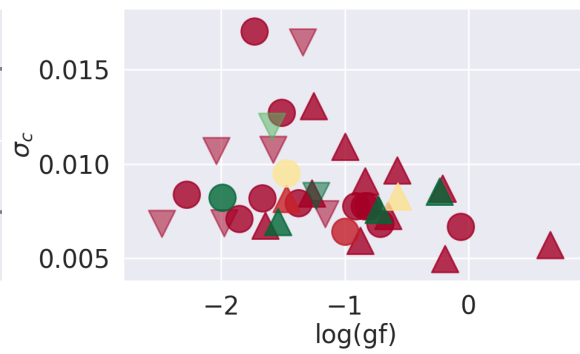
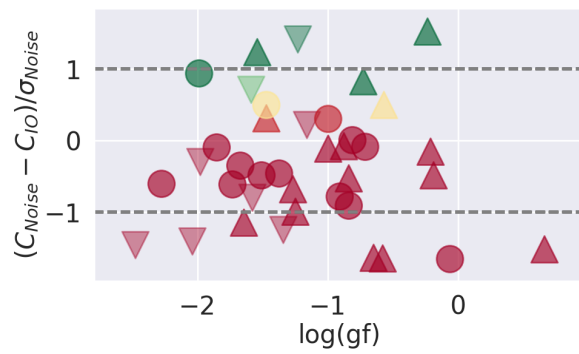
C.3.1. 0.75 angstrom band



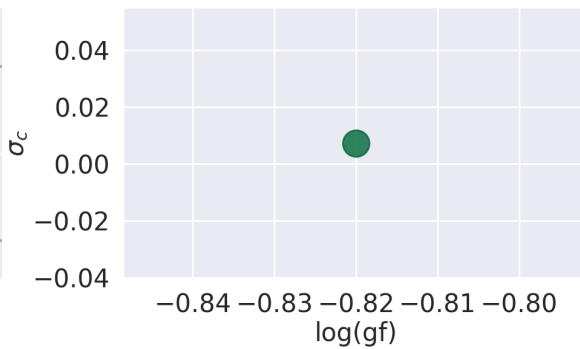
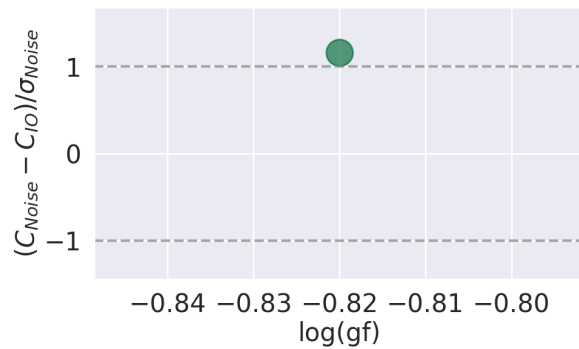




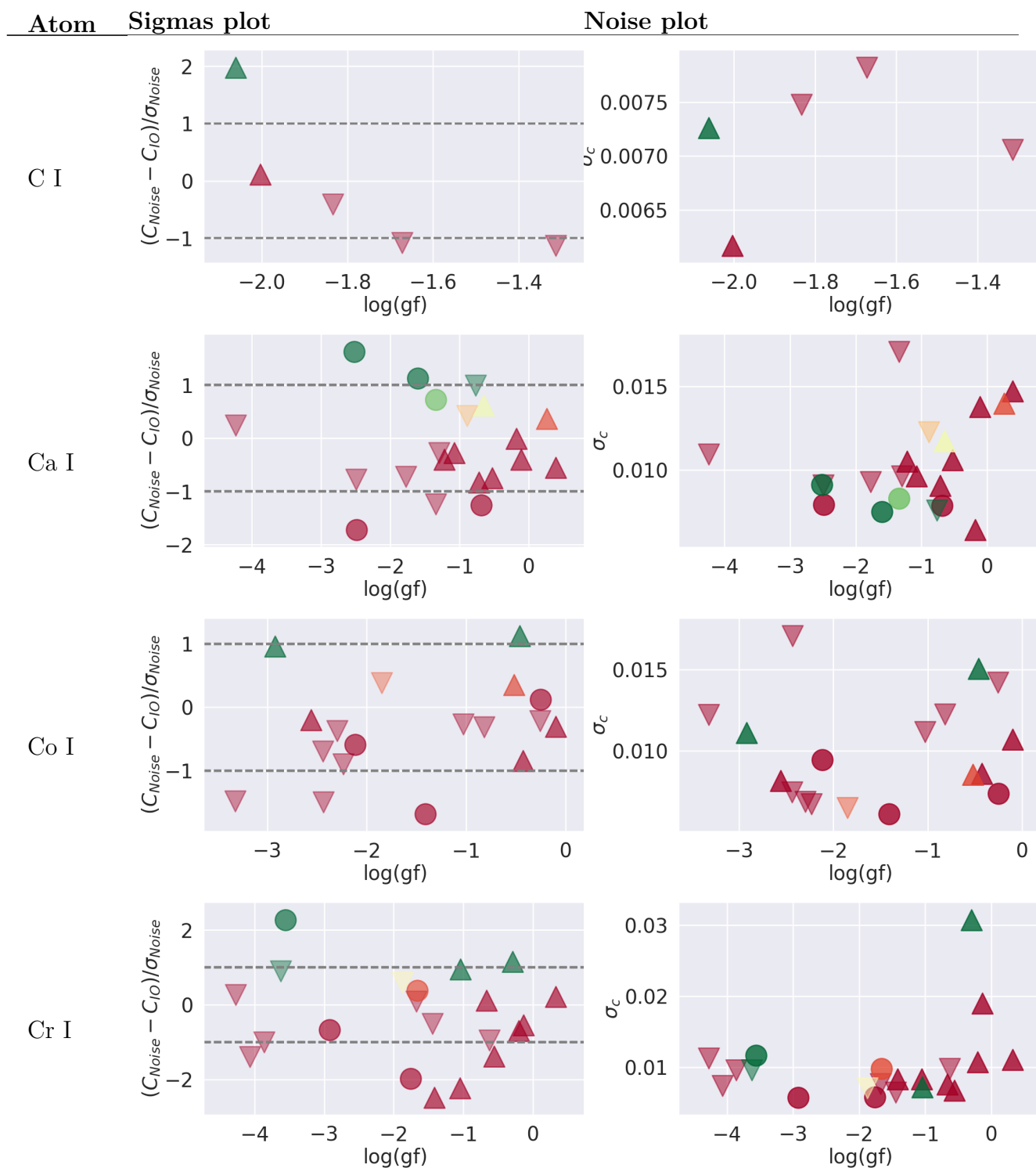
V I

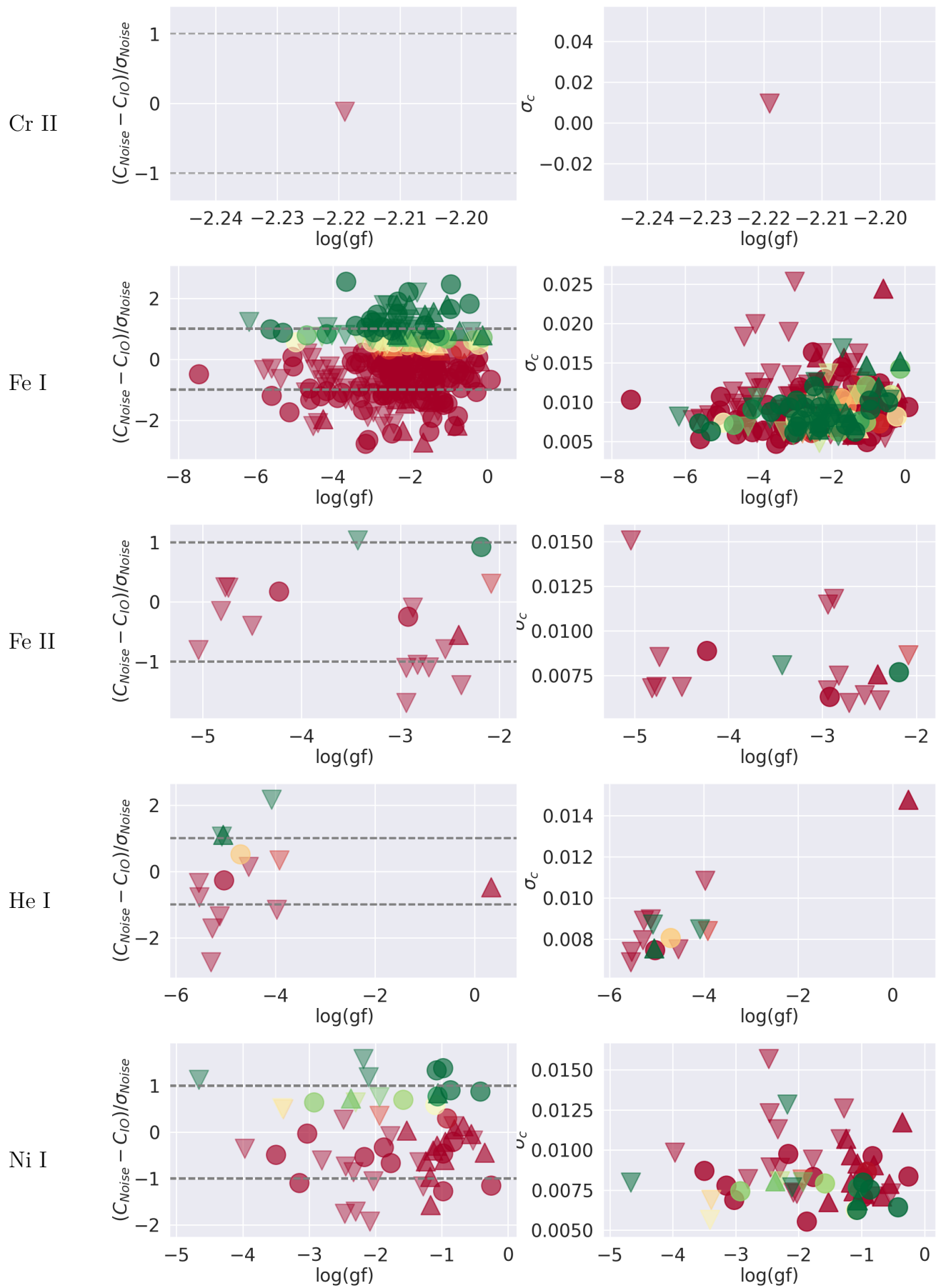


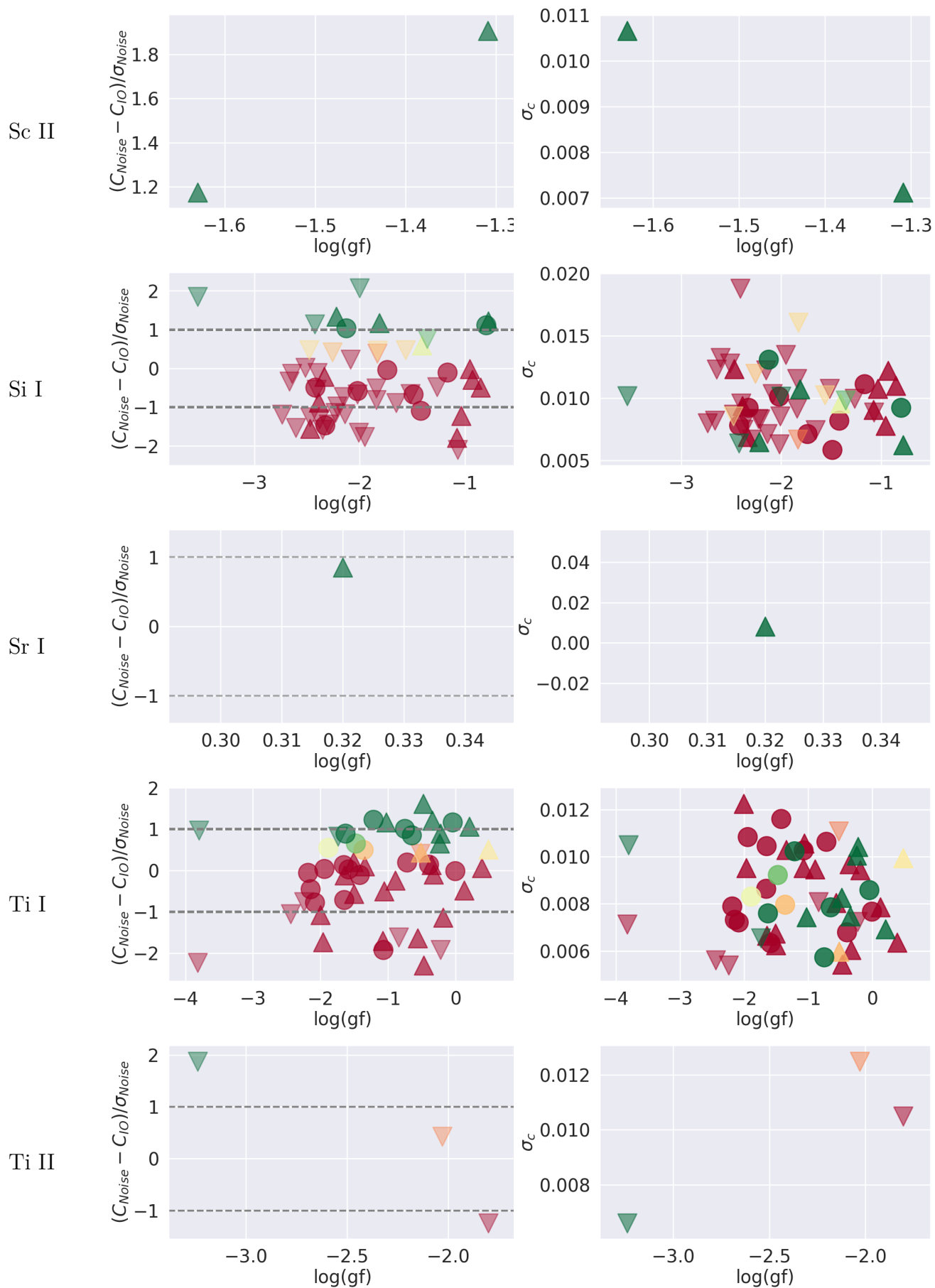
Y I



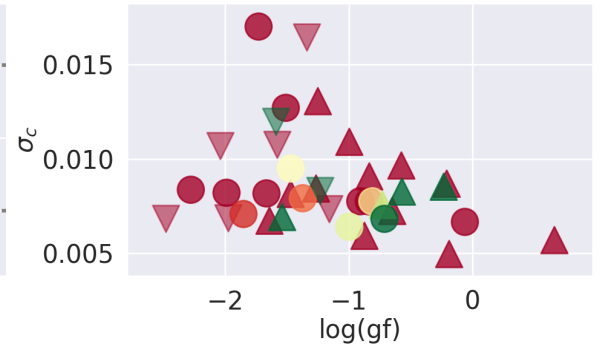
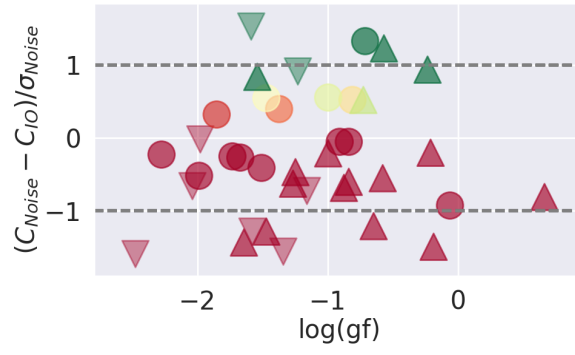
C.3.2. 1.0 angstrom band



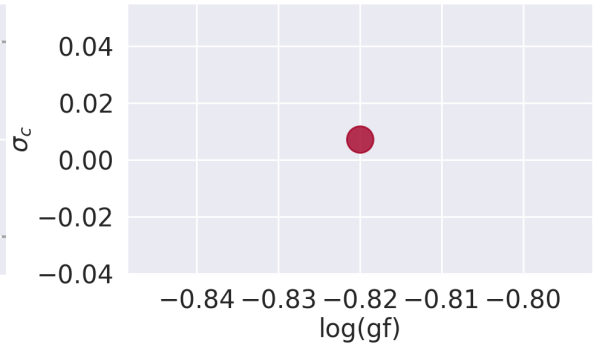
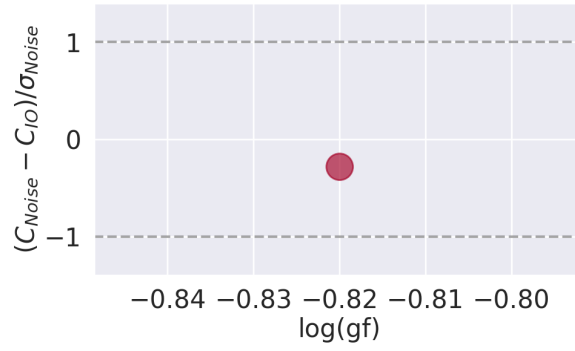




V I



Y I



C.4. Detected elements transitions

C.4.1. 0.75 angstrom band

Atom		$\lambda_{lab}(\lambda_{obs})$	log(gf)	normed depth	σ_{In-Out}	σ_{rel}	σ_c	
C I	△	6012.225(.011)	-2.0	0.25	-4.16	-1.25	0.006	
	△	5793.12(2.853)	-2.06	0.2	6.49	1.82	0.007	
Ca I	△	6439.075(8.827)	0.39	0.79	-1.45	-0.41	0.015	
	△	6462.567(.354)	0.26	0.78	0.09	0.04	0.014	
	△	6493.781(.564)	-0.11	0.7	-1.36	-0.38	0.014	
	△	5991.798(.685)	-0.18	0.14	3.29	0.94	0.006	
	△	6717.681(.434)	-0.52	0.63	-2.53	-0.64	0.011	
	△	6499.65(.402)	-0.65	0.62	1.09	0.33	0.012	
	○	6471.662(.444)	-0.69	0.64	-6.48	-1.82	0.008	
	△	6475.236(.401)	-0.72	0.44	-3.71	-1.03	0.009	
	△	5809.118(8.995)	-1.07	0.38	-0.04	-0.01	0.01	
	△	6360.298(.599)	-1.22	0.1	-3.22	-0.94	0.011	
	○	6455.598(.373)	-1.34	0.5	-0.56	-0.17	0.008	
	Co I	△	6007.677(.738)	-0.1	0.41	-0.96	-0.27	0.011
		○	6454.99(.775)	-0.25	0.11	-2.39	-0.66	0.007
△		6107.918(.875)	-0.43	0.47	-2.73	-0.8	0.009	
△		6232.383(.417)	-0.46	0.53	4.7	1.4	0.015	
△		6082.422(.52)	-0.52	0.35	-3.55	-1.0	0.009	
○		6444.675(.419)	-1.41	0.02	-7.0	-2.08	0.006	
○		6771.033(0.782)	-2.12	0.18	-2.64	-0.78	0.009	
△		6551.446(.448)	-2.56	0.12	1.13	0.3	0.008	
△		6129.094(8.764)	-2.92	0.25	4.62	1.34	0.011	
	△	5790.957(.761)	0.32	0.6	-0.23	-0.05	0.011	

	△	5787.918(.701)	-0.13	0.46	-2.72	-0.76	0.019
	△	6218.951(9.054)	-0.21	0.6	0.61	0.18	0.011
	△	5783.85(.657)	-0.29	0.4	3.86	1.07	0.031
	△	6669.281(.063)	-0.56	0.07	-1.08	-0.31	0.007
	△	5702.306(.124)	-0.67	0.24	2.87	0.8	0.008
	△	6597.55(.341)	-1.04	0.31	1.37	0.36	0.007
	△	6608.936(.893)	-1.05	0.49	-6.81	-1.96	0.008
	△	6643.035(.374)	-1.42	0.56	-8.04	-2.21	0.008
	○	5719.816(.584)	-1.66	0.09	0.21	0.07	0.01
	○	5844.595(.372)	-1.76	0.08	-5.72	-1.57	0.006
	<hr/>						
	○	6024.049(3.862)	0.09	0.61	-3.91	-1.08	0.009
	△	5862.357(.131)	-0.13	0.52	0.8	0.27	0.015
	○	5914.201(3.949)	-0.13	0.6	2.89	0.82	0.014
	△	5984.815(.599)	-0.2	0.49	-0.06	0.0	0.011
Fe I	○	5930.173(9.985)	-0.23	0.52	5.38	1.08	0.008
	○	6419.942(.732)	-0.24	0.48	-0.42	-0.11	0.01
	○	6020.17(9.941)	-0.28	0.54	-1.85	-0.5	0.009
	○	6078.491(.3)	-0.32	0.48	-1.91	-0.4	0.008
	△	5762.99(.768)	-0.37	0.59	-3.69	-1.02	0.008
	○	5914.112(3.932)	-0.38	0.6	2.85	0.81	0.011
	○	5987.065(6.849)	-0.43	0.44	-1.87	-0.52	0.011
	<hr/>						
	○	6456.383(.165)	-2.19	0.2	2.25	0.63	0.008
	△	6383.722(.51)	-2.41	0.05	0.65	0.17	0.008
Fe II	○	6149.258(.038)	-2.92	0.09	0.66	0.2	0.006
	○	6369.462(.25)	-4.23	0.05	-0.79	-0.22	0.009
	<hr/>						
	△	6678.154(7.767)	0.33	0.67	-2.79	-0.8	0.015
He I	○	6659.707(.603)	-4.71	0.04	2.2	0.66	0.008

	○	6648.79(9.071)	-5.03	0.02	-2.98	-0.84	0.007
	△	6648.189(7.84)	-5.06	0.13	2.88	0.49	0.008
	○	6176.807(.591)	-0.26	0.39	-3.96	-1.05	0.008
	△	5715.066(4.871)	-0.35	0.48	-1.28	-0.38	0.012
	○	6086.276(.089)	-0.42	0.27	5.61	1.55	0.006
	△	6175.36(.149)	-0.56	0.31	-2.57	-0.74	0.008
Ni I	△	6116.174(5.981)	-0.68	0.37	1.57	0.41	0.007
	△	6339.11(8.673)	-0.81	0.29	-0.69	-0.17	0.009
	○	6378.247(.025)	-0.83	0.22	-2.7	-0.74	0.01
	○	6111.066(0.847)	-0.87	0.23	3.84	1.08	0.008
	○	6314.659(.443)	-0.92	0.51	0.18	0.02	0.009
	△	6186.709(.49)	-0.95	0.2	-0.67	-0.15	0.007
	△	6130.13(9.907)	-0.96	0.14	-1.14	-0.19	0.009
	△	6604.601(.356)	-1.31	0.21	6.65	1.93	0.007
Sc II	△	6309.92(.942)	-1.63	0.16	3.03	0.85	0.011
	△	5948.541(.324)	-0.78	0.39	6.91	1.91	0.006
	○	6155.134(4.91)	-0.8	0.31	4.36	1.2	0.009
	△	5721.021(0.691)	-0.85	0.13	3.39	0.93	0.011
	△	6254.188(.045)	-0.93	0.6	-3.83	-1.08	0.012
Si I	△	6370.574(.147)	-0.95	0.1	-2.11	-0.56	0.008
	△	6414.98(.756)	-1.03	0.16	-3.45	-0.98	0.011
	△	6527.202(6.955)	-1.07	0.14	-0.76	-0.2	0.009
	○	6555.463(.211)	-1.17	0.15	-3.28	-0.94	0.011
	△	6518.129(.128)	-1.41	0.45	-1.38	-0.41	0.01
	○	6145.016(4.8)	-1.42	0.16	-4.73	-1.34	0.008
	○	6195.433(.211)	-1.49	0.07	-1.66	-0.44	0.006
Sr I	△	6503.991(.921)	0.32	0.18	5.53	1.59	0.008

	△	5774.027(3.811)	0.48	0.16	3.95	1.14	0.01
	△	5766.359(.109)	0.39	0.16	0.77	0.21	0.006
	△	6668.376(.166)	0.2	0.05	4.36	1.2	0.007
	△	6667.734(.48)	0.13	0.1	-4.67	-1.29	0.008
Ti I	○	6098.658(.433)	-0.01	0.11	4.54	1.29	0.008
	○	6763.963(.749)	-0.05	0.04	6.27	1.73	0.009
	△	5866.368(.246)	-0.19	0.53	-6.82	-1.89	0.009
	△	6215.233(4.94)	-0.22	0.42	1.68	0.48	0.01
	△	6258.706(.493)	-0.24	0.58	5.37	0.63	0.01
	△	5953.16(2.966)	-0.33	0.42	5.67	1.55	0.006
	△	6180.303(9.984)	-0.34	0.46	3.55	1.03	0.007
	△	5846.353(.025)	0.66	0.07	-5.27	-1.51	0.006
	○	6090.214(9.993)	-0.06	0.46	-5.77	-1.64	0.007
	△	5727.048(6.828)	-0.19	0.57	-1.78	-0.48	0.005
	△	5703.575(.354)	-0.21	0.45	-0.62	-0.15	0.009
V I	△	5698.52(.29)	-0.24	0.54	5.42	1.53	0.009
	△	5772.411(1.982)	-0.57	0.19	1.82	0.51	0.008
	△	6081.441(.254)	-0.58	0.34	-5.89	-1.64	0.01
	△	6039.722(.529)	-0.65	0.3	-6.07	-1.63	0.007
	○	6111.645(.427)	-0.71	0.31	-0.27	-0.08	0.007
	△	5731.241(.048)	-0.73	0.3	3.14	0.83	0.008
	○	6326.84(.629)	-0.81	0.07	-0.04	0.01	0.008
Y I	○	6435.004(4.783)	-0.82	0.08	4.02	1.16	0.007

C.4.2. 1.0 angstrom band

Atom		$\lambda_{lab}(\lambda_{obs})$	$\log(gf)$	normed depth	σ_{In-Out}	σ_{rel}	σ_c
C I	△	6012.225(.011)	-2.0	0.25	0.46	0.11	0.006
	△	5793.12(2.853)	-2.06	0.2	7.01	1.98	0.007
Ca I	△	6439.075(8.827)	0.39	0.79	-2.01	-0.55	0.015
	△	6462.567(.354)	0.26	0.78	1.29	0.37	0.014
	△	6493.781(.564)	-0.11	0.7	-1.42	-0.4	0.014
	△	5991.798(.685)	-0.18	0.14	-0.07	-0.01	0.006
	△	6717.681(.434)	-0.52	0.63	-2.64	-0.75	0.011
	△	6499.65(.402)	-0.65	0.62	2.07	0.62	0.012
	○	6471.662(.444)	-0.69	0.64	-4.56	-1.26	0.008
	△	6475.236(.401)	-0.72	0.44	-2.97	-0.83	0.009
	△	5809.118(8.995)	-1.07	0.38	-0.94	-0.27	0.01
	△	6360.298(.599)	-1.22	0.1	-1.38	-0.4	0.011
Co I	○	6455.598(.373)	-1.34	0.5	2.57	0.72	0.008
	△	6007.677(.738)	-0.1	0.41	-1.04	-0.3	0.011
	○	6454.99(.775)	-0.25	0.11	0.48	0.13	0.007
	△	6107.918(.875)	-0.43	0.47	-3.08	-0.85	0.009
	△	6232.383(.417)	-0.46	0.53	3.71	1.13	0.015
	△	6082.422(.52)	-0.52	0.35	1.25	0.35	0.009
	○	6444.675(.419)	-1.41	0.02	-5.64	-1.68	0.006
	○	6771.033(0.782)	-2.12	0.18	-2.03	-0.59	0.009
	△	6551.446(.448)	-2.56	0.12	-0.65	-0.2	0.008
	△	6129.094(8.764)	-2.92	0.25	4.78	0.96	0.011
Cr I	△	5790.957(.761)	0.32	0.6	0.71	0.22	0.011
	△	5787.918(.701)	-0.13	0.46	-1.95	-0.54	0.019

	△	6218.951(9.054)	-0.21	0.6	-2.61	-0.7	0.011
	△	5783.85(.657)	-0.29	0.4	4.35	1.15	0.031
	△	6669.281(.063)	-0.56	0.07	-4.96	-1.39	0.007
	△	5702.306(.124)	-0.67	0.24	0.34	0.12	0.008
	△	6597.55(.341)	-1.04	0.31	3.71	0.96	0.007
	△	6608.936(.893)	-1.05	0.49	-7.78	-2.23	0.008
	△	6643.035(.374)	-1.42	0.56	-9.11	-2.48	0.008
	○	5719.816(.584)	-1.66	0.09	1.29	0.38	0.01
	○	5844.595(.372)	-1.76	0.08	-7.12	-1.97	0.006
	<hr/>						
	○	6024.049(3.862)	0.09	0.61	-2.42	-0.67	0.009
	△	5862.357(.131)	-0.13	0.52	2.98	0.79	0.015
	○	5914.201(3.949)	-0.13	0.6	2.57	0.72	0.014
	△	5984.815(.599)	-0.2	0.49	-0.18	-0.06	0.011
Fe I	○	5930.173(9.985)	-0.23	0.52	1.89	0.48	0.008
	○	6419.942(.732)	-0.24	0.48	0.17	0.07	0.01
	○	6020.17(9.941)	-0.28	0.54	-3.71	-1.07	0.009
	○	6078.491(.3)	-0.32	0.48	-0.54	-0.14	0.008
	△	5762.99(.768)	-0.37	0.59	-2.14	-0.59	0.008
	○	5914.112(3.932)	-0.38	0.6	2.17	0.62	0.011
	○	5987.065(6.849)	-0.43	0.44	-2.51	-0.67	0.011
	<hr/>						
	○	6456.383(.165)	-2.19	0.2	3.29	0.92	0.008
	△	6383.722(.51)	-2.41	0.05	-1.94	-0.55	0.008
Fe II	○	6149.258(.038)	-2.92	0.09	-1.0	-0.24	0.006
	○	6369.462(.25)	-4.23	0.05	0.61	0.17	0.009
	<hr/>						
	△	6678.154(7.767)	0.33	0.67	-1.62	-0.47	0.015
He I	○	6659.707(.603)	-4.71	0.04	1.72	0.51	0.008
	○	6648.79(9.071)	-5.03	0.02	-0.91	-0.26	0.007

	△	6648.189(7.84)	-5.06	0.13	5.29	1.1	0.008
	○	6176.807(.591)	-0.26	0.39	-4.24	-1.16	0.008
	△	5715.066(4.871)	-0.35	0.48	-1.53	-0.44	0.012
	○	6086.276(.089)	-0.42	0.27	3.23	0.88	0.006
	△	6175.36(.149)	-0.56	0.31	-0.14	-0.05	0.008
Ni I	△	6116.174(5.981)	-0.68	0.37	0.43	0.13	0.007
	△	6339.11(8.673)	-0.81	0.29	0.19	0.07	0.009
	○	6378.247(.025)	-0.83	0.22	-0.81	-0.21	0.01
	○	6111.066(0.847)	-0.87	0.23	3.26	0.9	0.008
	○	6314.659(.443)	-0.92	0.51	1.06	0.29	0.009
	△	6186.709(.49)	-0.95	0.2	-0.83	-0.21	0.007
	△	6130.13(9.907)	-0.96	0.14	-1.98	-0.6	0.009
	△	6604.601(.356)	-1.31	0.21	6.79	1.91	0.007
Sc II	△	6309.92(.942)	-1.63	0.16	4.12	1.18	0.011
	△	5948.541(.324)	-0.78	0.39	4.48	1.22	0.006
	○	6155.134(4.91)	-0.8	0.31	4.01	1.12	0.009
	△	5721.021(0.691)	-0.85	0.13	-1.62	-0.49	0.011
	△	6254.188(.045)	-0.93	0.6	-1.02	-0.3	0.012
Si I	△	6370.574(.147)	-0.95	0.1	0.05	-0.01	0.008
	△	6414.98(.756)	-1.03	0.16	-4.31	-1.23	0.011
	△	6527.202(6.955)	-1.07	0.14	-6.31	-1.79	0.009
	○	6555.463(.211)	-1.17	0.15	-0.42	-0.11	0.011
	△	6518.129(.128)	-1.41	0.45	2.12	0.59	0.01
	○	6145.016(4.8)	-1.42	0.16	-4.04	-1.09	0.008
	○	6195.433(.211)	-1.49	0.07	-2.37	-0.67	0.006
Sr I	△	6503.991(.921)	0.32	0.18	3.0	0.85	0.008
	△	5774.027(3.811)	0.48	0.16	1.87	0.5	0.01

	△	5766.359(.109)	0.39	0.16	0.12	0.06	0.006
	△	6668.376(.166)	0.2	0.05	3.83	1.06	0.007
	△	6667.734(.48)	0.13	0.1	-1.73	-0.48	0.008
	○	6098.658(.433)	-0.01	0.11	-0.02	-0.01	0.008
	○	6763.963(.749)	-0.05	0.04	4.14	1.17	0.009
	△	5866.368(.246)	-0.19	0.53	-4.01	-1.14	0.009
	△	6215.233(4.94)	-0.22	0.42	3.12	0.89	0.01
	△	6258.706(.493)	-0.24	0.58	11.24	0.65	0.01
	△	5953.16(2.966)	-0.33	0.42	-0.26	-0.09	0.006
	△	6180.303(9.984)	-0.34	0.46	4.33	1.21	0.007
	△	5846.353(.025)	0.66	0.07	-2.74	-0.81	0.006
	○	6090.214(9.993)	-0.06	0.46	-3.12	-0.92	0.007
	△	5727.048(6.828)	-0.19	0.57	-5.36	-1.49	0.005
	△	5703.575(.354)	-0.21	0.45	-0.7	-0.2	0.009
V I	△	5698.52(.29)	-0.24	0.54	3.44	0.94	0.009
	△	5772.411(1.982)	-0.57	0.19	4.4	1.23	0.008
	△	6081.441(.254)	-0.58	0.34	-2.01	-0.55	0.01
	△	6039.722(.529)	-0.65	0.3	-4.44	-1.21	0.007
	○	6111.645(.427)	-0.71	0.31	4.82	1.32	0.007
	△	5731.241(.048)	-0.73	0.3	2.26	0.52	0.008
	○	6326.84(.629)	-0.81	0.07	1.82	0.52	0.008
Y I	○	6435.004(4.783)	-0.82	0.08	-1.04	-0.28	0.007

Appendix D

HD 189733b extensive analysis (HARPS dataset)

D.1. Global element analysis

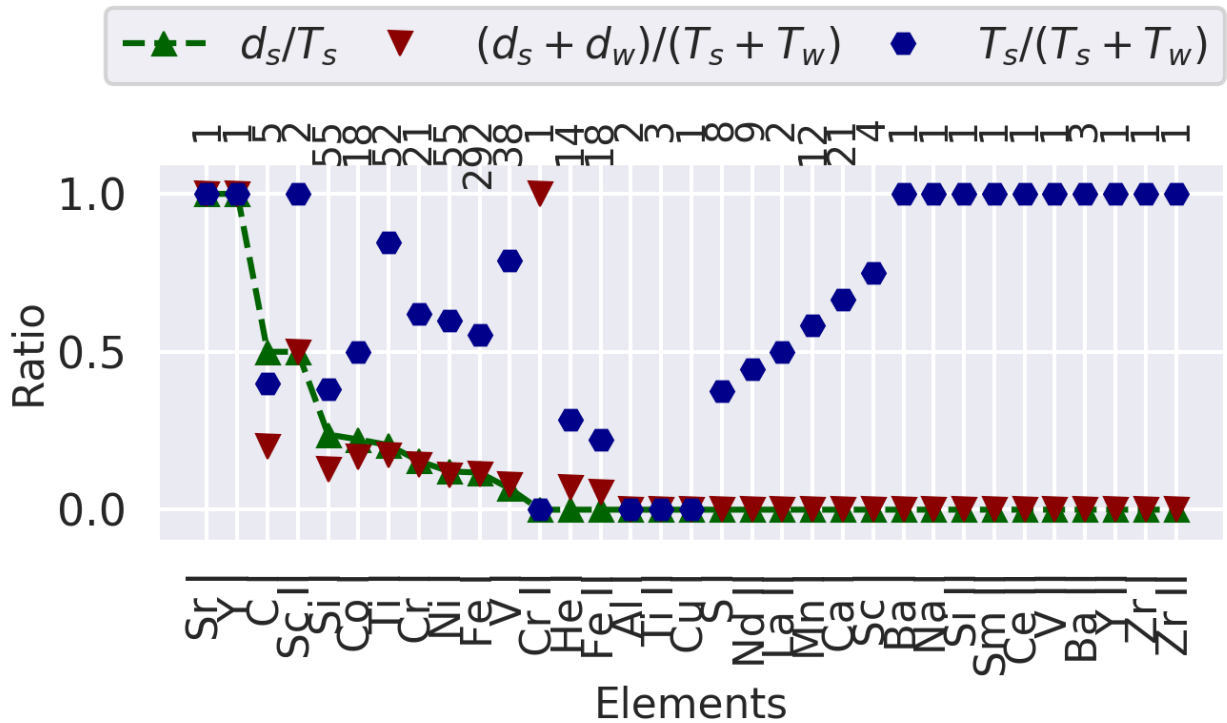


Figure D.1: Summary for elements on band 0.75

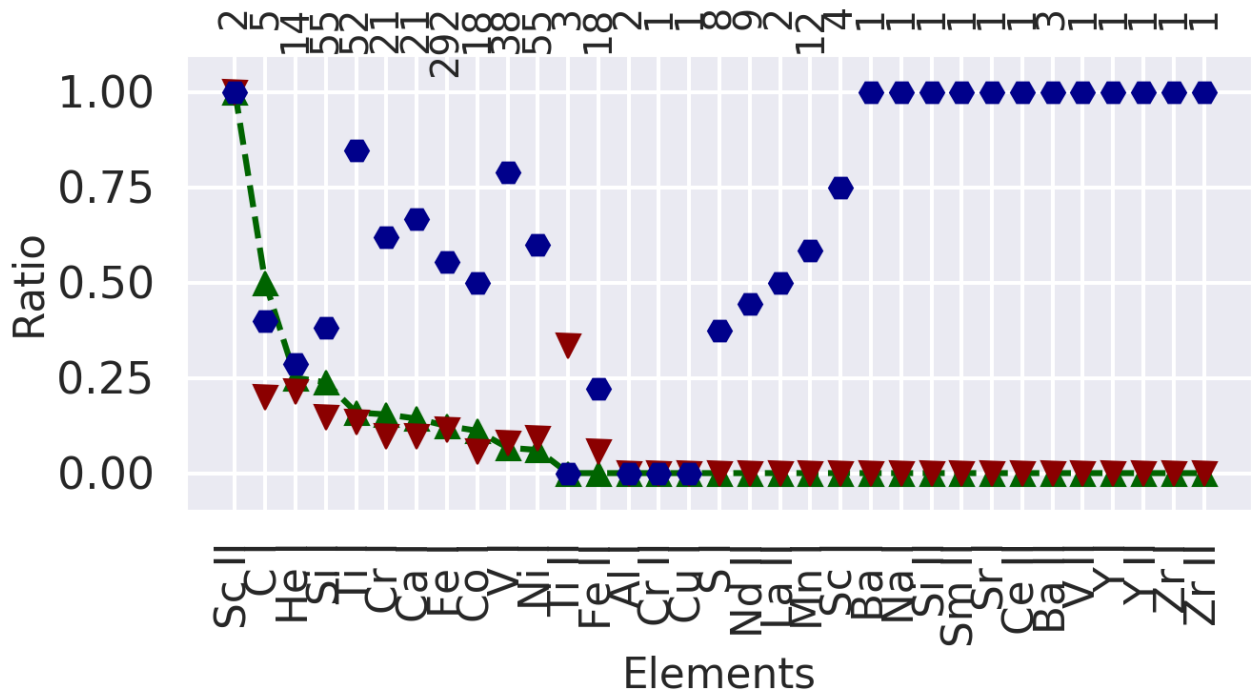


Figure D.2: Summary for elements on band 1.0

D.2. Algorithm parameters:

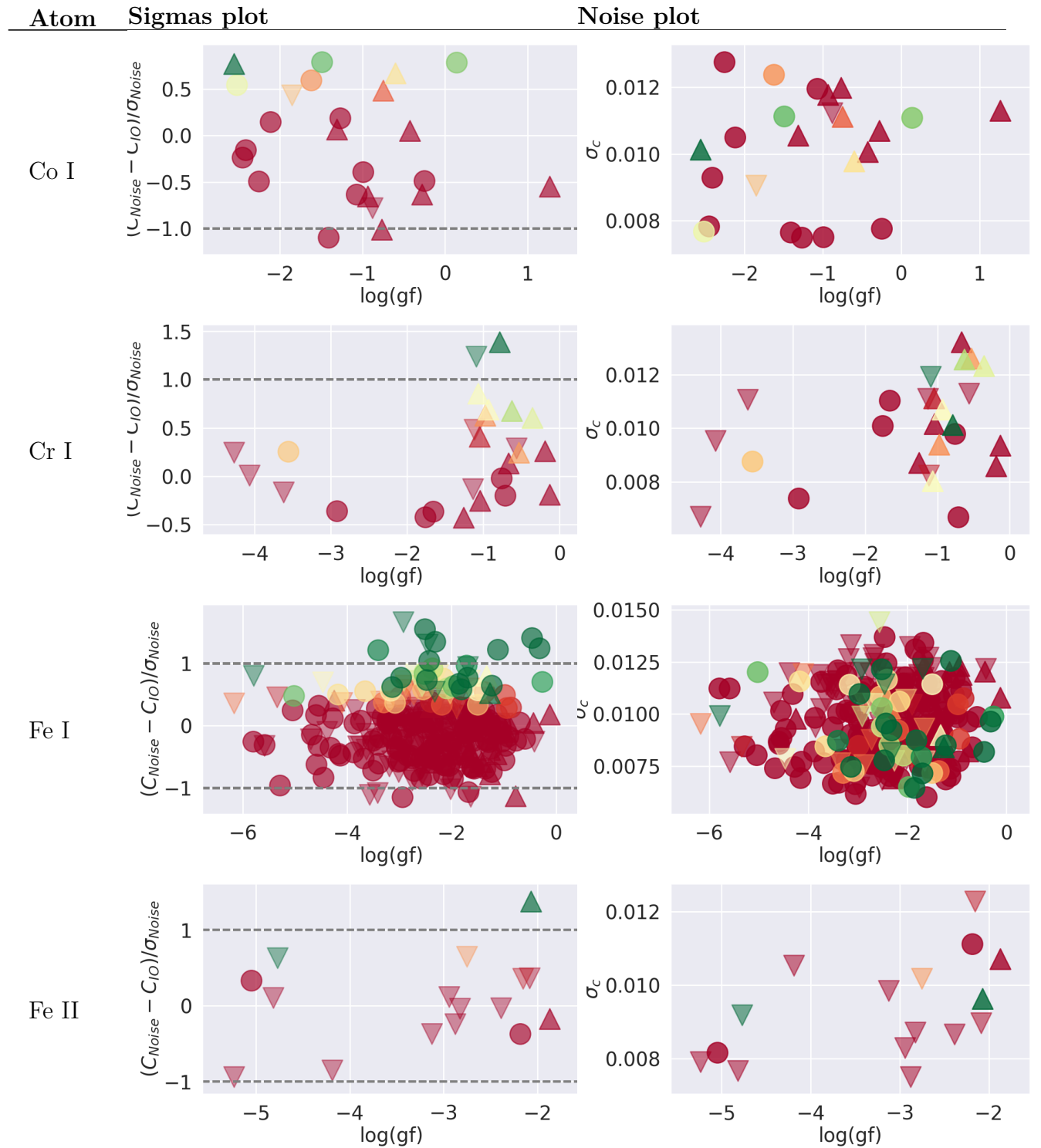
Parameter name	Value
N_FWHM	30
N_pixs	180
N_shifts	2500
cut_order	100
delta_max_shift	1
dlt_epochs	0
do_1stdopp	True
doppler_pixs	500
dtransit	0.07527
error_gain	1.36
general_warnings	indexFWHM and N_pixs changed due to wavelength binning
in_epochs	10
indexFWHM	6
interpolate_ref	True
merge_epoch_as	
n_binning	3
n_epoch_merge	0
n_epochs	18
near_indline	6
near_tolerance	0.001
norm_high	3
norm_min_pixs	1
norm_polyorder	3
norm_width	5
normalize_hists	False
orders	0
orders_length	0.009999999999763531
period	2.21857567
plot_time_binning	0
radial_velocity	-2.55
redf_loops	3000
redfield_bins	50
renorm_scale	1
smart_merge	True
t_start	53986.0470905603
t_transit	2454279.436714
telescope	harps
tell_only_out	False
test_boundary	0.013
test_percent	0.7
test_pixs_near	15
test_times_near	10
test_var_amplitude	0.06
test_var_mu	0.06
time_average_corr	True
times_indline	1
wave_binning	2

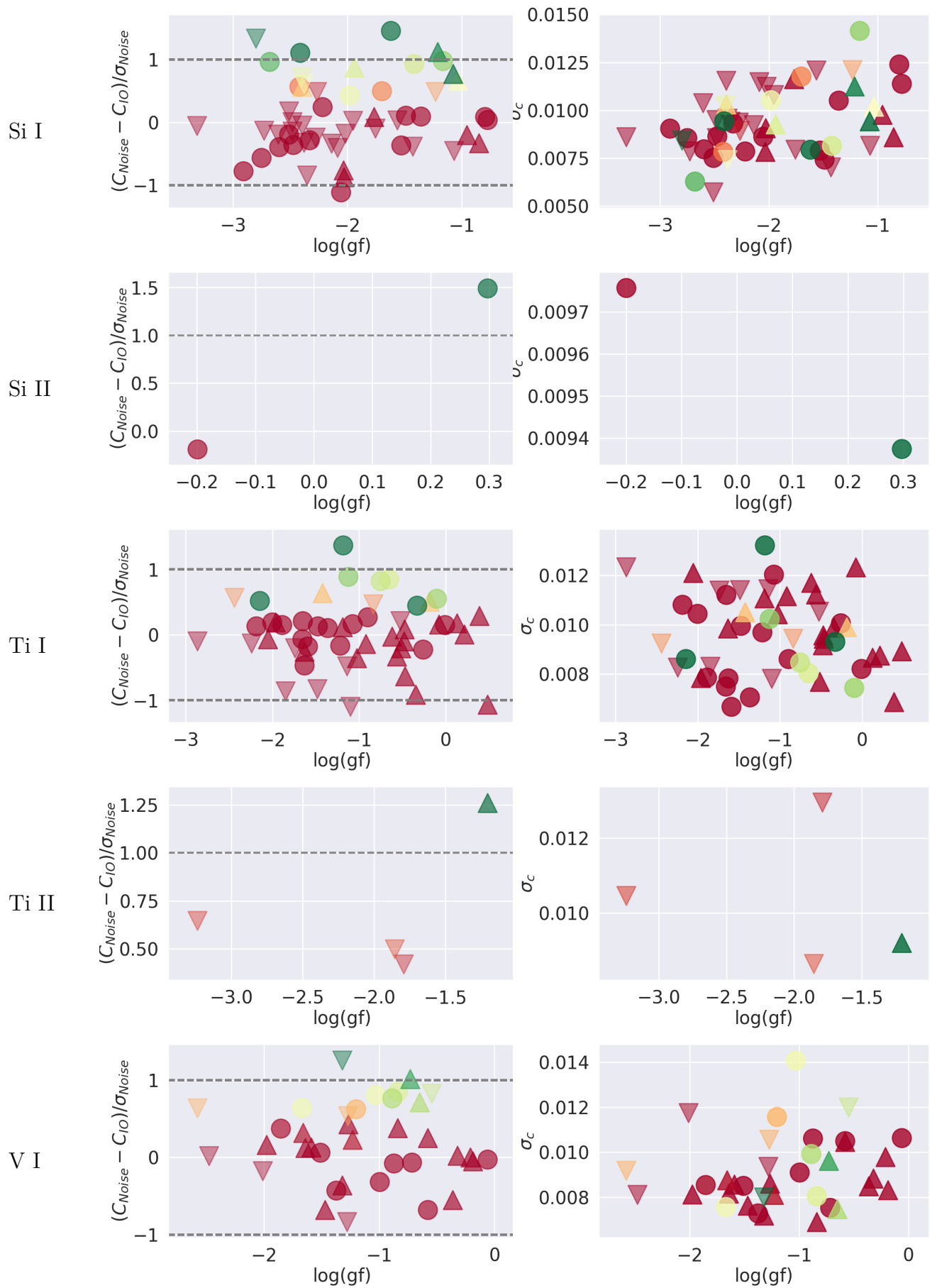
D.2.1. Object information:

Parameter name	Value
TELESCOP	ESO-3P6
INSTRUME	HARPS
OBJECT	HD189733
DATE	2010-08-05T02:14:33.376

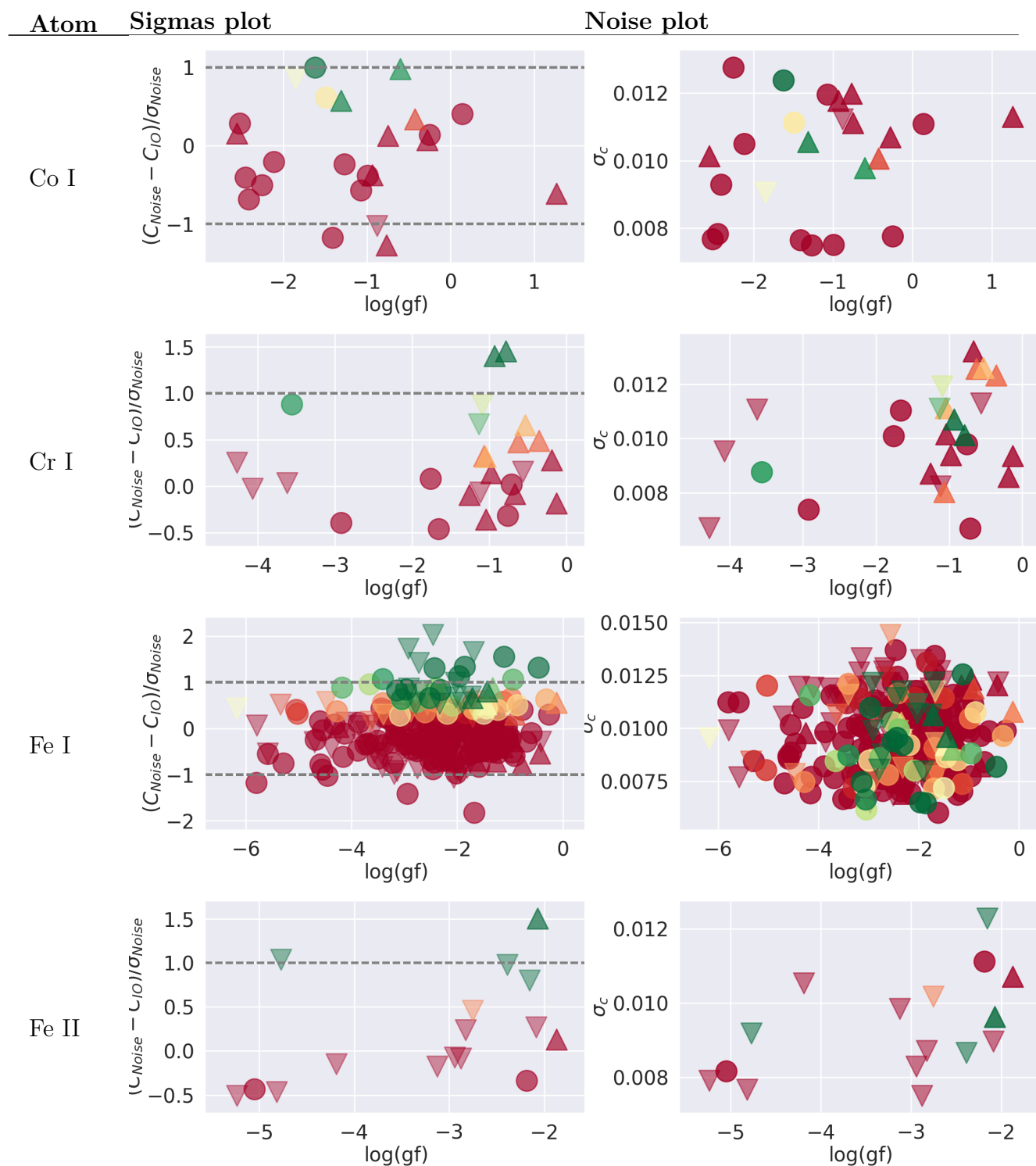
D.3. Elements with detections

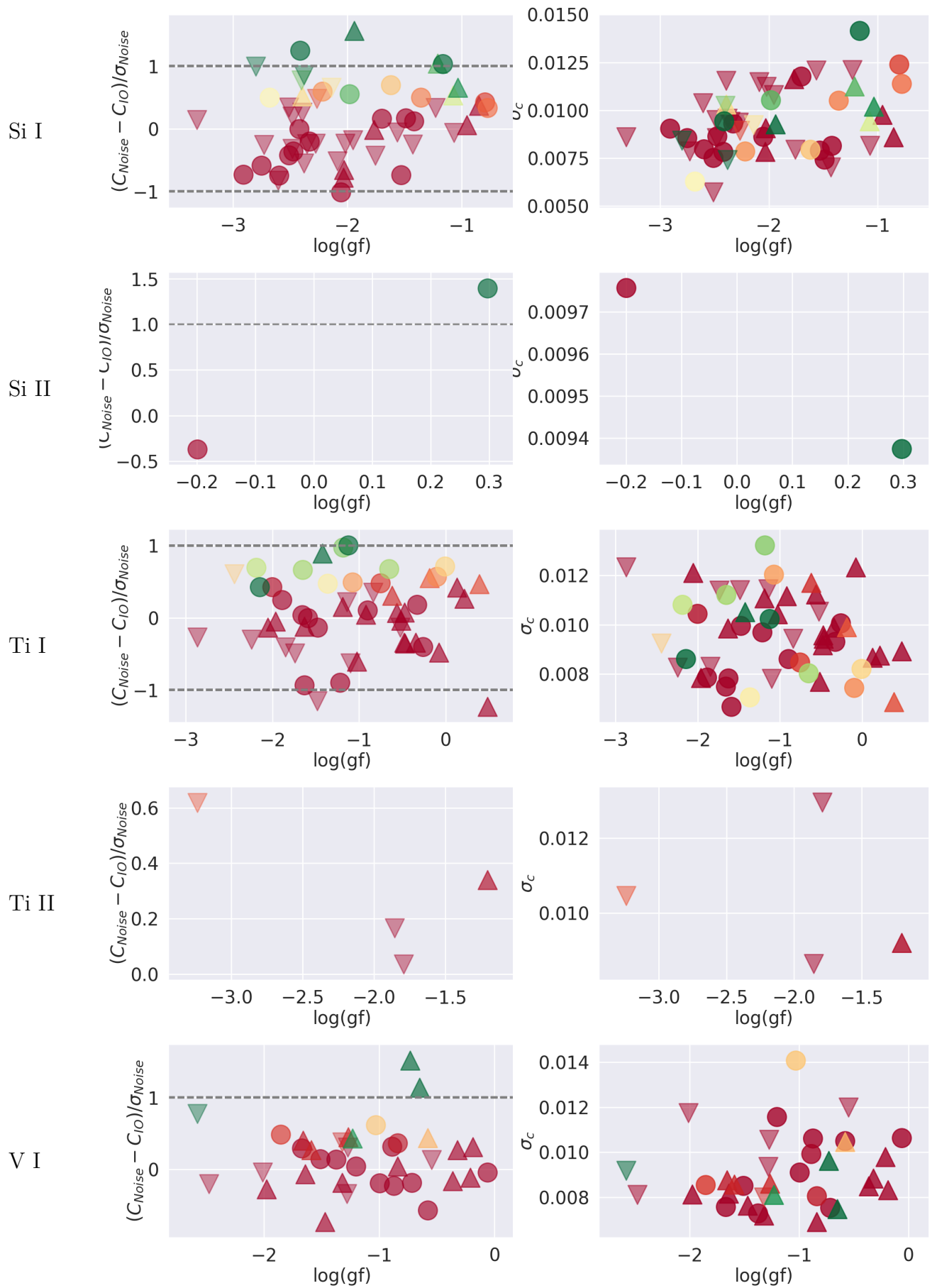
D.3.1. 0.75 angstrom band





D.3.2. 1.0 angstrom band





D.4. Detected elements transitions

D.4.1. 0.75 angstrom band

Atom	$\lambda_{lab}(\lambda_{obs})$	log(gf)	normed depth	σ_{In-Out}	σ_{rel}	σ_c
Co I	△ 5343.392(.44)	1.26	0.51	-1.34	-0.55	0.011
	○ 5359.192(.221)	0.14	0.1	2.51	0.79	0.011
	○ 6454.99(5.01)	-0.25	0.13	-1.27	-0.49	0.008
	△ 4821.142(.126)	-0.28	0.29	-3.01	-0.63	0.011
	△ 6107.918(8.117)	-0.43	0.54	0.17	0.05	0.01
	△ 6271.468(.288)	-0.6	0.27	1.83	0.67	0.01
	△ 5546.965(7.012)	-0.75	0.33	1.35	0.48	0.011
	△ 5637.143(.133)	-0.77	0.3	-2.86	-1.01	0.012
	△ 5257.609(.66)	-0.93	0.3	-2.02	-0.65	0.012
	○ 6000.663(.676)	-0.99	0.06	-1.09	-0.39	0.008
	○ 5946.485(.636)	-1.07	0.1	-2.39	-0.63	0.012
Cr I	△ 5787.918(.934)	-0.13	0.51	-1.52	-0.19	0.009
	△ 6661.075(.072)	-0.19	0.15	0.69	0.26	0.009
	△ 5243.298(.37)	-0.35	0.33	2.14	0.6	0.012
	△ 5553.549(.602)	-0.53	0.41	1.55	0.25	0.013
	△ 6219.187(.288)	-0.63	0.66	2.33	0.67	0.013
	△ 5702.306(.324)	-0.67	0.3	0.34	0.14	0.013
	○ 6729.734(.752)	-0.71	0.05	-0.58	-0.2	0.007
	○ 5628.643(.653)	-0.76	0.25	-0.08	-0.02	0.01
	△ 5386.967(.981)	-0.79	0.34	6.32	1.39	0.01
	△ 5387.562(.551)	-0.93	0.31	1.99	0.69	0.011
	△ 6715.473(.392)	-0.97	0.22	1.5	0.63	0.009
△ 5862.357(.375)	-0.13	0.58	0.5	0.18	0.011	

	○	5633.946(.963)	-0.27	0.5	2.76	0.7	0.01
	○	6078.491(.507)	-0.32	0.53	3.97	1.24	0.01
	△	5554.882(.892)	-0.44	0.61	0.22	0.05	0.012
	○	6055.992(6.007)	-0.46	0.51	3.51	1.41	0.008
	○	5816.373(.384)	-0.6	0.51	-0.37	-0.21	0.01
	○	5975.35(.366)	-0.69	0.41	0.15	0.05	0.008
	○	6469.192(.19)	-0.77	0.42	-0.69	-0.24	0.01
	△	6290.965(.969)	-0.77	0.44	-2.78	-1.13	0.008
	○	5638.262(.273)	-0.87	0.59	1.14	0.29	0.011
	△	5650.704(.693)	-0.91	0.32	0.14	0.03	0.012
	<hr/>						
	△	5466.908(.982)	-1.87	0.36	-0.85	-0.17	0.011
	△	6331.954(.969)	-2.07	0.05	3.42	1.38	0.01
Fe II	○	6456.383(.4)	-2.19	0.23	-1.37	-0.37	0.011
	○	5932.055(1.875)	-5.05	0.22	0.97	0.33	0.008
	<hr/>						
	○	6784.883(.983)	-0.78	0.06	0.12	0.04	0.011
	○	6155.134(.147)	-0.8	0.32	0.26	0.09	0.012
	△	5721.021(0.914)	-0.85	0.16	-0.94	-0.33	0.009
	△	6370.574(.369)	-0.95	0.12	-0.61	-0.2	0.01
Si I	△	6414.98(.98)	-1.03	0.18	2.0	0.66	0.01
	△	6527.202(.221)	-1.07	0.14	4.11	0.77	0.009
	○	6555.463(.481)	-1.17	0.15	2.46	0.97	0.014
	△	6303.606(.769)	-1.21	0.26	2.9	1.12	0.011
	○	5772.146(.144)	-1.36	0.27	0.44	0.09	0.011
	○	6145.016(.037)	-1.42	0.18	2.21	0.93	0.008
	○	6195.433(.468)	-1.49	0.07	0.43	0.11	0.007
	<hr/>						
Si II	○	6347.109(.089)	0.3	0.08	4.17	1.49	0.009
	○	6371.371(.349)	-0.2	0.05	-0.89	-0.19	0.01
	<hr/>						

	△	5774.027(.044)	0.48	0.2	-2.57	-1.06	0.009
	△	5766.359(.334)	0.39	0.19	0.92	0.29	0.007
	△	6565.502(.521)	0.21	0.09	0.08	0.01	0.009
	△	6667.734(.732)	0.13	0.11	0.56	0.18	0.009
Ti I	○	6098.658(.657)	-0.01	0.14	0.44	0.15	0.008
	△	5877.657(.795)	-0.08	0.19	0.17	0.16	0.012
	○	6548.325(.381)	-0.1	0.21	2.41	0.55	0.007
	△	5866.368(.465)	-0.19	0.63	1.71	0.51	0.01
	○	5648.565(.573)	-0.26	0.24	-0.54	-0.22	0.01
	○	5953.16(.176)	-0.33	0.46	3.24	0.45	0.009
	△	6180.303(.218)	-0.34	0.51	-2.37	-0.91	0.01
Ti II	△	6605.897(.961)	-1.21	0.1	3.42	1.26	0.009
	○	6090.214(.227)	-0.06	0.54	-0.1	-0.03	0.011
	△	5727.048(.064)	-0.19	0.63	-0.17	-0.05	0.008
	△	5703.575(.584)	-0.21	0.55	-0.1	0.0	0.01
	△	6119.523(.537)	-0.32	0.46	-0.03	0.02	0.009
V I	△	5627.633(.643)	-0.36	0.51	-1.8	-0.55	0.009
	○	5670.853(.863)	-0.58	0.49	-2.1	-0.68	0.011
	△	6081.441(.457)	-0.58	0.4	0.95	0.25	0.01
	△	6039.722(.736)	-0.65	0.37	2.36	0.72	0.007
	○	6111.645(.667)	-0.71	0.36	-0.02	-0.06	0.008
	△	5731.241(.254)	-0.73	0.3	2.73	1.02	0.01
	△	6358.817(.699)	-0.84	0.63	0.97	0.38	0.007

D.4.2. 1.0 angstrom band

Atom	$\lambda_{lab}(\lambda_{obs})$	$\log(gf)$	normed depth	σ_{In-Out}	σ_{rel}	σ_c
Co I	\triangle 5343.392(.44)	1.26	0.51	-1.57	-0.61	0.011
	\circ 5359.192(.221)	0.14	0.1	0.91	0.4	0.011
	\circ 6454.99(5.01)	-0.25	0.13	0.49	0.14	0.008
	\triangle 4821.142(.126)	-0.28	0.29	0.43	0.07	0.011
	\triangle 6107.918(8.117)	-0.43	0.54	1.25	0.34	0.01
	\triangle 6271.468(.288)	-0.6	0.27	2.83	0.98	0.01
	\triangle 5546.965(7.012)	-0.75	0.33	0.59	0.13	0.011
	\triangle 5637.143(.133)	-0.77	0.3	-3.71	-1.27	0.012
	\triangle 5257.609(.66)	-0.93	0.3	-1.74	-0.37	0.012
	\circ 6000.663(.676)	-0.99	0.06	-0.93	-0.38	0.008
\circ 5946.485(.636)	-1.07	0.1	-1.71	-0.57	0.012	
Cr I	\triangle 5787.918(.934)	-0.13	0.51	-2.14	-0.18	0.009
	\triangle 6661.075(.072)	-0.19	0.15	0.77	0.28	0.009
	\triangle 5243.298(.37)	-0.35	0.33	1.37	0.49	0.012
	\triangle 5553.549(.602)	-0.53	0.41	1.63	0.66	0.013
	\triangle 6219.187(.288)	-0.63	0.66	1.35	0.47	0.013
	\triangle 5702.306(.324)	-0.67	0.3	-0.24	-0.08	0.013
	\circ 6729.734(.752)	-0.71	0.05	0.06	0.02	0.007
	\circ 5628.643(.653)	-0.76	0.25	-0.85	-0.32	0.01
	\triangle 5386.967(.981)	-0.79	0.34	4.38	1.46	0.01
	\triangle 5387.562(.551)	-0.93	0.31	4.29	1.41	0.011
\triangle 6715.473(.392)	-0.97	0.22	0.25	0.14	0.009	
\triangle 5862.357(.375)	-0.13	0.58	1.44	0.56	0.011	
\circ 5633.946(.963)	-0.27	0.5	0.89	0.3	0.01	

	○	6078.491(.507)	-0.32	0.53	1.58	0.63	0.01
	△	5554.882(.892)	-0.44	0.61	-2.35	-0.53	0.012
	○	6055.992(6.007)	-0.46	0.51	3.99	1.32	0.008
	○	5816.373(.384)	-0.6	0.51	-0.11	-0.09	0.01
	○	5975.35(.366)	-0.69	0.41	-1.94	-0.28	0.008
	○	6469.192(.19)	-0.77	0.42	0.98	0.4	0.01
	△	6290.965(.969)	-0.77	0.44	-2.06	-0.79	0.008
	○	5638.262(.273)	-0.87	0.59	1.8	0.51	0.011
	△	5650.704(.693)	-0.91	0.32	1.27	0.3	0.012
	<hr/>						
Fe II	△	5466.908(.982)	-1.87	0.36	0.91	0.13	0.011
	△	6331.954(.969)	-2.07	0.05	3.89	1.51	0.01
	○	6456.383(.4)	-2.19	0.23	-1.22	-0.34	0.011
	○	5932.055(1.875)	-5.05	0.22	-1.66	-0.43	0.008
	<hr/>						
Si I	○	6784.883(.983)	-0.78	0.06	1.4	0.34	0.011
	○	6155.134(.147)	-0.8	0.32	1.25	0.43	0.012
	△	5721.021(0.914)	-0.85	0.16	0.94	0.37	0.009
	△	6370.574(.369)	-0.95	0.12	0.18	0.06	0.01
	△	6414.98(.98)	-1.03	0.18	2.84	0.66	0.01
	△	6527.202(.221)	-1.07	0.14	2.19	0.54	0.009
	○	6555.463(.481)	-1.17	0.15	3.46	1.04	0.014
	△	6303.606(.769)	-1.21	0.26	2.64	1.04	0.011
	○	5772.146(.144)	-1.36	0.27	1.46	0.5	0.011
	○	6145.016(.037)	-1.42	0.18	0.31	0.13	0.008
	○	6195.433(.468)	-1.49	0.07	0.93	0.17	0.007
	<hr/>						
Si II	○	6347.109(.089)	0.3	0.08	3.98	1.4	0.009
	○	6371.371(.349)	-0.2	0.05	-1.03	-0.37	0.01
	<hr/>						
	△	5774.027(.044)	0.48	0.2	-3.36	-1.23	0.009

	△	5766.359(.334)	0.39	0.19	1.28	0.47	0.007
	△	6565.502(.521)	0.21	0.09	0.62	0.27	0.009
	△	6667.734(.732)	0.13	0.11	0.92	0.42	0.009
	○	6098.658(.657)	-0.01	0.14	1.76	0.71	0.008
	△	5877.657(.795)	-0.08	0.19	-1.11	-0.48	0.012
	○	6548.325(.381)	-0.1	0.21	1.49	0.57	0.007
	△	5866.368(.465)	-0.19	0.63	1.33	0.55	0.01
	○	5648.565(.573)	-0.26	0.24	-1.04	-0.4	0.01
	○	5953.16(.176)	-0.33	0.46	0.75	0.18	0.009
	△	6180.303(.218)	-0.34	0.51	-1.02	-0.34	0.01
Ti II	△	6605.897(.961)	-1.21	0.1	1.05	0.34	0.009
	○	6090.214(.227)	-0.06	0.54	-0.17	-0.04	0.011
	△	5727.048(.064)	-0.19	0.63	0.79	0.31	0.008
	△	5703.575(.584)	-0.21	0.55	-0.3	-0.11	0.01
	△	6119.523(.537)	-0.32	0.46	0.66	0.27	0.009
V I	△	5627.633(.643)	-0.36	0.51	-0.51	-0.16	0.009
	○	5670.853(.863)	-0.58	0.49	-1.38	-0.57	0.011
	△	6081.441(.457)	-0.58	0.4	1.63	0.44	0.01
	△	6039.722(.736)	-0.65	0.37	5.05	1.14	0.007
	○	6111.645(.667)	-0.71	0.36	-0.56	-0.18	0.008
	△	5731.241(.254)	-0.73	0.3	3.58	1.52	0.01
	△	6358.817(.699)	-0.84	0.63	0.19	0.05	0.007

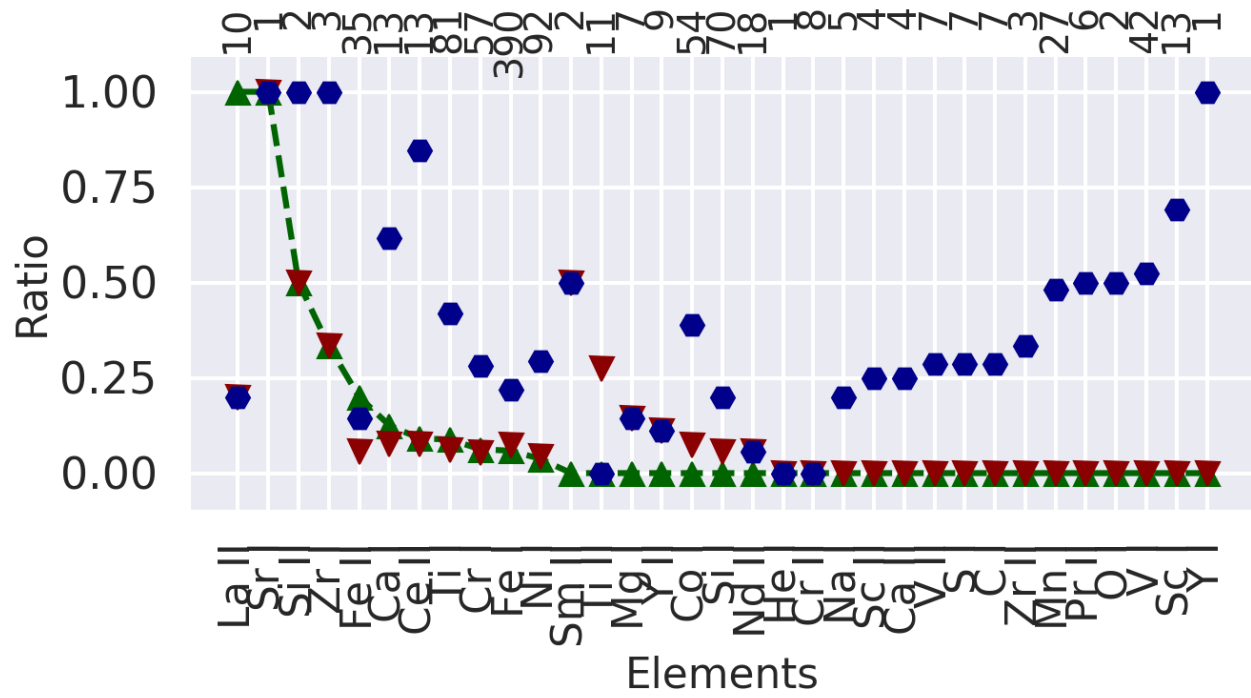


Figure E.2: Summary for elements on band 1.0

E.2. Algorithm parameters:

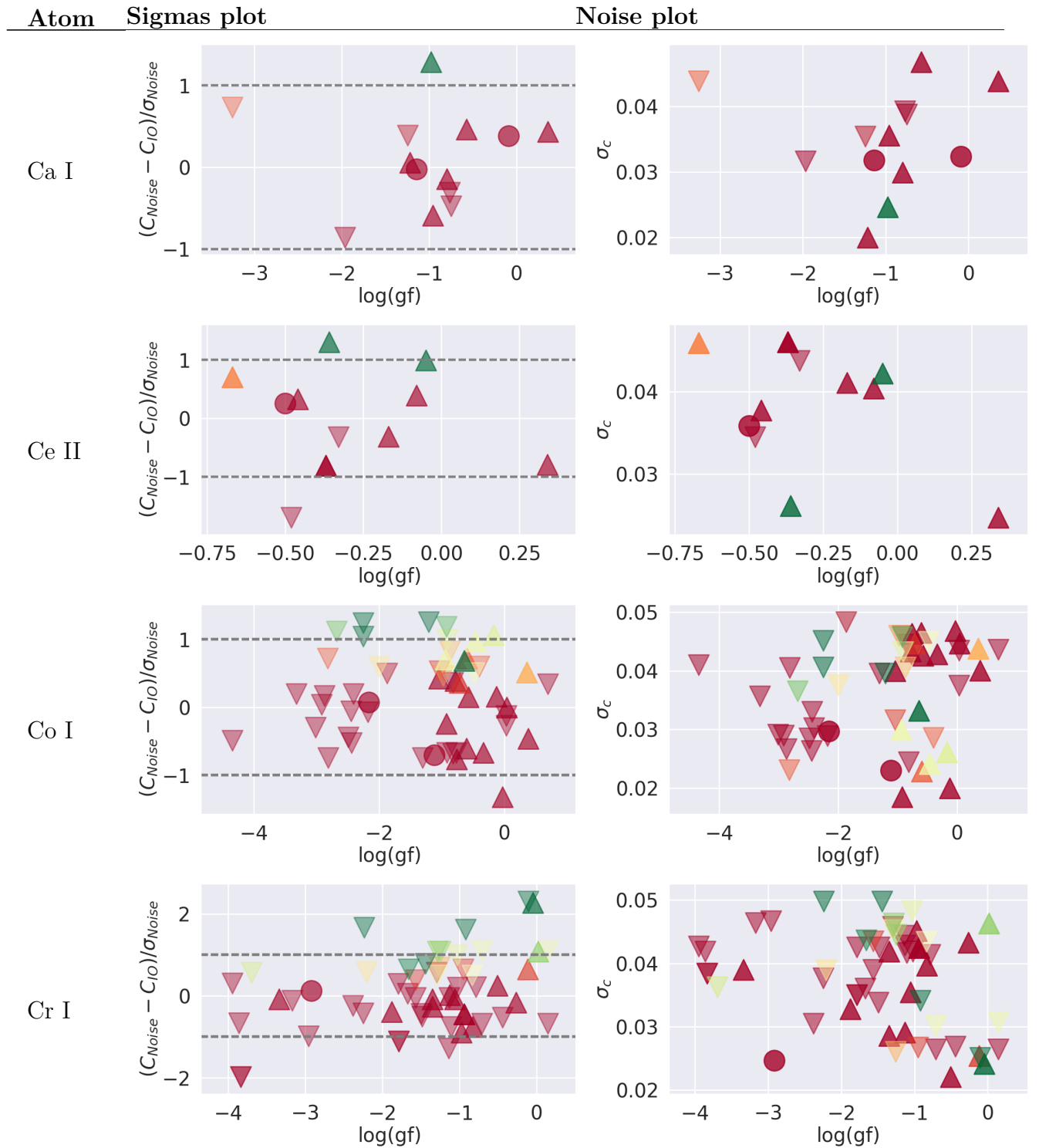
Parameter name	Value
N_pixs	700
N_shifts	2500
cut_order	100
delta_max_shift	1
dlt_epochs	0
do_1stdopp	True
doppler_pixs	500
dtransit	0.07408328592
error_gain	2.09
general_warnings	WARNING: Your data is not equally spaced.
in_epochs	30
indexFWHM	14
interpolate_ref	True
merge_epoch_as	['0:2', '2', '3:5', '5:7', '7:10', '11:15', '15:19', '19:23', '23:27', '27:31', '31:34', '34:37', '37:40', '42:45', '45:48', '48:51', '52:54', '54:56']
n_binning	3
n_epoch_merge	0
n_epochs	56
near_indline	28
near_tolerance	0.001
norm_high	3.5
norm_min_pixs	1
norm_polyorder	3
norm_width	5
normalize_hists	False
orders	17
orders_length	0.024220238919095957
period	2.4706132
plot_time_binning	0
radial_velocity	7.22
redf_loops	3000
redfield_bins	50
renorm_scale	1
smart_merge	True
t_start	54216.51120035792
t_transit	2456230.598
telescope	keck
tell_only_out	False
test_boundary	0.05
test_percent	0.7
test_pixs_near	15
test_times_near	10
test_var_amplitude	0.06
test_var_mu	0.06
time_average_corr	True
times_indline	2
wave_binning	0

E.2.1. Object information:

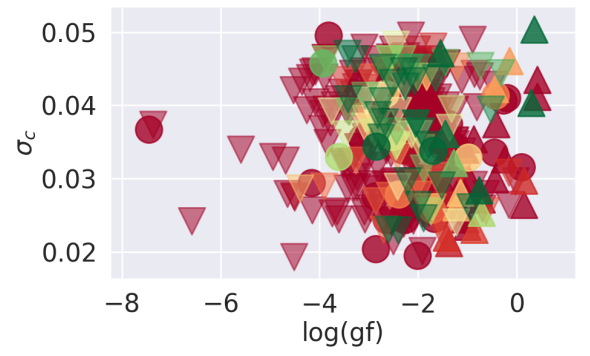
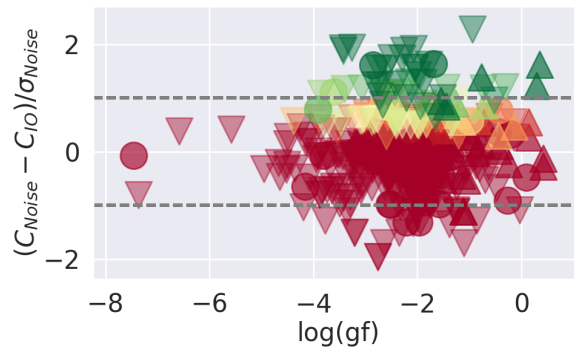
Parameter name	Value
TELESCOP	Keck I
INSTRUME	HIRES: High Resolution Echelle
OBJECT	Spectrometer object (Flux)
DATE	2007-04-26T11:13:32

E.3. Elements with detections

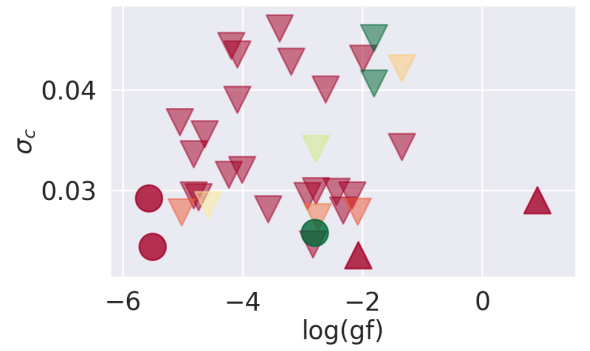
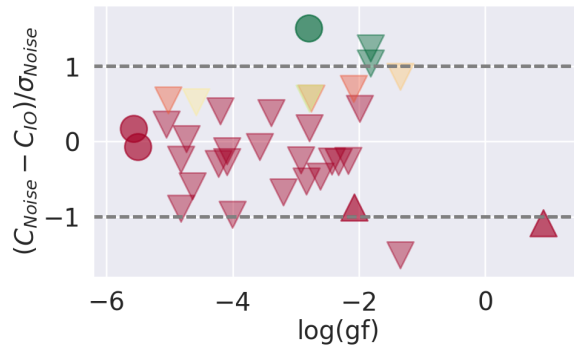
E.3.1. 0.75 angstrom band



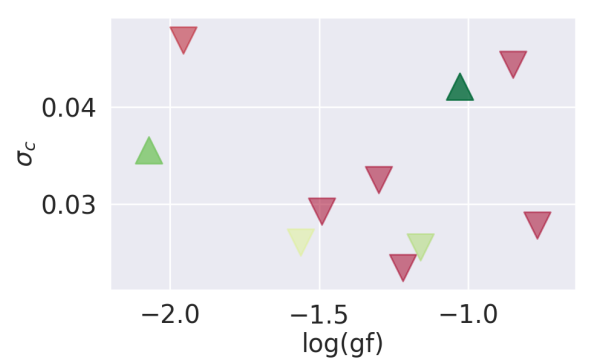
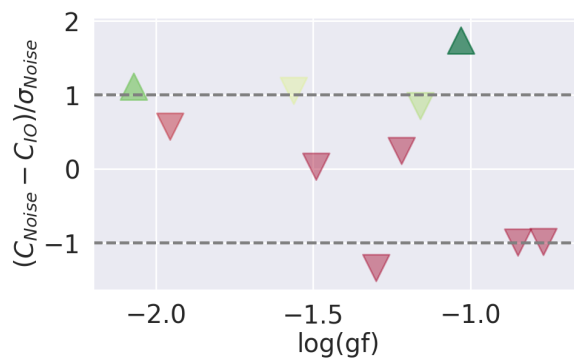
Fe I



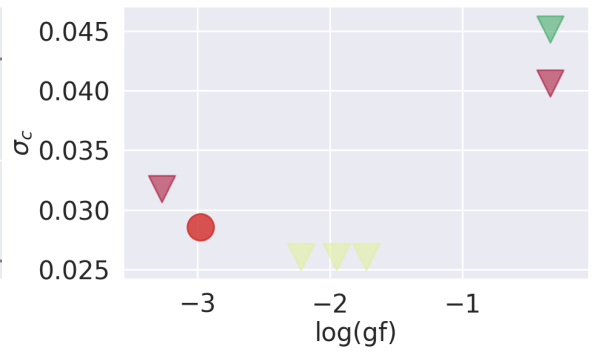
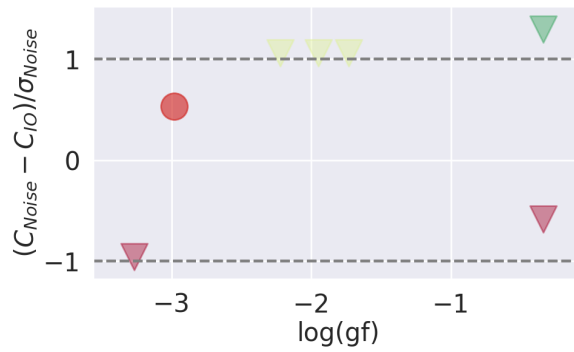
Fe II



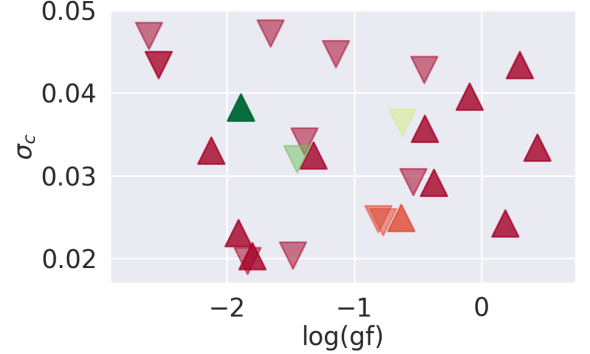
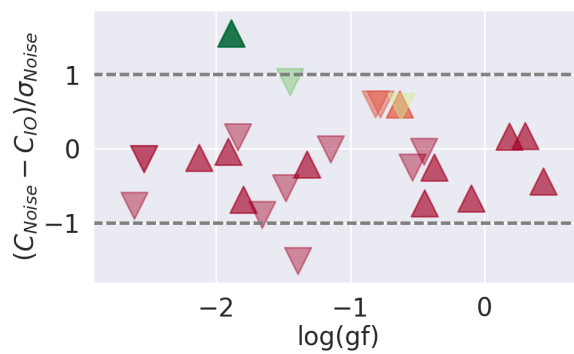
La II

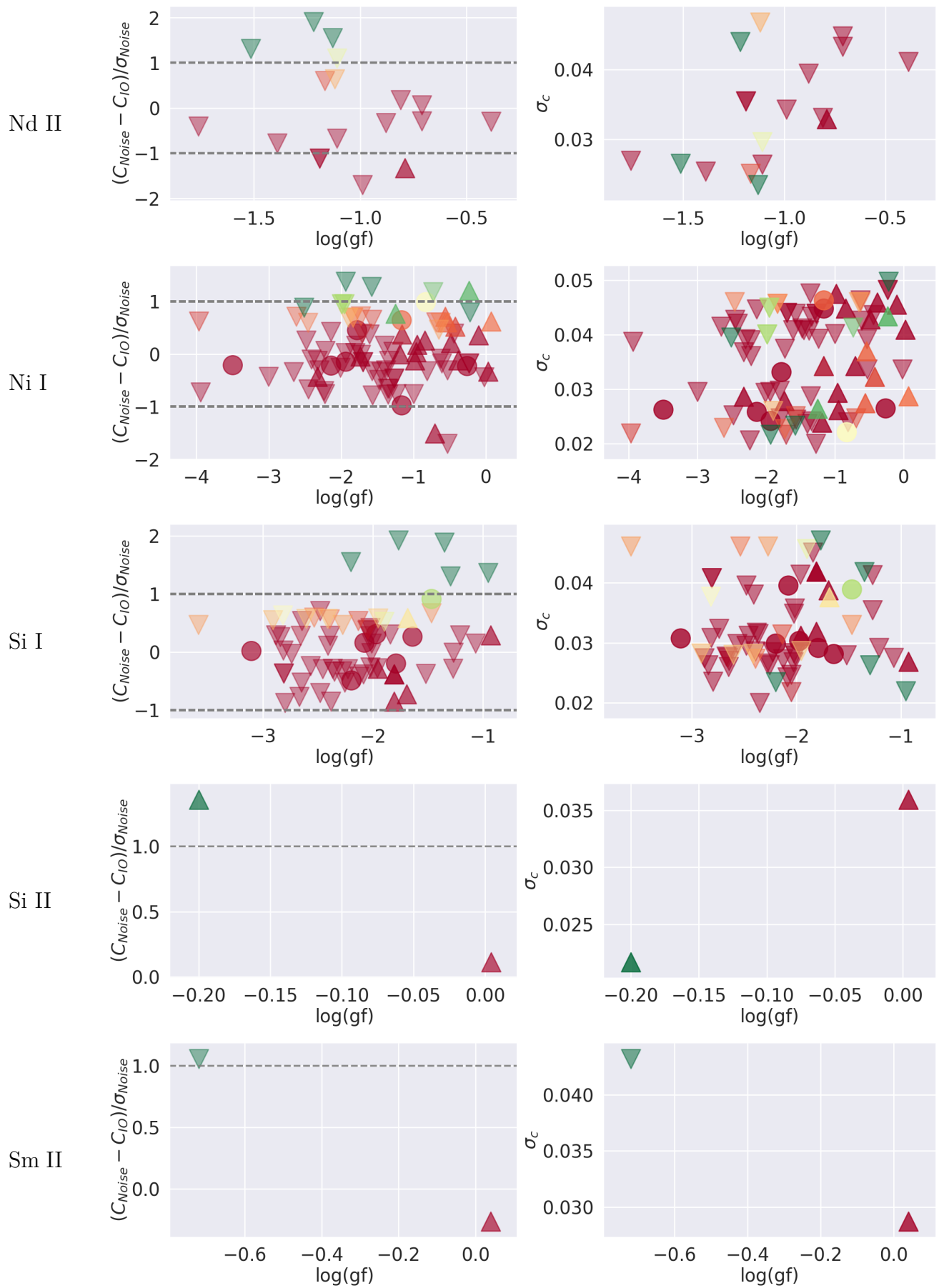


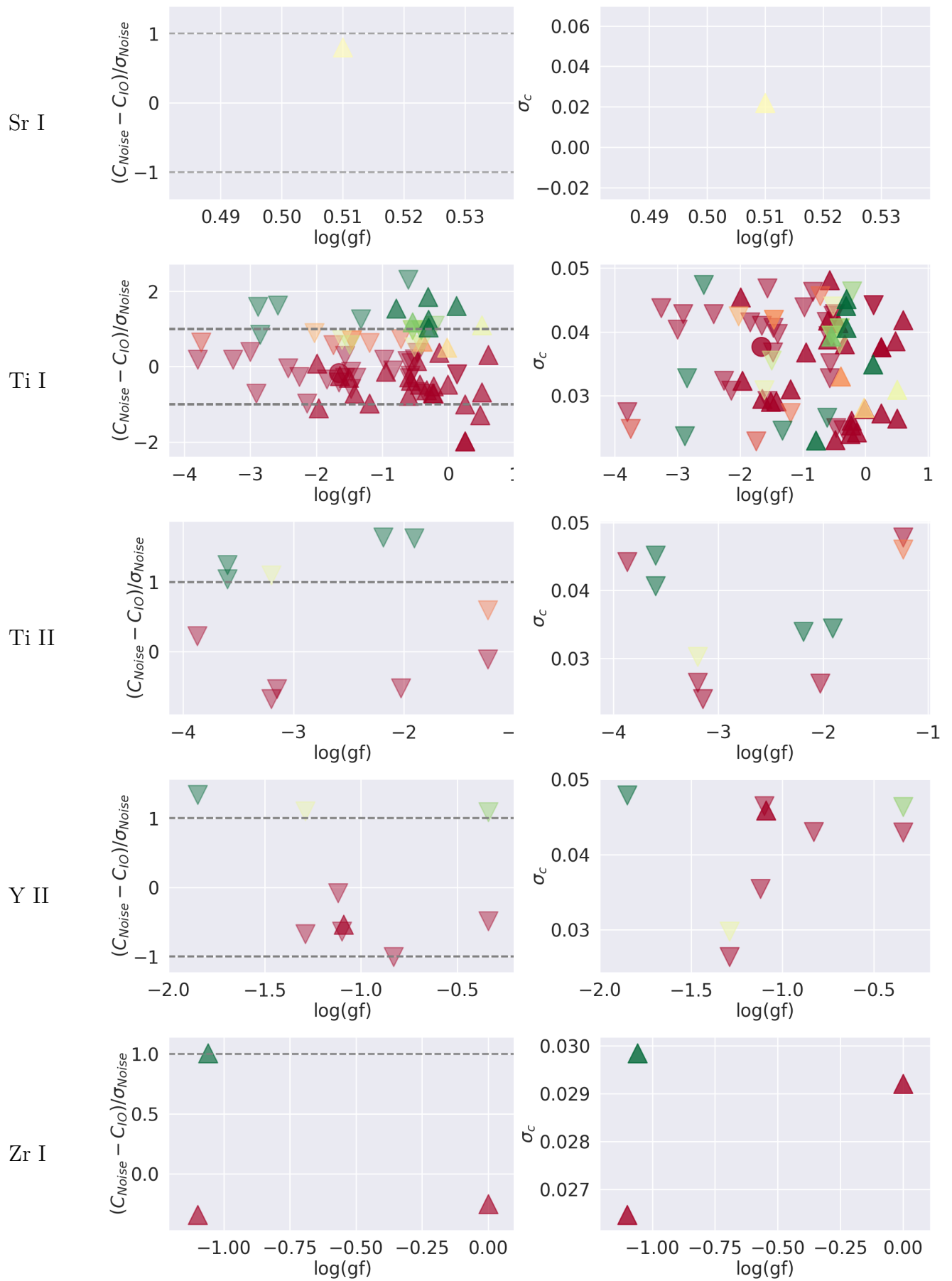
Mg I



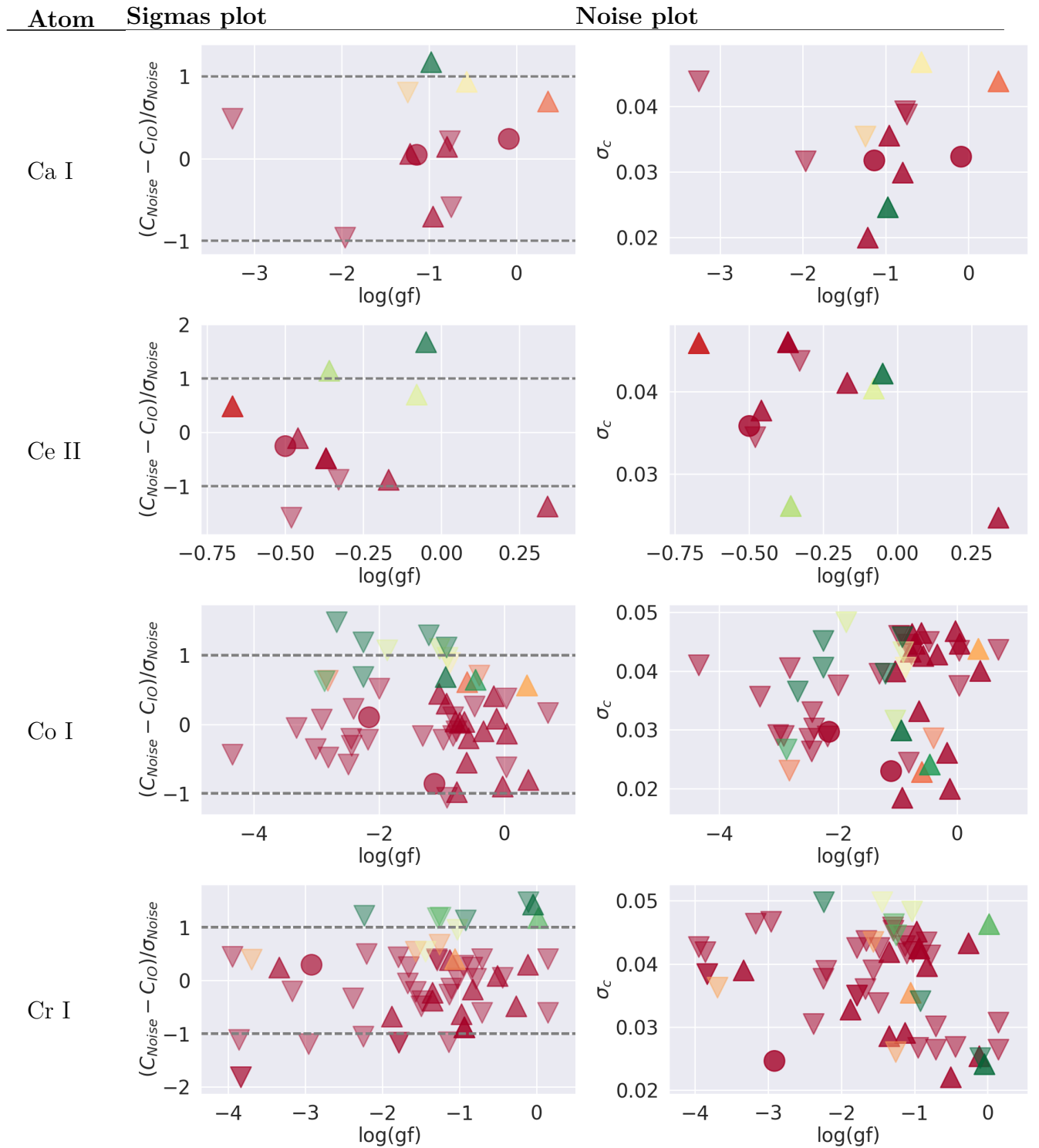
Mn I



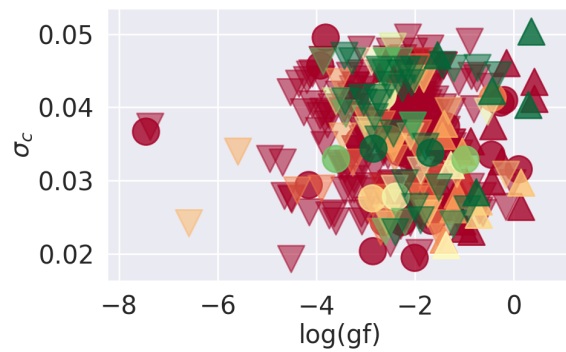
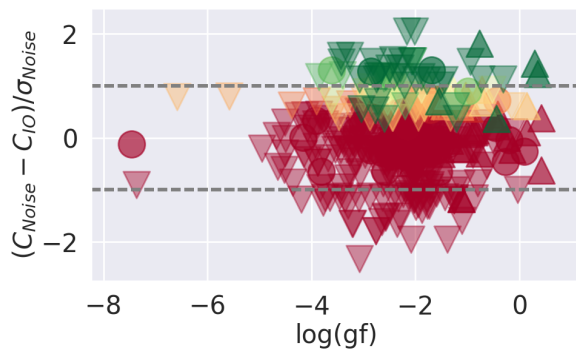




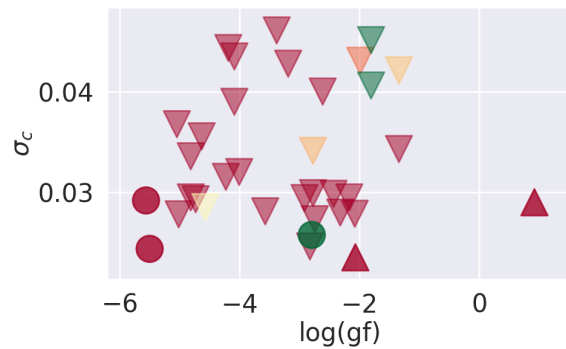
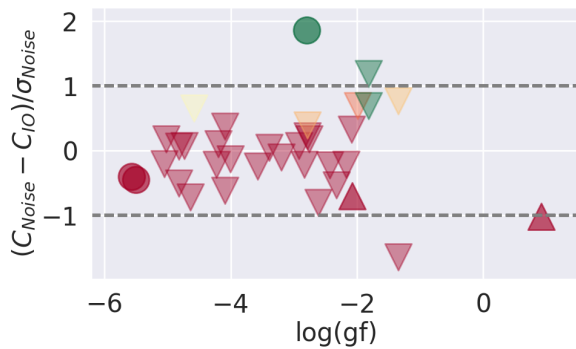
E.3.2. 1.0 angstrom band



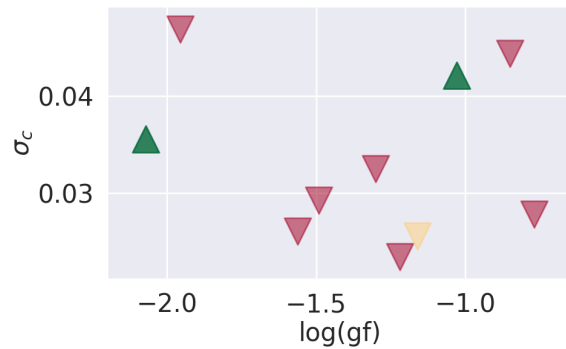
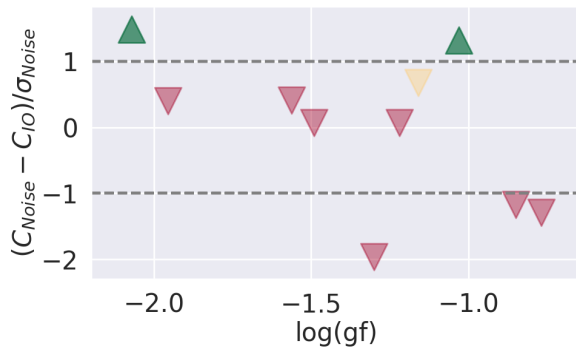
Fe I



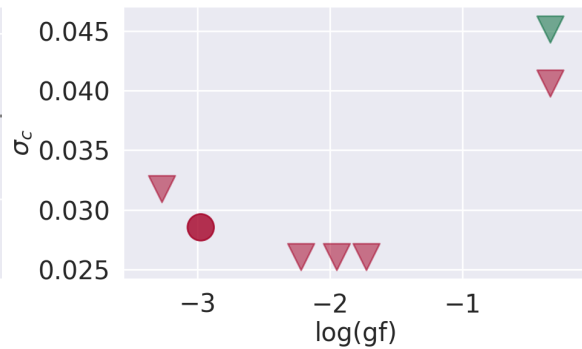
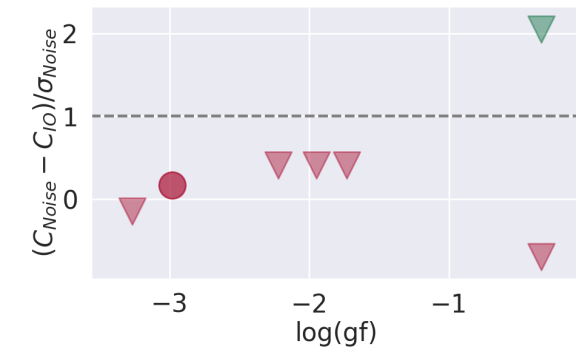
Fe II



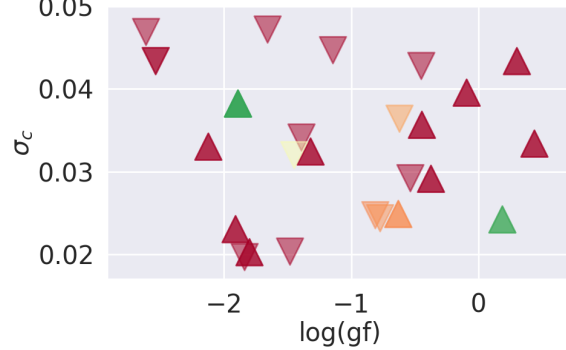
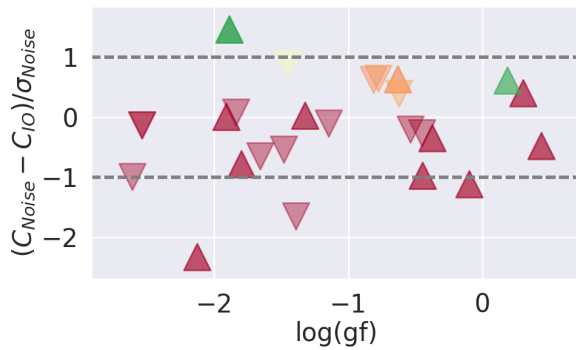
La II

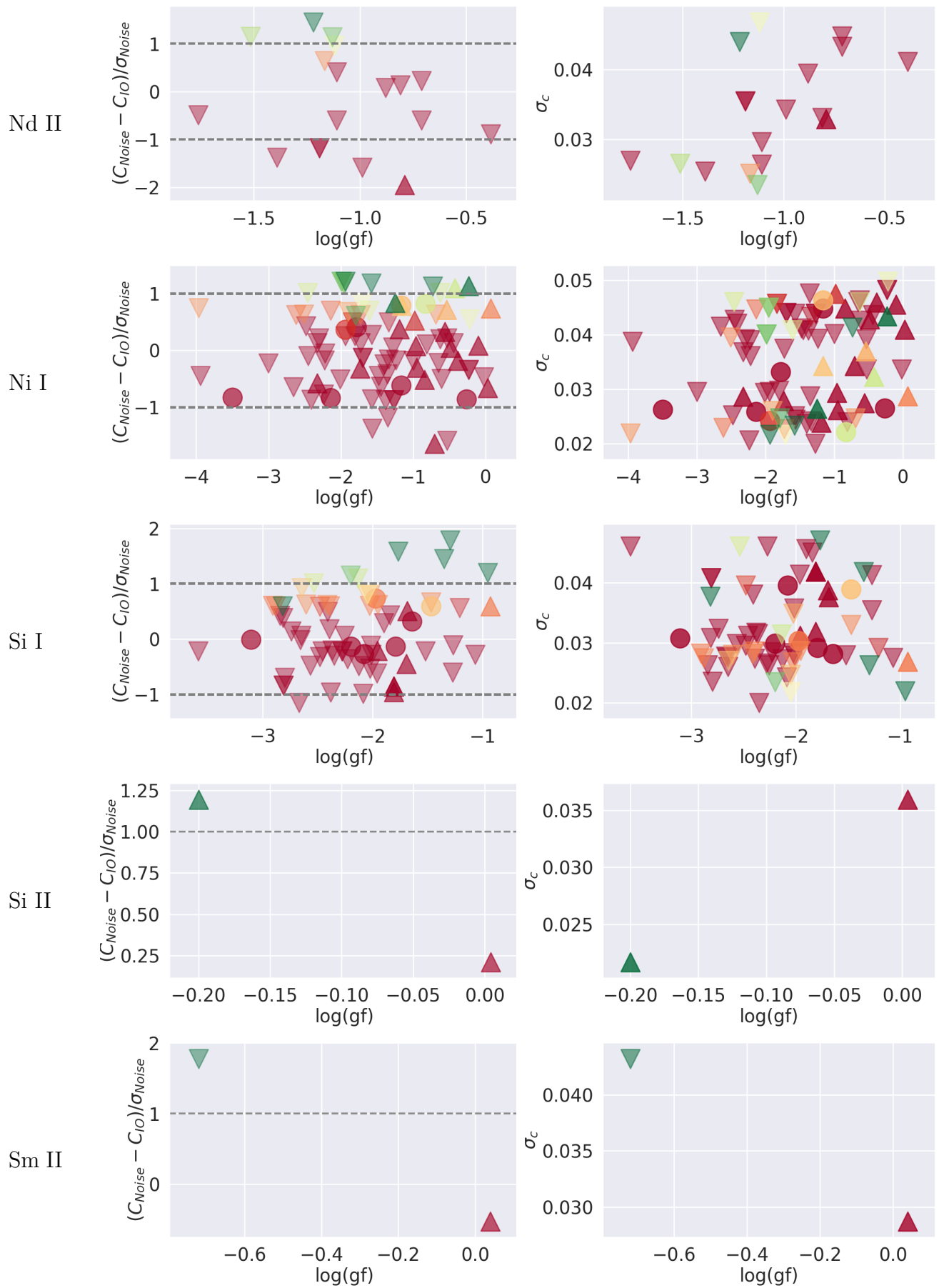


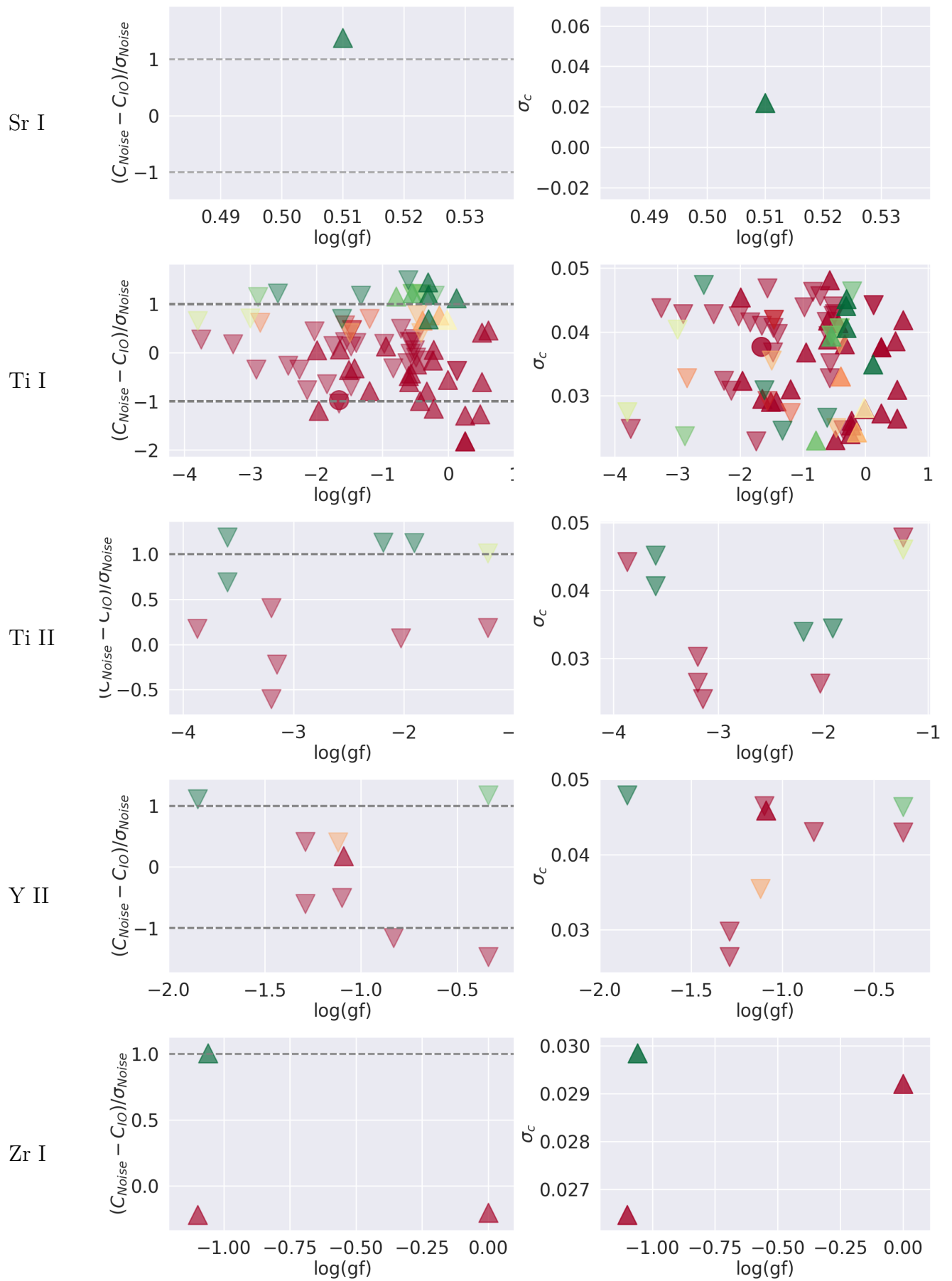
Mg I



Mn I







E.4. Detected elements transitions

E.4.1. 0.75 angstrom band

Atom		$\lambda_{lab}(\lambda_{obs})$	log(gf)	normed depth	σ_{In-Out}	σ_{rel}	σ_c
Ca I	△	5588.749(.206)	0.36	0.66	0.69	0.44	0.044
	○	6162.173(.855)	-0.09	0.37	0.69	0.39	0.032
	△	5590.114(.184)	-0.57	0.71	0.99	0.47	0.047
	△	6169.042(8.025)	-0.8	0.42	-0.27	-0.15	0.03
	△	5733.015(.231)	-0.96	0.38	-1.61	-0.59	0.036
	△	4995.167(.428)	-0.98	0.65	4.81	1.29	0.025
	○	6166.439(.948)	-1.14	0.24	-0.18	-0.02	0.032
	△	6360.298(.31)	-1.22	0.41	0.2	0.06	0.02
Ce II	△	4971.494(.203)	0.34	0.51	-2.23	-0.79	0.025
	△	5117.169(6.727)	-0.05	0.52	4.17	0.99	0.042
	△	5468.371(7.786)	-0.08	0.49	0.83	0.39	0.04
	△	5076.485(.056)	-0.17	0.65	-0.79	-0.31	0.041
	△	4943.441(.749)	-0.36	0.52	3.14	1.31	0.026
	△	5512.064(1.385)	-0.37	0.48	-2.67	-0.8	0.046
	△	5512.064(1.385)	-0.37	0.48	-2.67	-0.8	0.046
	△	5975.818(6.891)	-0.46	0.38	0.85	0.33	0.038
	○	6043.373(.65)	-0.5	0.26	0.69	0.26	0.036
	△	5518.489(.239)	-0.67	0.34	1.49	0.7	0.046
	△	5518.489(.239)	-0.67	0.34	1.49	0.7	0.046
	Co I	△	5362.774(.982)	0.38	0.43	-0.91	-0.46
△		5508.385(.194)	0.36	0.72	1.63	0.52	0.044
△		5508.385(.194)	0.36	0.72	1.63	0.52	0.044
△		5341.325(.311)	0.04	0.76	-0.16	-0.0	0.045

	△	5381.768(2.191)	-0.03	0.39	-4.38	-1.32	0.047
	△	6347.846(8.718)	-0.12	0.2	0.25	0.15	0.02
	△	6320.416(9.65)	-0.17	0.51	2.16	1.06	0.026
	△	5283.484(.153)	-0.34	0.69	-1.7	-0.67	0.043
	△	6232.383(.33)	-0.46	0.63	2.09	0.97	0.024
	△	5636.123(5.391)	-0.57	0.47	0.21	0.15	0.043
	△	6271.468(.828)	-0.6	0.31	1.36	0.72	0.023
	△	5206.037(5.877)	0.02	0.79	2.47	1.09	0.046
	△	4973.328(2.629)	-0.05	0.41	4.73	2.27	0.024
	△	4967.976(.363)	-0.12	0.66	1.26	0.65	0.025
	△	5694.731(5.098)	-0.27	0.31	-0.4	-0.17	0.043
Cr I	△	6263.095(2.712)	-0.51	0.29	0.42	0.25	0.022
	△	5642.358(.384)	-0.83	0.44	-1.56	-0.75	0.04
	△	5032.548(.311)	-0.94	0.51	-1.22	-0.45	0.043
	△	5032.548(.311)	-0.94	0.51	-1.22	-0.45	0.043
	△	5420.054(.166)	-0.97	0.53	-3.5	-0.9	0.045
	△	5729.206(8.57)	-1.06	0.22	-0.38	-0.09	0.035
	△	6172.046(.078)	-1.13	0.44	-0.03	0.02	0.029
	△	5133.681(2.771)	0.41	0.52	-0.86	-0.27	0.041
	△	5133.681(2.791)	0.41	0.55	-0.26	-0.13	0.044
	△	5367.466(6.273)	0.35	0.55	3.29	1.62	0.05
	△	5364.858(.264)	0.29	0.51	3.02	1.23	0.04
Fe I	△	4982.499(3.035)	0.14	0.69	1.17	0.55	0.03
	△	4982.499(3.05)	0.14	0.62	0.85	0.27	0.026
	○	6024.049(3.316)	0.09	0.49	-1.29	-0.47	0.032
	△	5125.112(.049)	-0.14	0.63	1.54	0.47	0.046
	○	5984.815(5.222)	-0.2	0.37	0.45	0.32	0.041

	△	5014.941(5.509)	-0.25	0.68	-0.23	-0.23	0.033
	○	5633.946(4.432)	-0.27	0.31	-2.21	-0.91	0.041
	△	5001.959(.642)	0.92	0.46	-2.55	-1.08	0.029
	△	6331.954(2.426)	-2.07	0.18	-2.09	-0.87	0.024
Fe II	○	6179.384(8.391)	-2.8	0.37	4.9	1.51	0.026
	○	6219.565(.328)	-5.51	0.04	-0.32	-0.07	0.024
	○	6307.529(.651)	-5.57	0.14	0.38	0.17	0.029
	△	5114.559(.772)	-1.03	0.36	4.22	1.74	0.042
La II	△	5936.21(.19)	-2.07	0.52	2.54	1.11	0.036
Mg I	○	6287.63(.788)	-2.98	0.11	1.19	0.53	0.029
	△	5017.638(.459)	0.44	0.43	-1.39	-0.44	0.033
	△	5308.921(.726)	0.3	0.47	0.54	0.18	0.043
	△	4974.345(.383)	0.19	0.56	0.74	0.17	0.024
	△	5020.715(1.317)	-0.1	0.55	-1.47	-0.67	0.04
	△	5008.058(.533)	-0.38	0.75	-0.6	-0.25	0.029
Mn I	△	5495.915(6.275)	-0.45	0.26	-1.71	-0.73	0.036
	△	4998.126(.127)	-0.63	0.31	1.28	0.6	0.025
	△	6014.374(5.033)	-1.32	0.41	-0.49	-0.21	0.032
	△	6382.187(.362)	-1.8	0.27	-1.39	-0.68	0.02
	△	5029.796(.41)	-1.89	0.49	3.0	1.56	0.038
	△	5029.796(.41)	-1.89	0.49	3.0	1.56	0.038
Nd II	△	4987.16(6.84)	-0.79	0.64	-2.78	-1.32	0.033
	△	4980.166(9.886)	0.07	0.6	1.4	0.62	0.029
	△	5084.089(.643)	0.03	0.65	-0.9	-0.33	0.041
	△	5099.927(0.013)	-0.1	0.65	0.79	0.36	0.046
	△	5142.775(3.074)	-0.23	0.43	2.65	1.2	0.043
Ni I	○	6176.807(.949)	-0.26	0.27	-0.48	-0.23	0.027

	△	5048.843(9.738)	-0.38	0.5	-0.47	-0.12	0.046
	△	6086.276(.827)	-0.42	0.26	1.24	0.52	0.032
	△	5663.975(.957)	-0.48	0.53	0.54	0.21	0.043
	△	5082.339(1.824)	-0.54	0.58	1.35	0.61	0.037
	△	6175.36(4.934)	-0.56	0.39	1.32	0.71	0.027
	△	5018.278(.867)	-0.7	0.54	-4.44	-1.51	0.034
	△	6254.188(.151)	-0.93	0.58	0.7	0.29	0.027
	○	5810.768(.683)	-1.47	0.25	2.35	0.92	0.039
	○	6299.599(.428)	-1.64	0.42	0.79	0.27	0.028
	△	5915.494(.709)	-1.69	0.54	1.85	0.59	0.038
Si I	△	5795.0(.42)	-1.69	0.26	-1.8	-0.73	0.039
	○	6308.825(.397)	-1.79	0.19	-0.29	-0.2	0.029
	△	6087.805(.854)	-1.81	0.26	-1.75	-0.85	0.032
	△	5502.939(.871)	-1.81	0.68	-1.14	-0.38	0.042
	△	5502.939(.871)	-1.81	0.68	-1.14	-0.38	0.042
	△	6112.928(.66)	-1.96	0.23	-0.75	-0.28	0.031
	○	6076.925(.957)	-1.98	0.05	-0.28	0.31	0.03
Si II	△	5978.93(.316)	0.0	0.36	0.38	0.11	0.036
	△	6371.371(.08)	-0.2	0.12	4.95	1.36	0.022
Sm II	△	6104.781(.284)	0.04	0.63	-0.58	-0.26	0.029
Sr I	△	6408.459(9.642)	0.51	0.46	1.98	0.8	0.022
	△	5785.976(6.785)	0.6	0.32	0.69	0.31	0.042
	△	4981.731(.464)	0.5	0.6	2.09	1.1	0.031
	△	4981.731(.456)	0.5	0.55	-1.58	-0.67	0.026
	△	5774.027(3.615)	0.48	0.4	-2.43	-1.29	0.039
Ti I	△	5025.57(6.14)	0.25	0.44	-4.06	-1.97	0.038
	△	5025.57(6.14)	0.25	0.44	-4.06	-1.97	0.038

	△	4999.503(.507)	0.25	0.34	-2.55	-0.99	0.027
	△	5013.28(.373)	0.12	0.76	4.78	1.61	0.035
	△	6098.658(.236)	-0.01	0.21	-1.03	-0.47	0.028
	△	5000.99(.794)	-0.02	0.63	1.78	0.51	0.028
	△	6220.474(.858)	-0.14	0.48	0.96	0.37	0.024
Y II	△	5544.611(.251)	-1.09	0.4	-0.04	-0.54	0.046
	△	6304.341(.101)	0.0	0.44	-0.5	-0.25	0.029
Zr I	△	6127.475(.782)	-1.06	0.11	3.15	1.01	0.03
	△	6143.252(.293)	-1.1	0.66	-0.8	-0.34	0.026

E.4.2. 1.0 angstrom band

Atom		$\lambda_{lab}(\lambda_{obs})$	$\log(gf)$	normed depth	σ_{In-Out}	σ_{rel}	σ_c
Ca I	△	5588.749(.206)	0.36	0.66	1.38	0.7	0.044
	○	6162.173(.855)	-0.09	0.37	0.8	0.24	0.032
	△	5590.114(.184)	-0.57	0.71	1.89	0.94	0.047
	△	6169.042(8.025)	-0.8	0.42	0.33	0.15	0.03
	△	5733.015(.231)	-0.96	0.38	-1.47	-0.7	0.036
	△	4995.167(.428)	-0.98	0.65	4.66	1.18	0.025
	○	6166.439(.948)	-1.14	0.24	-0.12	0.05	0.032
	△	6360.298(.31)	-1.22	0.41	0.17	0.06	0.02
Ce II	△	4971.494(.203)	0.34	0.51	-4.43	-1.37	0.025
	△	5117.169(6.727)	-0.05	0.52	3.62	1.68	0.042
	△	5468.371(7.786)	-0.08	0.49	2.16	0.71	0.04
	△	5076.485(.056)	-0.17	0.65	-1.31	-0.87	0.041
	△	4943.441(.749)	-0.36	0.52	2.35	1.15	0.026
	△	5512.064(1.385)	-0.37	0.48	-1.67	-0.47	0.046
	△	5512.064(1.385)	-0.37	0.48	-1.67	-0.47	0.046
	△	5975.818(6.891)	-0.46	0.38	-0.11	-0.1	0.038
	○	6043.373(.65)	-0.5	0.26	0.23	-0.25	0.036
	△	5518.489(.239)	-0.67	0.34	1.15	0.48	0.046
△	5518.489(.239)	-0.67	0.34	1.15	0.48	0.046	
Co I	△	5362.774(.982)	0.38	0.43	-1.7	-0.8	0.04
	△	5508.385(.194)	0.36	0.72	1.61	0.57	0.044
	△	5508.385(.194)	0.36	0.72	1.61	0.57	0.044
	△	5341.325(.311)	0.04	0.76	-0.16	-0.13	0.045
	△	5381.768(2.191)	-0.03	0.39	-2.33	-0.89	0.047

	△	6347.846(8.718)	-0.12	0.2	0.18	0.09	0.02
	△	6320.416(9.65)	-0.17	0.51	0.84	0.41	0.026
	△	5283.484(.153)	-0.34	0.69	-0.49	-0.1	0.043
	△	6232.383(.33)	-0.46	0.63	2.8	0.64	0.024
	△	5636.123(5.391)	-0.57	0.47	-0.01	-0.2	0.043
	△	6271.468(.828)	-0.6	0.31	1.39	0.62	0.023
<hr/>							
	△	5206.037(5.877)	0.02	0.79	2.63	1.18	0.046
	△	4973.328(2.629)	-0.05	0.41	3.82	1.43	0.024
	△	4967.976(.363)	-0.12	0.66	0.39	0.3	0.025
	△	5694.731(5.098)	-0.27	0.31	-1.19	-0.48	0.043
Cr I	△	6263.095(2.712)	-0.51	0.29	0.17	0.09	0.022
	△	5642.358(.384)	-0.83	0.44	-1.01	-0.17	0.04
	△	5032.548(.311)	-0.94	0.51	-1.98	-0.88	0.043
	△	5032.548(.311)	-0.94	0.51	-1.98	-0.88	0.043
	△	5420.054(.166)	-0.97	0.53	-2.85	-0.63	0.045
	△	5729.206(8.57)	-1.06	0.22	1.55	0.41	0.035
	△	6172.046(.078)	-1.13	0.44	0.84	0.38	0.029
<hr/>							
	△	5133.681(2.771)	0.41	0.52	-2.79	-0.62	0.041
	△	5133.681(2.791)	0.41	0.55	0.79	0.38	0.044
	△	5367.466(6.273)	0.35	0.55	3.06	1.24	0.05
	△	5364.858(.264)	0.29	0.51	3.35	1.43	0.04
Fe I	△	4982.499(3.05)	0.14	0.62	0.27	0.11	0.026
	△	4982.499(3.035)	0.14	0.69	1.69	0.62	0.03
	○	6024.049(3.316)	0.09	0.49	-0.73	-0.26	0.032
	△	5125.112(.049)	-0.14	0.63	-1.05	-0.22	0.046
	○	5984.815(5.222)	-0.2	0.37	-0.05	-0.04	0.041
	△	5014.941(5.509)	-0.25	0.68	0.11	0.0	0.033

	○	5633.946(4.432)	-0.27	0.31	-1.15	-0.46	0.041
	△	5001.959(.642)	0.92	0.46	-2.41	-1.02	0.029
	△	6331.954(2.426)	-2.07	0.18	-1.68	-0.7	0.024
Fe II	○	6179.384(8.391)	-2.8	0.37	4.65	1.87	0.026
	○	6219.565(.328)	-5.51	0.04	-1.1	-0.45	0.024
	○	6307.529(.651)	-5.57	0.14	-0.97	-0.4	0.029
	△	5114.559(.772)	-1.03	0.36	3.08	1.32	0.042
La II	△	5936.21(.19)	-2.07	0.52	3.56	1.49	0.036
Mg I	○	6287.63(.788)	-2.98	0.11	0.52	0.16	0.029
	△	5017.638(.459)	0.44	0.43	-1.4	-0.47	0.033
	△	5308.921(.726)	0.3	0.47	0.98	0.41	0.043
	△	4974.345(.383)	0.19	0.56	2.7	0.61	0.024
	△	5020.715(1.317)	-0.1	0.55	-2.52	-1.11	0.04
	△	5008.058(.533)	-0.38	0.75	-0.93	-0.35	0.029
Mn I	△	5495.915(6.275)	-0.45	0.26	-1.9	-0.97	0.036
	△	4998.126(.127)	-0.63	0.31	1.5	0.63	0.025
	△	6014.374(5.033)	-1.32	0.41	0.19	0.03	0.032
	△	6382.187(.362)	-1.8	0.27	-1.84	-0.78	0.02
	△	5029.796(.41)	-1.89	0.49	2.72	1.47	0.038
	△	5029.796(.41)	-1.89	0.49	2.72	1.47	0.038
Nd II	△	4987.16(6.84)	-0.79	0.64	-4.71	-1.94	0.033
	△	4980.166(9.886)	0.07	0.6	1.46	0.74	0.029
	△	5084.089(.643)	0.03	0.65	-1.38	-0.66	0.041
	△	5099.927(0.013)	-0.1	0.65	0.47	0.09	0.046
	△	5142.775(3.074)	-0.23	0.43	3.98	1.14	0.043
Ni I	○	6176.807(.949)	-0.26	0.27	-2.03	-0.86	0.027
	△	5048.843(9.738)	-0.38	0.5	-0.51	-0.18	0.046

	△	6086.276(.827)	-0.42	0.26	2.25	1.1	0.032
	△	5663.975(.957)	-0.48	0.53	0.15	0.05	0.043
	△	5082.339(1.824)	-0.54	0.58	1.61	0.72	0.037
	△	6175.36(4.934)	-0.56	0.39	0.85	0.33	0.027
	△	5018.278(.867)	-0.7	0.54	-6.26	-1.64	0.034
	△	6254.188(.151)	-0.93	0.58	1.43	0.6	0.027
	○	5810.768(.683)	-1.47	0.25	1.67	0.59	0.039
	○	6299.599(.428)	-1.64	0.42	0.8	0.32	0.028
	△	5915.494(.709)	-1.69	0.54	0.89	0.51	0.038
Si I	△	5795.0(.42)	-1.69	0.26	-1.48	-0.45	0.039
	○	6308.825(.397)	-1.79	0.19	-0.31	-0.13	0.029
	△	6087.805(.854)	-1.81	0.26	-2.18	-0.96	0.032
	△	5502.939(.871)	-1.81	0.68	-3.06	-0.85	0.042
	△	5502.939(.871)	-1.81	0.68	-3.06	-0.85	0.042
	△	6112.928(.66)	-1.96	0.23	-0.32	-0.21	0.031
	○	6076.925(.957)	-1.98	0.05	1.43	0.74	0.03
Si II	△	5978.93(.316)	0.0	0.36	0.71	0.21	0.036
	△	6371.371(.08)	-0.2	0.12	3.75	1.2	0.022
Sm II	△	6104.781(.284)	0.04	0.63	-0.97	-0.52	0.029
Sr I	△	6408.459(9.642)	0.51	0.46	3.57	1.38	0.022
	△	5785.976(6.785)	0.6	0.32	0.96	0.46	0.042
	△	4981.731(.464)	0.5	0.6	0.91	0.41	0.031
	△	4981.731(.456)	0.5	0.55	-1.54	-0.6	0.026
	△	5774.027(3.615)	0.48	0.4	-2.89	-1.27	0.039
Ti I	△	4999.503(.507)	0.25	0.34	-3.27	-1.29	0.027
	△	5025.57(6.14)	0.25	0.44	-4.01	-1.82	0.038
	△	5025.57(6.14)	0.25	0.44	-4.01	-1.82	0.038

	△	5013.28(.373)	0.12	0.76	3.29	1.12	0.035
	△	6098.658(.236)	-0.01	0.21	-1.19	-0.56	0.028
	△	5000.99(.794)	-0.02	0.63	1.95	0.68	0.028
	△	6220.474(.858)	-0.14	0.48	1.62	0.77	0.024
Y II	△	5544.611(.251)	-1.09	0.4	0.69	0.18	0.046
	△	6304.341(.101)	0.0	0.44	-0.36	-0.2	0.029
Zr I	△	6127.475(.782)	-1.06	0.11	3.29	1.01	0.03
	△	6143.252(.293)	-1.1	0.66	-1.23	-0.22	0.026

Bibliography

- S. Albrecht, I. Snellen, E. de Mooij, and R. Le Poole. Ground-based detections of sodium in HD 209458b's atmosphere in two data sets. In Frédéric Pont, Dimitar Sasselov, and Matthew J. Holman, editors, *Transiting Planets*, volume 253 of *IAU Symposium*, pages 520–523, February 2009. doi: 10.1017/S1743921308027105.
- R. Allart, V. Bourrier, C. Lovis, D. Ehrenreich, J. Aceituno, A. Guizarro, F. Pepe, D. K. Sing, J. J. Spake, and A. Wyttenbach. High-resolution confirmation of an extended helium atmosphere around WASP-107b. *A&A*, 623:A58, March 2019. doi: 10.1051/0004-6361/201834917.
- N. Astudillo-Defru and P. Rojo. Ground-based detection of calcium and possibly scandium and hydrogen in the atmosphere of HD 209458b. *A&A*, 557:A56, Sep 2013. doi: 10.1051/0004-6361/201219018.
- L. Ben-Jaffel and G. E. Ballester. Hubble Space Telescope detection of oxygen in the atmosphere of exoplanet HD 189733b. *A&A*, 553:A52, May 2013. doi: 10.1051/0004-6361/201221014.
- Maya Ben-Yami, Nikku Madhusudhan, Samuel H. C. Cabot, Savvas Constantinou, Anjali Piette, Siddharth Gandhi, and Luis Welbanks. Neutral Cr and V in the Atmosphere of Ultra-hot Jupiter WASP-121 b. *ApJ*, 897(1):L5, July 2020. doi: 10.3847/2041-8213/ab94aa.
- Björn Benneke. Strict Upper Limits on the Carbon-to-Oxygen Ratios of Eight Hot Jupiters from Self-Consistent Atmospheric Retrieval. *arXiv e-prints*, art. arXiv:1504.07655, April 2015.
- Björn Benneke, Ian Wong, Caroline Piaulet, Heather A. Knutson, Joshua Lothringer, Caroline V. Morley, Ian J. M. Crossfield, Peter Gao, Thomas P. Greene, Courtney Dress-

- ing, Diana Dragomir, Andrew W. Howard, Peter R. McCullough, Eliza M. R. Kempton, Jonathan J. Fortney, and Jonathan Fraine. Water Vapor and Clouds on the Habitable-zone Sub-Neptune Exoplanet K2-18b. *ApJ*, 887(1):L14, December 2019. doi: 10.3847/2041-8213/ab59dc.
- V. Bourrier, A. Lecavelier des Etangs, H. Dupuy, D. Ehrenreich, A. Vidal-Madjar, G. Hébrard, G. E. Ballester, J. M. Désert, R. Ferlet, D. K. Sing, and P. J. Wheatley. Atmospheric escape from HD 189733b observed in H I Lyman- α : detailed analysis of HST/STIS September 2011 observations. *A&A*, 551:A63, March 2013. doi: 10.1051/0004-6361/201220533.
- N. Casasayas-Barris, E. Pallé, F. Yan, G. Chen, R. Luque, M. Stangret, E. Nagel, M. Zechmeister, M. Oshagh, J. Sanz-Forcada, L. Nortmann, F. J. Alonso-Floriano, P. J. Amado, J. A. Caballero, S. Czesla, S. Khalafinejad, M. López-Puertas, J. López-Santiago, K. Molaverdikhani, D. Montes, A. Quirrenbach, A. Reiners, I. Ribas, A. Sánchez-López, and M. R. Zapatero Osorio. Is there Na I in the atmosphere of HD 209458b?. Effect of the centre-to-limb variation and Rossiter-McLaughlin effect in transmission spectroscopy studies. *A&A*, 635:A206, March 2020. doi: 10.1051/0004-6361/201937221.
- David Charbonneau, Timothy M. Brown, Robert W. Noyes, and Ronald L. Gilliland. Detection of an Extrasolar Planet Atmosphere. *ApJ*, 568(1):377–384, Mar 2002. doi: 10.1086/338770.
- G. Chen, N. Casasayas-Barris, E. Pallé, F. Yan, M. Stangret, H. M. Cegla, R. Allart, and C. Lovis. Detection of Na, K, and H α absorption in the atmosphere of WASP-52b using ESPRESSO. *A&A*, 635:A171, March 2020. doi: 10.1051/0004-6361/201936986.
- Patricio E. Cubillos, Luca Fossati, Tommi Koskinen, Mitchell E. Young, Michael Salz, Kevin France, A. G. Sreejith, and Carole A. Haswell. Near-ultraviolet Transmission Spectroscopy of HD 209458b: Evidence of Ionized Iron Beyond the Planetary Roche Lobe. *AJ*, 159(3): 111, March 2020. doi: 10.3847/1538-3881/ab6a0b.
- Xavier Dumusque, Aldo S. Bonomo, Raphaëlle D. Haywood, Luca Malavolta, Damien Ségransan, Lars A. Buchhave, Andrew Collier Cameron, David W. Latham, Emilio Molinari, Francesco Pepe, Stéphane Udry, David Charbonneau, Rosario Cosentino, Courtney D. Dressing, Pedro Figueira, Aldo F. M. Fiorenzano, Sara Gettel, Avet Harutyunyan,

- Keith Horne, Mercedes Lopez-Morales, Christophe Lovis, Michel Mayor, Giusi Micela, Fatemeh Motalebi, Valerio Nascimbeni, David F. Phillips, Giampaolo Piotto, Don Pollacco, Didier Queloz, Ken Rice, Dimitar Sasselov, Alessandro Sozzetti, Andrew Szegedy, and Chris Watson. The Kepler-10 Planetary System Revisited by HARPS-N: A Hot Rocky World and a Solid Neptune-Mass Planet. *ApJ*, 789(2):154, July 2014. doi: 10.1088/0004-637X/789/2/154.
- François Fressin, Guillermo Torres, David Charbonneau, Stephen T. Bryson, Jessie Christiansen, Courtney D. Dressing, Jon M. Jenkins, Lucianne M. Walkowicz, and Natalie M. Batalha. The False Positive Rate of Kepler and the Occurrence of Planets. *ApJ*, 766(2): 81, April 2013. doi: 10.1088/0004-637X/766/2/81.
- Benjamin J. Fulton and Erik A. Petigura. The California-Kepler Survey. VII. Precise Planet Radii Leveraging Gaia DR2 Reveal the Stellar Mass Dependence of the Planet Radius Gap. *AJ*, 156(6):264, December 2018. doi: 10.3847/1538-3881/aae828.
- Benjamin J. Fulton, Erik A. Petigura, Andrew W. Howard, Howard Isaacson, Geoffrey W. Marcy, Phillip A. Cargile, Leslie Hebb, Lauren M. Weiss, John Asher Johnson, Timothy D. Morton, Evan Sinukoff, Ian J. M. Crossfield, and Lea A. Hirsch. The California-Kepler Survey. III. A Gap in the Radius Distribution of Small Planets. *AJ*, 154(3):109, September 2017. doi: 10.3847/1538-3881/aa80eb.
- Andrea Gebek and Apurva V. Oza. Alkaline Exospheres of Exoplanet Systems: Evaporative Transmission Spectra. *arXiv e-prints*, art. arXiv:2005.02536, May 2020.
- H. J. Hoeijmakers, R. J. de Kok, I. A. G. Snellen, M. Brogi, J. L. Birkby, and H. Schwarz. A search for TiO in the optical high-resolution transmission spectrum of HD 209458b: Hindrance due to inaccuracies in the line database. *A&A*, 575:A20, Mar 2015. doi: 10.1051/0004-6361/201424794.
- H. J. Hoeijmakers, D. Ehrenreich, D. Kitzmann, R. Allart, S. L. Grimm, J. V. Seidel, A. Wyttenbach, L. Pino, L. D. Nielsen, C. Fisher, P. B. Rimmer, V. Bourrier, H. M. Cegla, B. Lavie, C. Lovis, A. B. C. Patzer, J. W. Stock, F. A. Pepe, and Kevin Heng. A spectral survey of an ultra-hot Jupiter. Detection of metals in the transmission spectrum of KELT-9 b. *A&A*, 627:A165, July 2019. doi: 10.1051/0004-6361/201935089.
- H. Jens Hoeijmakers, David Ehrenreich, Kevin Heng, Daniel Kitzmann, Simon L. Grimm,

- Romain Allart, Russell Deitrick, Aurélien Wyttenbach, Maria Oreshenko, Lorenzo Pino, Paul B. Rimmer, Emilio Molinari, and Luca Di Fabrizio. Atomic iron and titanium in the atmosphere of the exoplanet KELT-9b. *Nature*, 560(7719):453–455, August 2018. doi: 10.1038/s41586-018-0401-y.
- H. Jens Hoeijmakers, Samuel H. C. Cabot, Lily Zhao, Lars A. Buchhave, René Tronsgaard, Daniel Kitzmann, Simon L. Grimm, Heather M. Cegla, Vincent Bourrier, David Ehrenreich, Kevin Heng, Christophe Lovis, and Debra A. Fischer. High-resolution Transmission Spectroscopy of MASCARA-2 b with EXPRES. *arXiv e-prints*, art. arXiv:2004.08415, April 2020.
- Andrew W. Howard, Geoffrey W. Marcy, John Asher Johnson, Debra A. Fischer, Jason T. Wright, Howard Isaacson, Jeff A. Valenti, Jay Anderson, Doug N. C. Lin, and Shigeru Ida. The Occurrence and Mass Distribution of Close-in Super-Earths, Neptunes, and Jupiters. *Science*, 330(6004):653, October 2010. doi: 10.1126/science.1194854.
- S. Khalafinejad, C. von Essen, H. J. Hoeijmakers, G. Zhou, T. Klocová, J. H. M. M. Schmitt, S. Dreizler, M. Lopez-Morales, T. O. Husser, T. O. B. Schmidt, and R. Collet. Exoplanetary atmospheric sodium revealed by orbital motion. Narrow-band transmission spectroscopy of HD 189733b with UVES. *A&A*, 598:A131, February 2017. doi: 10.1051/0004-6361/201629473.
- F. Kupka, N. Piskunov, T. A. Ryabchikova, H. C. Stempels, and W. W. Weiss. VALD-2: Progress of the Vienna Atomic Line Data Base. *A&AS*, 138:119–133, Jul 1999. doi: 10.1051/aas:1999267.
- M. Lendl, A. H. M. J. Triaud, D. R. Anderson, A. Collier Cameron, L. Delrez, A. P. Doyle, M. Gillon, C. Hellier, E. Jehin, P. F. L. Maxted, M. Neveu-VanMalle, F. Pepe, D. Pollacco, D. Queloz, D. Ségransan, B. Smalley, A. M. S. Smith, S. Udry, V. Van Grootel, and R. G. West. WASP-117b: a 10-day-period Saturn in an eccentric and misaligned orbit. *A&A*, 568:A81, August 2014. doi: 10.1051/0004-6361/201424481.
- Jack J. Lissauer, Daniel C. Fabrycky, Eric B. Ford, William J. Borucki, Francois Fressin, Geoffrey W. Marcy, Jerome A. Orosz, Jason F. Rowe, Guillermo Torres, William F. Welsh, Natalie M. Batalha, Stephen T. Bryson, Lars A. Buchhave, Douglas A. Caldwell, Joshua A. Carter, David Charbonneau, Jessie L. Christiansen, William D. Cochran,

- Jean-Michel Desert, Edward W. Dunham, Michael N. Fanelli, Jonathan J. Fortney, III Gautier, Thomas N., John C. Geary, Ronald L. Gilliland, Michael R. Haas, Jennifer R. Hall, Matthew J. Holman, David G. Koch, David W. Latham, Eric Lopez, Sean McCauliff, Neil Miller, Robert C. Morehead, Elisa V. Quintana, Darin Ragozzine, Dimitar Sasselov, Donald R. Short, and Jason H. Steffen. A closely packed system of low-mass, low-density planets transiting Kepler-11. *Nature*, 470(7332):53–58, February 2011. doi: 10.1038/nature09760.
- A. Lobel. Spectro web: oscillator strength measurements of atomic absorption lines in the sun and procyon. In *Journal of Physics Conference Series*, volume 130 of *Journal of Physics Conference Series*, page 012015, Oct 2008. doi: 10.1088/1742-6596/130/1/012015.
- Nikku Madhusudhan. Exoplanetary Atmospheres: Key Insights, Challenges and Prospects. *arXiv e-prints*, art. arXiv:1904.03190, Apr 2019.
- M. Mayor, M. Marmier, C. Lovis, S. Udry, D. Ségransan, F. Pepe, W. Benz, J. L. Bertaux, F. Bouchy, X. Dumusque, G. Lo Curto, C. Mordasini, D. Queloz, and N. C. Santos. The HARPS search for southern extra-solar planets XXXIV. Occurrence, mass distribution and orbital properties of super-Earths and Neptune-mass planets. *arXiv e-prints*, art. arXiv:1109.2497, September 2011.
- Michel Mayor and Didier Queloz. A Jupiter-mass companion to a solar-type star. *Nature*, 378(6555):355–359, Nov 1995. doi: 10.1038/378355a0.
- Christoph Mordasini. Planetary Population Synthesis. art. 143, 2018. doi: 10.1007/978-3-319-55333-7_143.
- Lisa Nortmann, Enric Pallé, Michael Salz, Jorge Sanz-Forcada, Evangelos Nagel, F. Javier Alonso-Floriano, Stefan Czesla, Fei Yan, Guo Chen, Ignas A. G. Snellen, Mathias Zechmeister, Jürgen H. M. M. Schmitt, Manuel López-Puertas, Núria Casasayas-Barris, Florian F. Bauer, Pedro J. Amado, José A. Caballero, Stefan Dreizler, Thomas Henning, Manuel Lampón, David Montes, Karan Molaverdikhani, Andreas Quirrenbach, Ansgar Reiners, Ignasi Ribas, Alejandro Sánchez-López, P. Christian Schneider, and María R. Zapatero Osorio. Ground-based detection of an extended helium atmosphere in the Saturn-mass exoplanet WASP-69b. *Science*, 362(6421):1388–1391, December 2018. doi: 10.1126/science.aat5348.
- A. Odrzywolek and J. Rafelski. Classification of Exoplanets According to Density. *Acta*

Physica Polonica B, 49(11):1917, January 2018. doi: 10.5506/APhysPolB.49.1917.

J. F. Otegi, F. Bouchy, and R. Helled. Revisited mass-radius relations for exoplanets below 120 M_{\oplus} . *A&A*, 634:A43, February 2020. doi: 10.1051/0004-6361/201936482.

Seth Redfield, Michael Endl, William D. Cochran, and Lars Koesterke. Sodium Absorption from the Exoplanetary Atmosphere of HD 189733b Detected in the Optical Transmission Spectrum. *ApJ*, 673(1):L87, Jan 2008. doi: 10.1086/527475.

P. B. Rimmer and Ch Helling. A Chemical Kinetics Network for Lightning and Life in Planetary Atmospheres. *ApJS*, 224(1):9, May 2016. doi: 10.3847/0067-0049/224/1/9.

M. Salz, S. Czesla, P. C. Schneider, E. Nagel, J. H. M. M. Schmitt, L. Nortmann, F. J. Alonso-Floriano, M. López-Puertas, M. Lampón, F. F. Bauer, I. A. G. Snellen, E. Pallé, J. A. Caballero, F. Yan, G. Chen, J. Sanz-Forcada, P. J. Amado, A. Quirrenbach, I. Ribas, A. Reiners, V. J. S. Béjar, N. Casasayas-Barris, M. Cortés-Contreras, S. Dreizler, E. W. Guenther, T. Henning, S. V. Jeffers, A. Kaminski, M. Kürster, M. Lafarga, L. M. Lara, K. Molaverdikhani, D. Montes, J. C. Morales, A. Sánchez-López, W. Seifert, M. R. Zapatero Osorio, and M. Zechmeister. Detection of He I $\lambda 10830$ Å absorption on HD 189733 b with CARMENES high-resolution transmission spectroscopy. *A&A*, 620:A97, December 2018. doi: 10.1051/0004-6361/201833694.

A. Sánchez-López, F. J. Alonso-Floriano, M. López-Puertas, I. A. G. Snellen, B. Funke, E. Nagel, F. F. Bauer, P. J. Amado, J. A. Caballero, S. Czesla, L. Nortmann, E. Pallé, M. Salz, A. Reiners, I. Ribas, A. Quirrenbach, G. Anglada-Escudé, V. J. S. Béjar, N. Casasayas-Barris, D. Galadí-Enríquez, E. W. Guenther, Th. Henning, A. Kaminski, M. Kürster, M. Lampón, L. M. Lara, D. Montes, J. C. Morales, M. Stangret, L. Tal-Or, J. Sanz-Forcada, J. H. M. M. Schmitt, M. R. Zapatero Osorio, and M. Zechmeister. Water vapor detection in the transmission spectra of HD 209458 b with the CARMENES NIR channel. *arXiv e-prints*, art. arXiv:1908.08754, Aug 2019.

Elyar Sedaghati, Henri M. J. Boffin, Ryan J. MacDonald, Siddharth Gandhi, Nikku Madhusudhan, Neale P. Gibson, Mahmoudreza Oshagh, Antonio Claret, and Heike Rauer. Detection of titanium oxide in the atmosphere of a hot Jupiter. *Nature*, 549(7671):238–241, September 2017. doi: 10.1038/nature23651.

J. V. Seidel, D. Ehrenreich, V. Bourrier, R. Allart, O. Attia, H. J. Hoeijmakers, M. Lendl,

- E. Linder, A. Wyttenbach, N. Astudillo-Defru, D. Bayliss, H. M. Cegla, Kevin Heng, B. Lavie, C. Lovis, C. Melo, F. Pepe, L. A. dos Santos, D. Ségransan, and S. Udry. Hot Exoplanet Atmospheres Resolved with Transit Spectroscopy (HEARTS) V. Detection of sodium on the bloated super-Neptune WASP-166b. *arXiv e-prints*, art. arXiv:2007.01783, July 2020.
- I. Snellen, R. de Kok, J. L. Birkby, B. Brandl, M. Brogi, C. Keller, M. Kenworthy, H. Schwarz, and R. Stuik. Combining high-dispersion spectroscopy with high contrast imaging: Probing rocky planets around our nearest neighbors. *A&A*, 576:A59, April 2015. doi: 10.1051/0004-6361/201425018.
- I. A. G. Snellen, S. Albrecht, E. J. W. de Mooij, and R. S. Le Poole. Ground-based detection of sodium in the transmission spectrum of exoplanet HD 209458b. *A&A*, 487(1):357–362, Aug 2008. doi: 10.1051/0004-6361:200809762.
- M. Stangret, N. Casasayas-Barris, E. Pallé, F. Yan, A. Sánchez-López, and M. López-Puertas. Detection of Fe I and Fe II in the atmosphere of MASCARA-2b using a cross-correlation method. *A&A*, 638:A26, June 2020. doi: 10.1051/0004-6361/202037541.
- Giovanna Tinetti, Pierre Drossart, Paul Eccleston, Paul Hartogh, Astrid Heske, Jérémy Leconte, Giusi Micela, Marc Ollivier, Göran Pilbratt, Ludovic Puig, Diego Turrini, Bart Vandenbussche, Paulina Wolkenberg, Jean-Philippe Beaulieu, Lars A. Buchave, Martin Ferus, Matt Griffin, Manuel Guedel, Kay Justtanont, Pierre-Olivier Lagage, Pedro Machado, Giuseppe Malaguti, Michiel Min, Hans Ulrik Nørgaard-Nielsen, Mirek Rataj, Tom Ray, Ignasi Ribas, Mark Swain, Robert Szabo, Stephanie Werner, Joanna Barstow, Matt Burleigh, James Cho, Vincent Coudé du Foresto, Athena Coustenis, Leen Decin, Therese Encrenaz, Marina Galand, Michael Gillon, Ravit Helled, Juan Carlos Morales, Antonio García Muñoz, Andrea Moneti, Isabella Pagano, Enzo Pascale, Giuseppe Piccioni, David Pinfield, Subhajit Sarkar, Franck Selsis, Jonathan Tennyson, Amaury Triaud, Olivia Venot, Ingo Waldmann, David Waltham, Gillian Wright, Jerome Amiaux, Jean-Louis Auguères, Michel Berthé, Naidu Bezawada, Georgia Bishop, Neil Bowles, Deirdre Coffey, Josep Colomé, Martin Crook, Pierre-Elie Crouzet, Vania Da Peppo, Isabel Escudero Sanz, Mauro Focardi, Martin Frericks, Tom Hunt, Ralf Kohley, Kevin Middleton, Gianluca Morgante, Roland Ottensamer, Emanuele Pace, Chris Pearson, Richard Stam-

per, Kate Symonds, Miriam Rengel, Etienne Renotte, Peter Ade, Laura Affer, Christophe Alard, Nicole Allard, Francesca Altieri, Yves André, Claudio Arena, Ioannis Argyriou, Alan Aylward, Cristian Baccani, Gaspar Bakos, Marek Banaszkiwicz, Mike Barlow, Virginie Batista, Giancarlo Bellucci, Serena Benatti, Pernelle Bernardi, Bruno Bézard, Maria Blecka, Emeline Bolmont, Bertrand Bonfond, Rosaria Bonito, Aldo S. Bonomo, John Robert Brucato, Allan Sacha Brun, Ian Bryson, Waldemar Bujwan, Sarah Casewell, Benjamin Charnay, Cesare Cecchi Pestellini, Guo Chen, Angela Ciaravella, Riccardo Claudi, Rodolphe Clédassou, Mario Damasso, Mario Damiano, Camilla Danielski, Pieter Deroo, Anna Maria Di Giorgio, Carsten Dominik, Vanessa Doublier, Simon Doyle, René Doyon, Benjamin Drummond, Bastien Duong, Stephen Eales, Billy Edwards, Maria Farina, Ettore Flaccomio, Leigh Fletcher, François Forget, Steve Fossey, Markus Fränz, Yuka Fujii, Álvaro García-Piquer, Walter Gear, Hervé Geoffray, Jean Claude Gérard, Lluís Gesa, H. Gomez, Rafał Graczyk, Caitlin Griffith, Denis Grodent, Mario Giuseppe Guarcello, Jacques Gustin, Keiko Hamano, Peter Hargrave, Yann Hello, Kevin Heng, Enrique Herero, Allan Hornstrup, Benoit Hubert, Shigeru Ida, Masahiro Ikoma, Nicolas Iro, Patrick Irwin, Christopher Jarchow, Jean Jaubert, Hugh Jones, Queyrel Julien, Shingo Kameda, Franz Kerschbaum, Pierre Kervella, Tommi Koskinen, Matthijs Krijger, Norbert Krupp, Marina Lafarga, Federico Landini, Emanuel Lellouch, Giuseppe Leto, A. Luntzer, Theresa Rank-Lüftinger, Antonio Maggio, Jesus Maldonado, Jean-Pierre Maillard, Urs Mall, Jean-Baptiste Marquette, Stéphane Mathis, Pierre Maxted, Taro Matsuo, Alexander Medvedev, Yamila Miguel, Vincent Minier, Giuseppe Morello, Alessandro Mura, Norio Narita, Valerio Nascimbeni, N. Nguyen Tong, Vladimiro Noce, Fabrizio Oliva, Enric Palle, Paul Palmer, Maurizio Pancrazzi, Andreas Papageorgiou, Vivien Parmentier, Manuel Perger, Antonino Petralia, Stefano Pezzuto, Ray Pierrehumbert, Ignazio Pillitteri, Giampaolo Piotto, Giampaolo Pisano, Loredana Prisinzano, Aikaterini Radioti, Jean-Michel Réess, Ladislav Rezac, Marco Rocchetto, Albert Rosich, Nicoletta Sanna, Alexandre Santerne, Giorgio Savini, Gaetano Scandariato, Bruno Sicardy, Carles Sierra, Giuseppe Sindoni, Konrad Skup, Ignas Snellen, Mateusz Sobiecki, Lauriane Soret, Alessandro Sozzetti, A. Stiepen, Antoine Strugarek, Jake Taylor, William Taylor, Luca Terenzi, Marcell Tessenyi, Angelos Tsiaras, C. Tucker, Diana Valencia, Gautam Vasisht, Allona Vazan, Francesc Vilardell, Sabine Vinatier, Serena Viti, Rens Waters, Piotr Wawer, Anna Wawrzaszek, Anthony Whitworth, Yuk L. Yung, Sergey N. Yurchenko, María Rosa Zapatero Osorio, Robert

- Zellem, Tiziano Zingales, and Frans Zwart. A chemical survey of exoplanets with ARIEL. *Experimental Astronomy*, 46(1):135–209, November 2018. doi: 10.1007/s10686-018-9598-x.
- H. D. Tran, R. Cohen, A. Colson, J. A. Mader, M. Swain, A. C. Laity, M. Kong, C. R. Gelino, and G. B. Berriman. Data reduction pipelines for the Keck Observatory Archive. In Proc. SPIE, volume 9910 of *Society of Photo-Optical Instrumentation Engineers (SPIE) Conference Series*, page 99102E, July 2016. doi: 10.1117/12.2230963.
- A. H. M. J. Triaud, D. Queloz, C. Hellier, M. Gillon, B. Smalley, L. Hebb, A. Collier Cameron, D. Anderson, I. Boisse, G. Hébrard, E. Jehin, T. Lister, C. Lovis, P. F. L. Maxted, F. Pepe, D. Pollacco, D. Ségransan, E. Simpson, S. Udry, and R. West. WASP-23b: a transiting hot Jupiter around a K dwarf and its Rossiter-McLaughlin effect. *A&A*, 531:A24, July 2011. doi: 10.1051/0004-6361/201016367.
- Julia Venturini, Octavio M. Guilera, Jonas Haldemann, M. Paula Ronco, and Christoph Mordasini. The Nature of the Radius Valley: Hints from Formation and Evolution Models. *arXiv e-prints*, art. arXiv:2008.05513, August 2020.
- C. von Essen, M. Mallonn, L. Welbanks, N. Madhusudhan, A. Pinhas, H. Bouy, and P. Weis Hansen. An optical transmission spectrum of the ultra-hot Jupiter WASP-33 b. First indication of aluminum oxide in an exoplanet. *A&A*, 622:A71, February 2019. doi: 10.1051/0004-6361/201833837.
- Luis Welbanks and Nikku Madhusudhan. On Degeneracies in Retrievals of Exoplanetary Transmission Spectra. *AJ*, 157(5):206, May 2019a. doi: 10.3847/1538-3881/ab14de.
- Luis Welbanks and Nikku Madhusudhan. On Degeneracies in Retrievals of Exoplanetary Transmission Spectra. *AJ*, 157(5):206, May 2019b. doi: 10.3847/1538-3881/ab14de.
- Joshua N. Winn, John Asher Johnson, Kathryn M. G. Peek, Geoffrey W. Marcy, Gaspar Á. Bakos, Keigo Enya, Norio Narita, Yasushi Suto, Edwin L. Turner, and Steven S. Vogt. Spin-Orbit Alignment for the Eccentric Exoplanet HD 147506b. *ApJ*, 665(2):L167–L170, August 2007. doi: 10.1086/521362.
- Joshua N. Winn, John Asher Johnson, Norio Narita, Yasushi Suto, Edwin L. Turner, Debra A. Fischer, R. Paul Butler, Steven S. Vogt, Francis T. O’Donovan, and B. Scott Gaudi. The Prograde Orbit of Exoplanet TrES-2b. *ApJ*, 682(2):1283–1288, August 2008.

doi: 10.1086/589235.

Joshua N. Winn, John Asher Johnson, Daniel Fabrycky, Andrew W. Howard, Geoffrey W. Marcy, Norio Narita, Ian J. Crossfield, Yasushi Suto, Edwin L. Turner, Gil Esquerdo, and Matthew J. Holman. On the Spin-Orbit Misalignment of the XO-3 Exoplanetary System. *ApJ*, 700(1):302–308, July 2009. doi: 10.1088/0004-637X/700/1/302.

Aaron S. Wolf, Gregory Laughlin, Gregory W. Henry, Debra A. Fischer, Geoff Marcy, Paul Butler, and Steve Vogt. A Determination of the Spin-Orbit Alignment of the Anomalously Dense Planet Orbiting HD 149026. *ApJ*, 667(1):549–556, September 2007. doi: 10.1086/503354.

A. Wyttenbach, D. Ehrenreich, C. Lovis, S. Udry, and F. Pepe. Spectrally resolved detection of sodium in the atmosphere of HD 189733b with the HARPS spectrograph. *A&A*, 577:A62, May 2015. doi: 10.1051/0004-6361/201525729.

A. Wyttenbach, C. Lovis, D. Ehrenreich, V. Bourrier, L. Pino, R. Allart, N. Astudillo-Defru, H. M. Cegla, K. Heng, B. Lavie, C. Melo, F. Murgas, A. Santerne, D. Ségransan, S. Udry, and F. Pepe. Hot Exoplanet Atmospheres Resolved with Transit Spectroscopy (HEARTS). I. Detection of hot neutral sodium at high altitudes on WASP-49b. *A&A*, 602:A36, June 2017. doi: 10.1051/0004-6361/201630063.